POLITECNICO DI TORINO

Corso di Laurea magistrale in Ingegneria Meccanica

Dipartimento di Ingegneria Meccanica e Aerospaziale

Uncertainty quantification in multibody dynamics

Application to the PKM Exechon robust dynamic analysis

Supervisors:

Prof. Elvio BONISOLI

Prof. John E. MOTTERSHEAD

Dr. Anas BATOU

Student :

Daniele STRAZZULLA

Matricola : s242401

Academic year

2017-2018

To my family...

Abstract

In many cases, when we want to study the dynamic behavior of complex mechanical systems that are subjected to large displacements and rotations, the resulting equation of motion is nonlinear. Therefore, the mathematical model is too complex to provide an analytical solution. Nowadays the dynamics of complex systems it is usually studied with multi-body codes through numerical integration of the equations. High-performance mechanical system requires a compromise between efficiency and effectiveness. The mathematical model, as well as the parameters of the model, are contaminated with uncertainties, therefore to improve the predictability of the model uncertainties must be taken into account. The aim of this project is to show through an industrial application, how to take into account all the possible source of uncertainties that may arise in a multi-body (MB) and in a flexible MB system, in order to increase the robustness of the model and understand through a sensitivity analysis which are the most influential parameters. This project will particularly focus on uncertainties related to (1) the inertial properties of the bodies, (2) the placement of sensor and actuators during experiments, (3) Controllers parameters (4) joint friction and (5) uncertainties related to the stiffness matrices of flexible parts of a flexible multibody system. Through the Maximum Entropy Principle the prior probability distribution of the random variable is constructed, then the stochastic dynamical equations are solved through the Monte Carlo simulation method, which will allow us through mathematical statistics, to obtain a confidence region of the response of the system and through a Variance-based sensitivity analysis understands the influence of certain group of parameters respect to frequency of the system. This will be useful to understand (1) how these uncertainties affect the response of the system and (2) which group of parameters influences the most the system.

Contents

Chapter 1

Introduction

1.1 Background

Nowadays the dynamics of complex systems it is usually studied with multi-body codes through numerical integration of the equations. A multi-body (MB) system consist of several rigid which interact with each other by joints or by internal forces (springs, dampers, actuators ...) [1]. Sometimes in order to optimize the system or have a more representative model, some of the main parts can no longer be modeled as a rigid bodies, because it is also important to evaluate the effect that the flexibility has on the dynamic behavior of the system, parameters such as stiffness have the main impact on the behavior of a mechanical system, therefore we need to switch to a Flexible multibody system (FMBS) [2]. The mathematical model, as well as the parameters of the model, are contaminated with uncertainties, therefore to improve the predictability of the model uncertainties must be taken into account. Data uncertainty are due to lack of knowledge of the exact value of parameters such as Young Modulus (E) density (ρ) and so on. Model uncertainties they may be due to simplifications and approximations of the physical behavior of the system, for example, since the property of the flexible component is usually obtained through a Finite Element approach, we already know that there is some uncertainty on the evaluation of the stiffness matrix which is intrinsic of the method and they can be reduced but not removed. However, over the years multibody analysis has proven to be a useful tool in the engineering field thank to the possibility of this tool to link different discipline, this is why a lot of efforts have been made to try to integrate uncertainty quantification methods with multibody analysis.

In [3] the authors propose a method to include epistemic uncertainties in MBS analysis, this approach is based on fuzzy arithmetic where the uncertain values are represented by fuzzy numbers.

In [4, 5] the authors propose a generalized polynomial chaos approach to model the uncertainty in a nonlinear multi-body dynamic system.

In this paper [6], the authors propose a nonparametric probabilistic approach based on the random matrix theory with uncertain rigid bodies, which is the same approach used in this report.

Two different numerical application are shown in this report for modeling the uncertainties in the MB system such as (mass, inertia, sensor position and orientation etc..), for the flexible multibody system we will focus only on the uncertainties related to the stiffness matrix of the flexible parts. The first application concern a MB model realized in **Simulink** of the **PKM** Exechon Fig.1.1, the Exechon Parallel Kinematic Machine (PKM) is a machine specially designed for accurate positioning and machining. A deterministic MB model of this machine has been constructed to predict and understand its kinematics and vibratory dynamics to support the future engineering of complex setups using the machine. To validate this model a specimen has been instrumented by **MTC** (manufacturing technology center) company and experimental data at certain locations have been collected. The results of this specimen show that the MB model is not in complete agreement with experimental results and uncertainties in both the MB model and the experimental procedure need to be analyzed. In the last application will be shown a method for modeling the uncertainties related to the stiffness matrices of flexible parts of a flexible multibody system, through a simplified model of the Exechon PKM realized in **MATLAB** in an in-house software based on the Floating frame of reference approach [1], provided by the University of Liverpool.

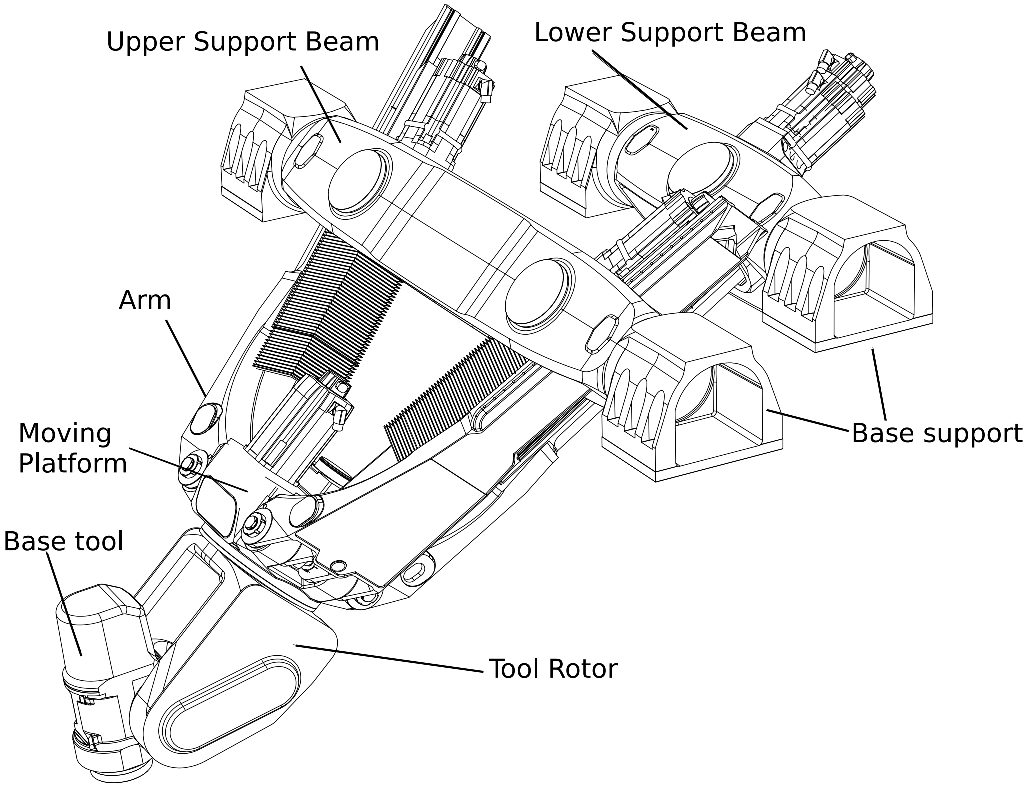

Figure 1.1: Parallel Kinematic Machine Exechon

1.2 Aim and objectives

The aim of this project consists in analyzing potential sources of uncertainty in the MB and FMB model of the Exechon PKM, in order to:

- improve the robustness of the model analyzed
- understand which parameters influence the most the dynamic response of the system
- understand how uncertainties affect the dynamic response of the system

This will be done by taking into account all the possible sources of uncertainties that may arise in a MB and FMB system, we will particularly focus on uncertainties related to (1) the inertial properties of the bodies, (2) the placement of sensor and actuators during experiments, (3) Controllers parameters and (4) joints friction and (5) uncertainties related to the stiffness matrices of flexible parts of a FMBS.

1.3 Scheduling

For the first objective, a stochastic model is constructed by replacing the uncertain parameters with random parameters, the prior probability distribution of the random variables are constructed by using the Maximum Entropy Principle [7], that maximizes the uncertainties in the model under the constraint defined by the available information. This method takes into account the physical/mathematical properties of the parameters during the construction and yields distribution with a maximum conservatism and controlled by a few numbers of parameters. The stochastic dynamical equations are solved through the Monte Carlo simulation method [8], that calculates a series of possible realizations of the phenomenon, hence through mathematical statistics, we obtain a confidence region and the Relative standard deviation of the output of the system obtaining a qualitative sensitivity analysis then for the multibody model only once obtained the more important parameters we used a variance-based sensitivity analysis [9], in order to understands the influence of certain group of parameters respect to Frequency of the system. Chapter 2 is devoted to the introduction of the two model used for the sensitivity analysis. In Chapter 3 we propose a probabilistic model for the uncertain parameters using the Maximum entropy principle. The last Chapter is devoted to the application of the method presented.

Chapter 2

Models description

The Exechon Parallel Kinematic Machine (PKM) is a 5-axis machine, mounted on a 2-axis G*ü*del gantry, specially designed for accurate positioning and machining. This machine presents a tripod structure, and it has a total of 14 joints, 5 of them actuated by Siemens motors and controllers, and 9 non-actuated rotational joints. This machine is composed of two **RRPR** and one **SPR** legs connected in parallel with the platform [10], where **R** indicate a Revolution joint , **P** a Prismatic joint and **S** a spherical joint. In Fig.2.1 a simplified representation of the DOF of the system is shown. The actuated joints are three prismatic joint **P** and the two rotational joint $\mathbf{R}_{base\_tool}$ and $\mathbf{R}_{tool}$.

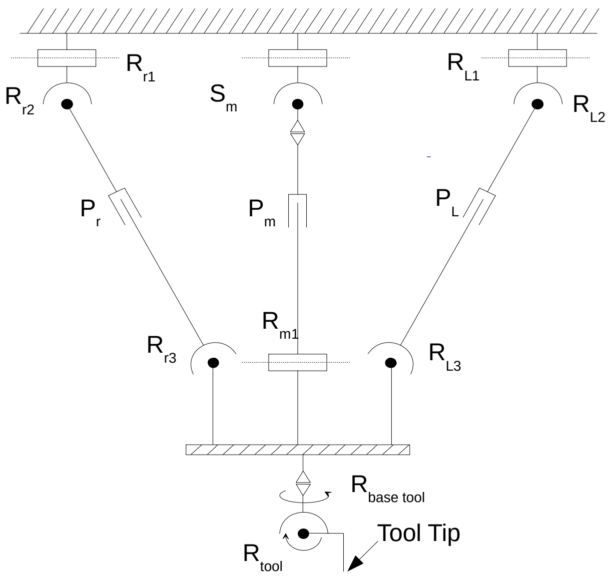

Figure 2.1: PKM kinematic description

2.1 MTC Multi Body model description

A kinematic model uses the constraint equations of a mechanical system to determine the configuration of the system based on geometric characteristics and restrictions. A kinematic model of a system can be direct or inverse, being the main difference between them the definition of the inputs and outputs: a direct kinematic model establishes the configuration of a system based on the given position of its joints, while an inverse kinematic model establishes the joints' positions to achieve a given system configuration. A dynamic model also accounts for time-dependent changes in the state of the system (being some of these positions, speeds, external and internal forces...) produced by mass and inertia effects and by the internal mechanic's behaviour. In the system under study here, both the direct and inverse kinematic models were obtained and validated. The inverse kinematic model (IKM) is used in this project to guide the dynamic model, i.e., the desired configuration/trajectory is passed to the IKM as an input, that returns the joint positions/motions necessary to achieve it, which are in turn passed as input to the dynamic model, as shown in figure 2.2. The PKM dynamics have

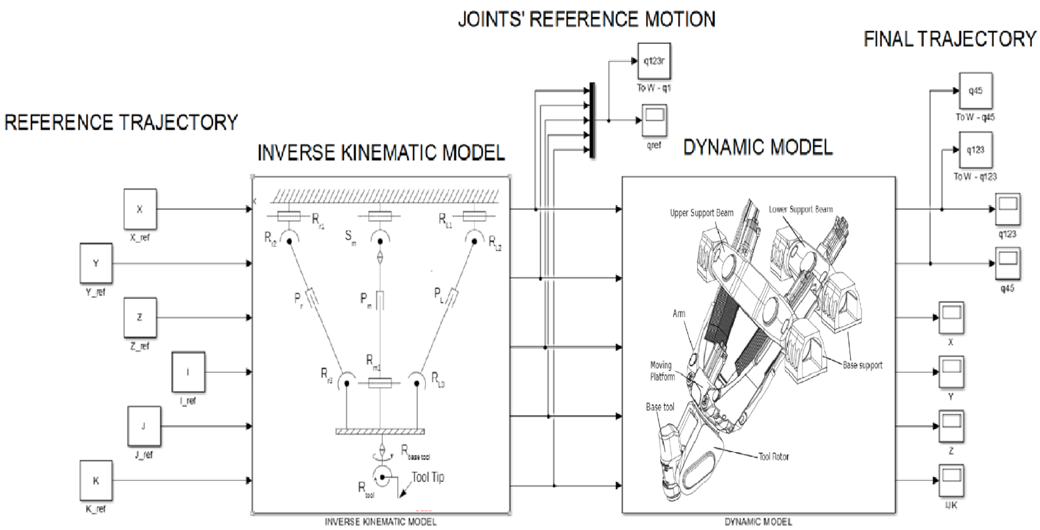

Figure 2.2: PKM inverse kinematic and dynamic models' information workflow

been modelled using a MB technique where the main parts of the physical system are modelled as rigid bodies related to each other by the joints. The model has been developed using Simscape MB, figure 2.3. Mass and inertia properties of

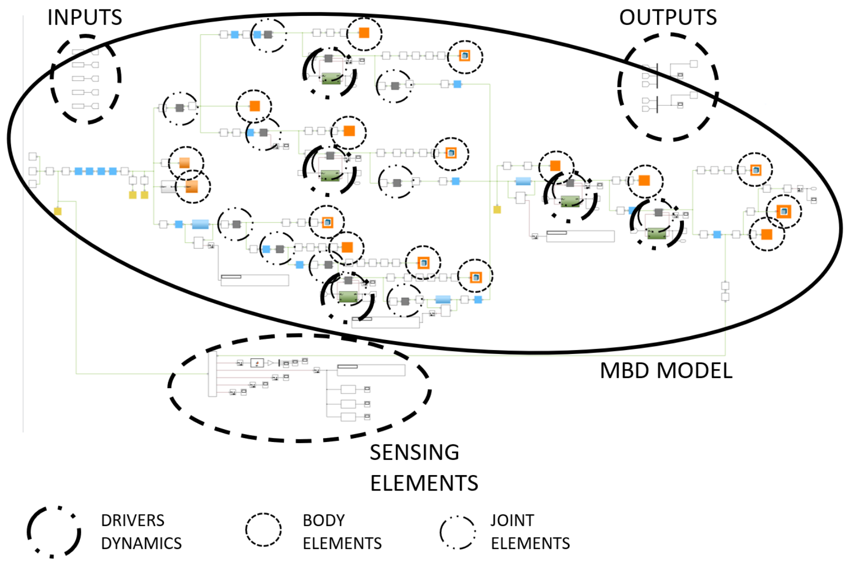

Figure 2.3: PKM dynamic model developed on SimScape/SimMechanics

the body elements have been obtained from a simplified CAD model with know material characteristics.

2.1.1 Experimental data processing

In the figure 2.5 we can see how the experiment was carried on, the experiment involved placing accelerometers onto the system at 20 different locations (figure 2.4) and measuring the accelerations when a vertical excitation force is applied to the tooltip through a shaker firmly clamped to the ground. The stinger rod was attached to the shaker by one end and to the force sensor by the other end. The latest was attached to a dummy tool specifically designed for this purpose, which is held in place by the PKM tool holder. Raw data, from all the sensors, of acceleration and force respect to the time (figure 2.7 and 2.6) were provided by the MTC, hence through a Discrete Fourier Transform (DFT) we were able to obtain the frequency spectrum of the acceleration figure 2.8 and force figure 2.9, then we obtained the inertance and phase of the response of the system, which correlates the acceleration outputs with the force inputs in the frequency domain, figures from 2.10 to 2.13. [1]

[1] For sake of simplicity, in this report, we will compare only the data of two sensors (1 and 3).we will refer to the figure 2.4 for sensor's labelling.

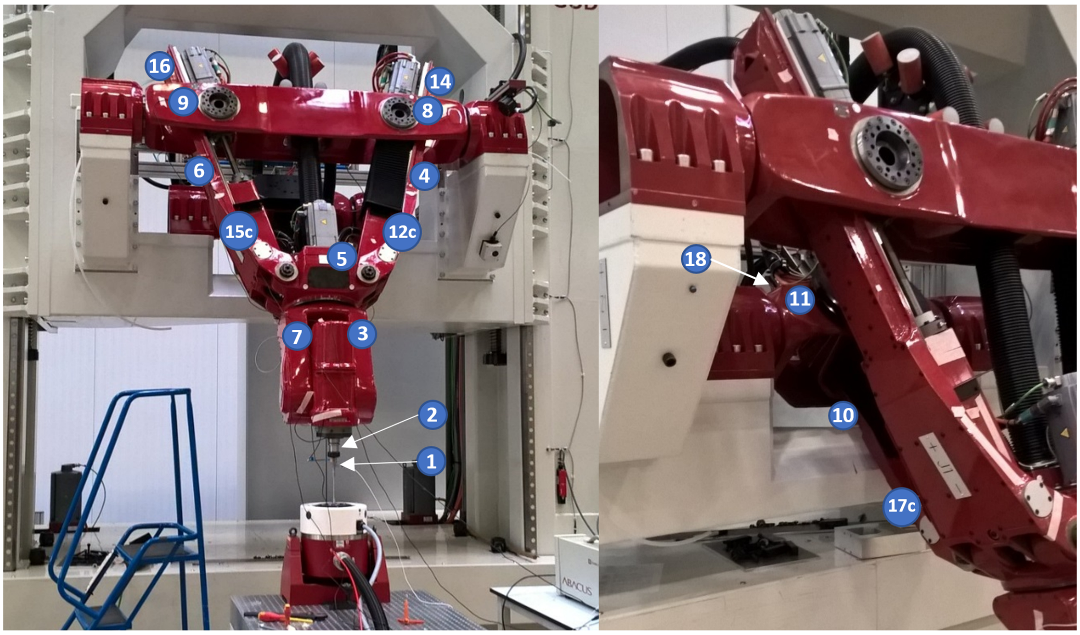

Figure 2.4: PKM label sensor placements

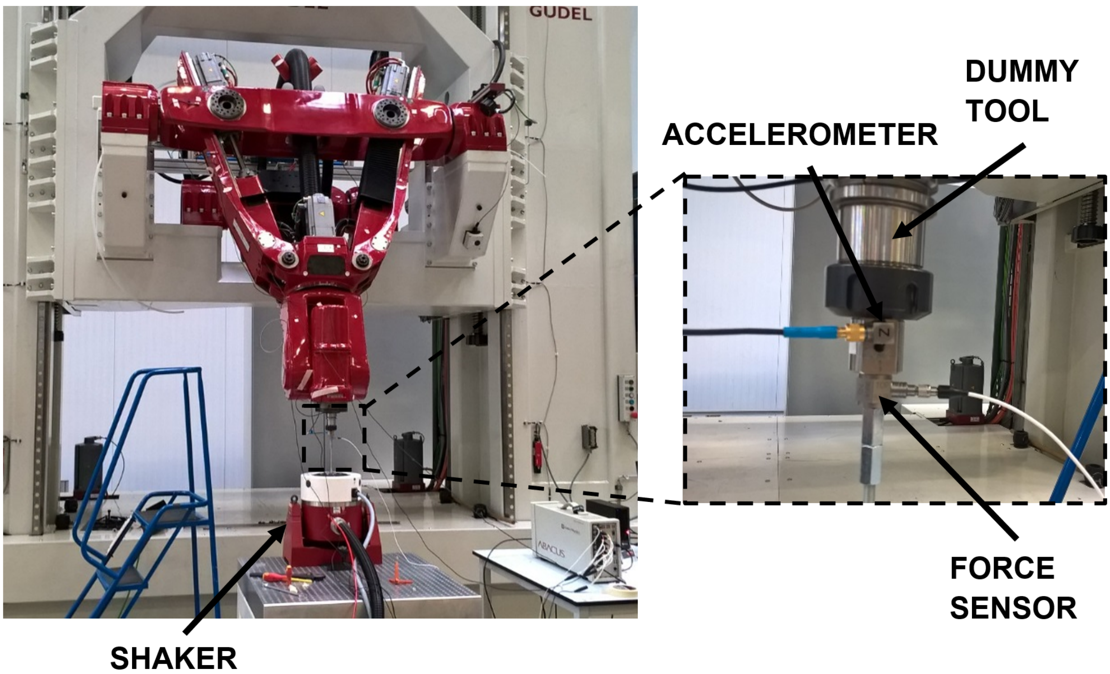

Figure 2.5: PKM and shaker position during the experiment

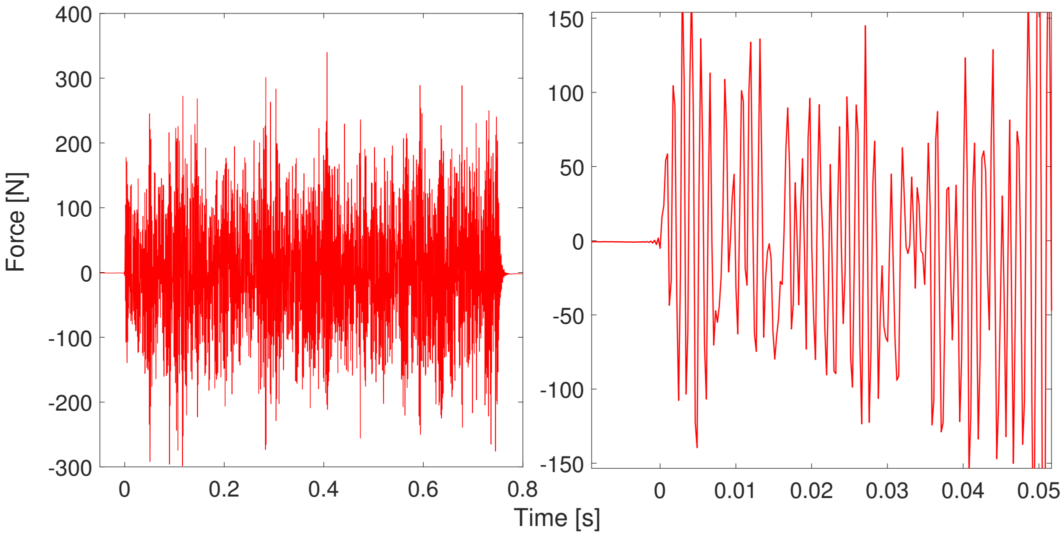

Figure 2.6: Excitation force in time

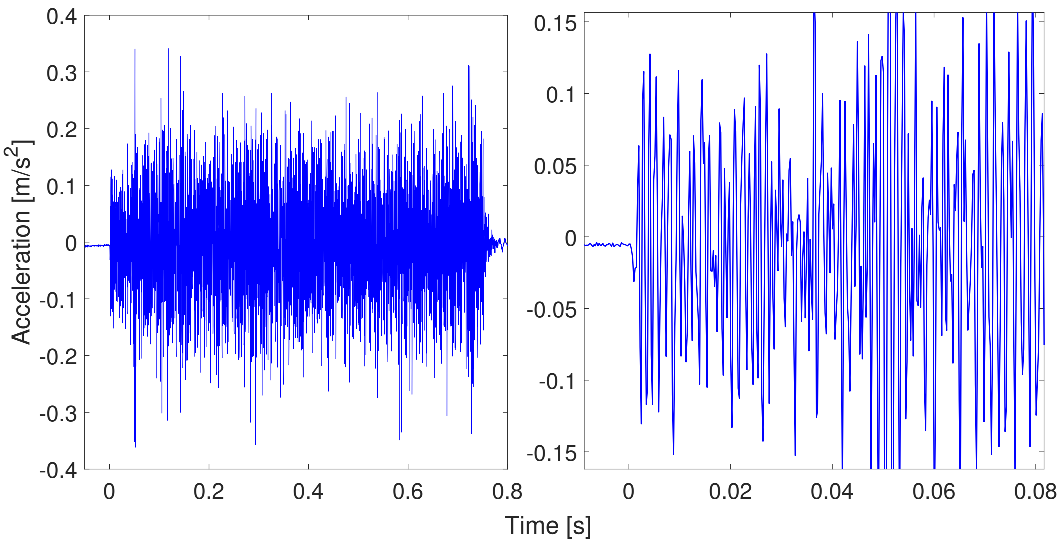

Figure 2.7: acceleration in time **sensor 1**

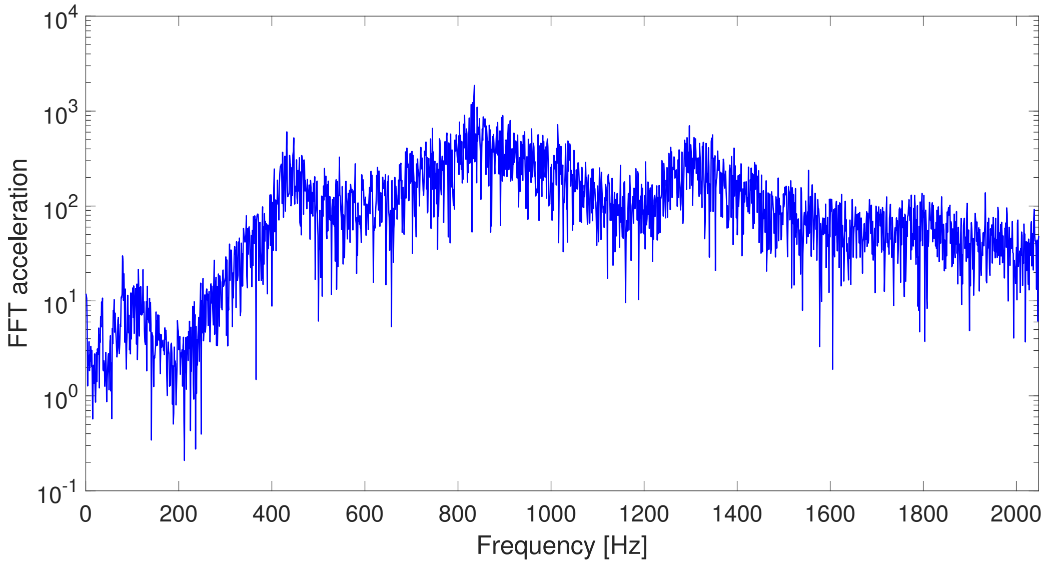

Figure 2.8: frequency spectrum of the acceleration **sensor 1**

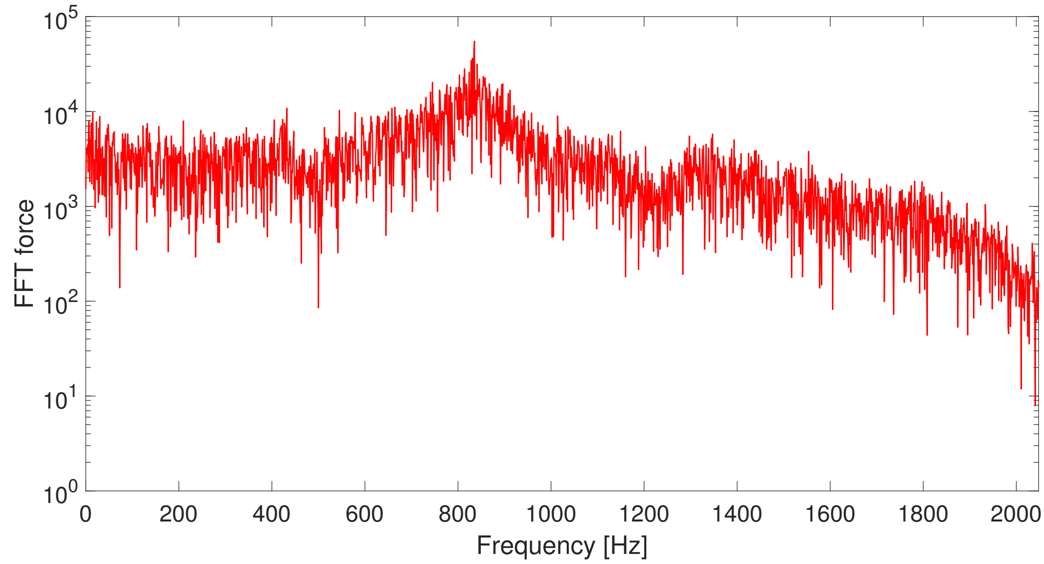

Figure 2.9: frequency spectrum of the force

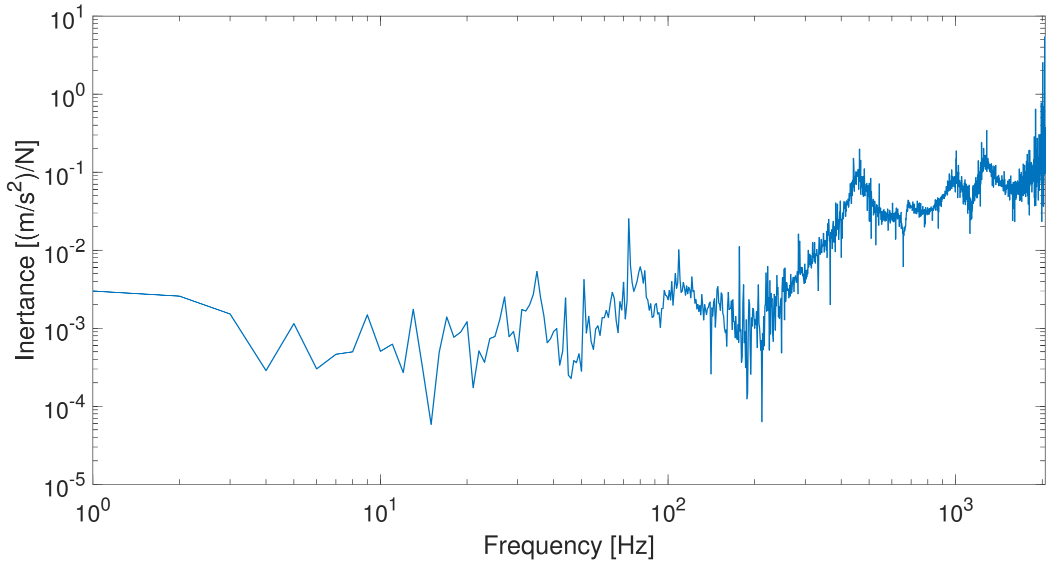

Figure 2.10: Experimental frequency response **sensor 1**

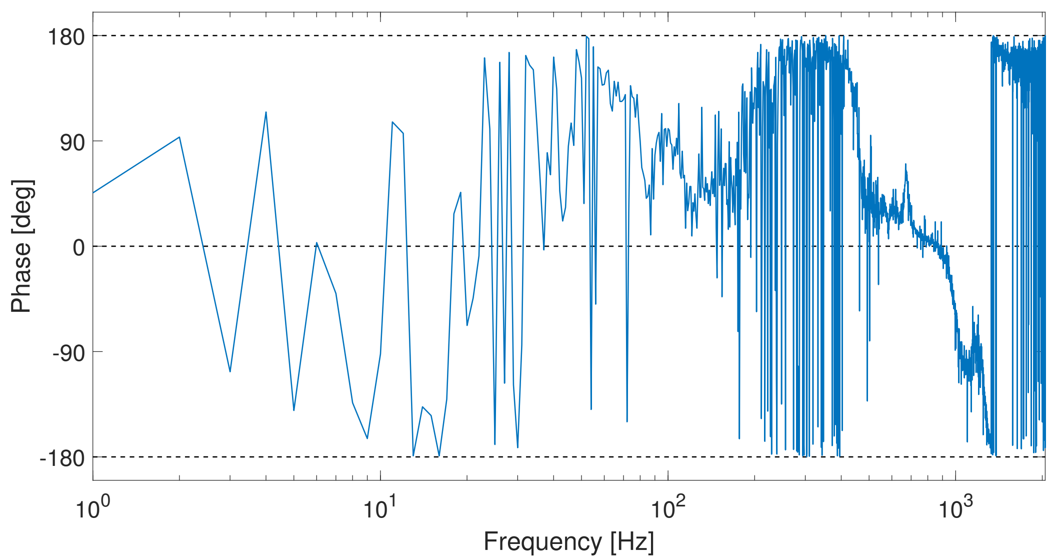

Figure 2.11: Experimental phase **sensor 1**

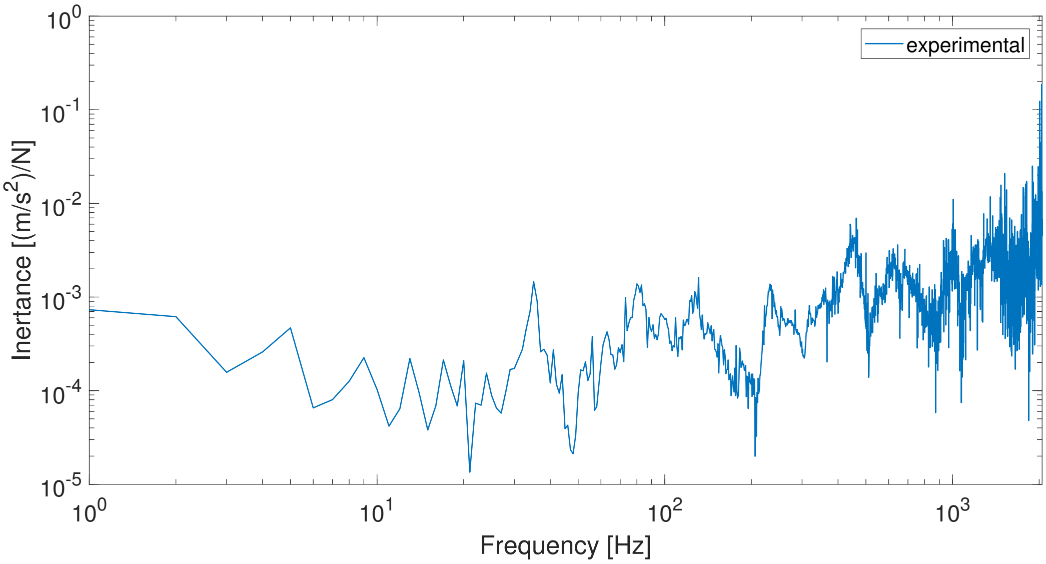

Figure 2.12: Experimental frequency response **sensor 3**

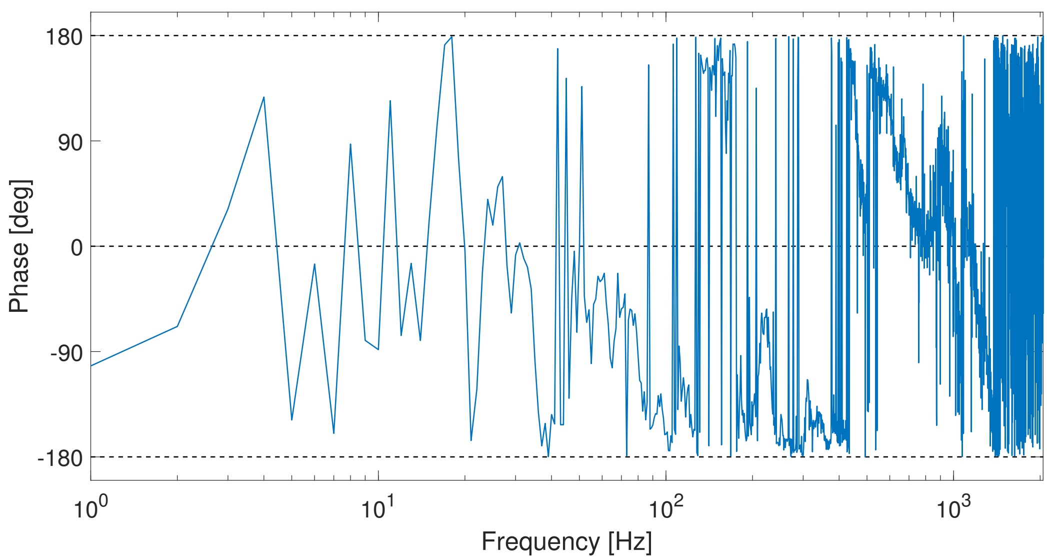

Figure 2.13: Experimental phase **sensor 3**

2.2 Flexible Multi Body model description

This numerical example focuses on modelling the uncertainty related to the stiffness matrix of flexible multibody systems (FMBS). The FMB software used is based on the *floating frame of reference formulation*(FFRF)[1] and it is combined with the *Craig-Bampton* sub-structuring method [11, 12] considering the interfaces of the substructure rigidly connected, in order to reduce the computational cost of the simulations.

2.2.1 Floating frame of reference formulation

The floating frame of reference formulations it is one of the most used methods to describe the kinematics of flexible multibody systems. In the floating frame of reference formulation each flexible bodies is described through two sets of coordinate: *reference* and *elastic* coordinates, figure 2.14. The reference coordinate

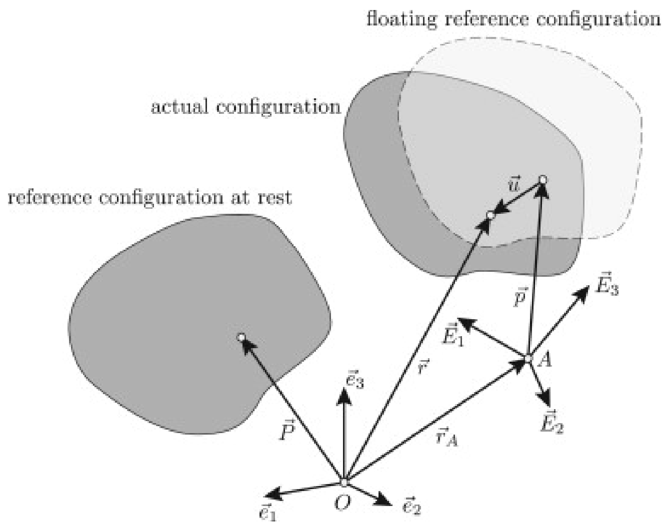

Figure 2.14: Floating frame of reference formulation, [13]

.

describes the location $\mathbf{R}_j$ and orientation $\boldsymbol{\theta}_j$ of the body in the inertial frame, instead, the elastic coordinates $\mathbf{u}_j^f$ describe the deformation with respect to the body coordinate system, [1]. Therefore the large rigid body displacement is described by reference coordinates, instead, the deformation of the body with respect to its coordinate system is described using the elastic coordinates through a set of local shape function. Using these two sets of coordinates and the methods of analytical mechanics, the equations of motion of the flexible body can be written as:

$$
\begin{bmatrix} \mathbf{m}_j^{RR} & \mathbf{m}_j^{R\theta} & \mathbf{m}_j^{Rf} \\ & \mathbf{m}_j^{\theta\theta} & \mathbf{m}_j^{\theta f} \\ Sym & & \mathbf{m}_j^{ff} \end{bmatrix}
\begin{bmatrix} \ddot{\mathbf{R}}_j \\ \ddot{\boldsymbol{\theta}}_j \\ \ddot{\mathbf{u}}_j^f \end{bmatrix}
+
\begin{bmatrix} \mathbf{0} & \mathbf{0} & \mathbf{0} \\ \mathbf{0} & \mathbf{0} & \mathbf{0} \\ \mathbf{0} & \mathbf{0} & \mathbf{k}_j^{ff} \end{bmatrix}
\begin{bmatrix} \mathbf{R}_j \\ \boldsymbol{\theta}_j \\ \mathbf{u}_j^f \end{bmatrix}
+
\begin{bmatrix} \mathbf{C}_{R_j}^T \\ \mathbf{C}_{\theta_j}^T \\ \mathbf{C}_{u_j^f}^T \end{bmatrix}
\boldsymbol{\lambda}
=
\begin{bmatrix} (\mathbf{Q}_j^e)_R \\ (\mathbf{Q}_j^e)_\theta \\ (\mathbf{Q}_j^e)_f \end{bmatrix}
+
\begin{bmatrix} (\mathbf{Q}_j^v)_R \\ (\mathbf{Q}_j^v)_\theta \\ (\mathbf{Q}_j^v)_f \end{bmatrix}
\tag{2.1}
$$

Where $\mathbf{R}_j$ is the set of the Cartesian coordinates that define location of origin of the j-th bodies, $\boldsymbol{\theta}_j$ is the set of rotational coordinates that describe the orientation of the bodies, $\mathbf{u}_j^f$ is the set of the generalized elastic coordinates, $\mathbf{Q}_j^v$ is a quadratic velocity vector resulting from the differentiation of the kinetic energy with respect to time and with respect to the body coordinates, $\mathbf{Q}_j^e$ is the vector of generalized forces associated with the generalized coordinates, $\mathbf{C}_j$ is the constraint Jacobian matrix and $\boldsymbol{\lambda}$ is the vector of Lagrange multipliers of body, $\mathbf{m}_j^{RR}$ is the matrix associated with the translation of the body reference is a constant[2] diagonal matrix, $\mathbf{m}_j^{R\theta}$ represents the inertia coupling between the translation and rotation of the body reference this matrix is null if we take as origin of the body the center of mass, $\mathbf{m}_j^{\theta\theta}$ is the matrix associated with the rotational coordinates of the body reference, $\mathbf{m}_j^{ff}$ is the matrix associated with elastic coordinates this matrix is constant, $\mathbf{m}_j^{\theta f}$ and $\mathbf{m}_j^{\theta f}$ represent the coupling between the reference motion and elastic deformation and $\mathbf{k}_j^{ff}$ is the symmetric positive semidefinite stiffness matrix associated with the elastic coordinates, this matrix as well as $\mathbf{m}_j^{ff}$ are the same matrices that appear in linear structural dynamics because the elastic coordinate are defined in the body-fixed reference frame, they are obtained through the finite element model of the flexible component.

2.2.2 Craig-Bampton method

When we are dealing with complex mechanical systems, we usually have dozens of bodies, since in most of them the flexibility cannot be neglected their stiff-

[2]the non constant matrices are function of time

ness must be considered. The stiffness matrices are usually obtained with a finite element approach, that through the discretization of the geometry into finite element, where each element is basically a model of a small deformable solid. The deformation of this solid element is described through the shape function, each element has two or more nodes that will become the degree of freedom (DOF) of the model, hence we pass from an infinite number of degree of freedom to a finite number of degree of freedom, this first approximation brings an overestimation of the stiffness matrix, but this is not the only approximation of this method. The number of DOF is chosen evaluating a benefit between computational cost, i.e. if we have a mesh that is too large, which means having a low number of degrees of freedom, this leads to a poorly precision of the results and vice-versa having a mesh too thick that means having a high number of degrees of freedom leads to a high computational cost. Usually, we are dealing with tens of thousands or even much more degree of freedom and since we need to lunch lots of simulation to perform the sensitivity analysis, we want to optimize computational time as much as possible. This is why we use the Craig Bampton method, that is a well-known model order reduction technique, will help us to decrease the degrees of freedom of the structure and therefore to decrease the computational cost. The generic equation of motion of the free behaviour of the substructure S_j[3], in the elastic coordinate:

$$\mathbf{M}_j\,\ddot{\mathbf{u}}_j + \mathbf{K}_j\,\mathbf{u}_j = \mathbf{0} \tag{2.2}$$

where in order to simplify the notation $\mathbf{M}_j$ and $\mathbf{K}_j$, are respectively, $\mathbf{m}_j^{ff}$ $\mathbf{K}_j^{ff}$ $(n_j \times n_j)$ matrix of the j-th substructure. Now we can write the equation of motion of the free body respect to his reference and reorganize the equation of motion accordingly with the Craig Bampton sub-structuring method:

$$\begin{bmatrix} \mathbf{M}_j^{II} & \mathbf{M}_j^{I\Gamma} \\ \mathbf{M}_j^{\Gamma I} & \mathbf{M}_j^{\Gamma\Gamma} \end{bmatrix} \begin{bmatrix} \ddot{\mathbf{u}}_j^{I} \\ \ddot{\mathbf{u}}_j^{\Gamma} \end{bmatrix} + \begin{bmatrix} \mathbf{K}_j^{II} & \mathbf{K}_j^{I\Gamma} \\ \mathbf{K}_j^{\Gamma I} & \mathbf{K}_j^{\Gamma\Gamma} \end{bmatrix} \begin{bmatrix} \mathbf{u}_j^{I} \\ \mathbf{u}_j^{\Gamma} \end{bmatrix} = \begin{bmatrix} 0 \\ 0 \end{bmatrix} \tag{2.3}$$

Where we indicated with (I) the inner DOF and with (Γ) the interface DOF. Hence we write the displacement vector u^I as the sum of the elastic modes of shape and constraint modes. Constraint modes are the deformation pattern due to the

[3]where $j = 1 \dots n_s$

displacement $\mathbf{u}^{\Gamma}$ when no force acts on the substructure [14].

$$\mathbf{u}_j^{I'} = -\mathbf{K}_j^{II}\mathbf{K}_j^{I\Gamma[-1]}\mathbf{u}_j^{\Gamma} \tag{2.4}$$

The elastic modes of shape, that are the natural modes of free vibraton[4] of the substructure with fixed interface DOF $\mathbf{u}_j^{\Gamma} = \mathbf{0}$ can be evaluated as follow:

$$\left(-\omega^2\mathbf{M}_j^{II} + \mathbf{K}_j^{II}\right)\mathbf{\Phi}_j^{I} = \mathbf{0} \tag{2.5}$$

where we consider only the first $\tilde{m}_j$ eigenvalues, usually $\tilde{m}_j$ is much less then the all the inner DOF and so we get the reduced-order model by projecting the internal DOF on the set of the $\tilde{m}$ elastic modes, accordingly once obtained the eigenvectors we can carry out the modal transformation

$$\mathbf{u}_j^{I''} = \mathbf{\Phi}_j^{I}\tilde{\mathbf{q}}_j \tag{2.6}$$

where $\tilde{\mathbf{q}}_j$ are the generalize coordinate related to normal modes of the substructures and $[\mathbf{\Phi}_j^{I}]_{n_j^I \times \tilde{m}_j}$ is the modal matrix. Hence we can finally write the Craig Bambpton transform matrix as follow:

$$\mathbf{\Psi}_{\boldsymbol{j}} = \begin{bmatrix} \mathbf{\Phi}_{\boldsymbol{j}}^{\boldsymbol{I}} & -\mathbf{K}_j^{II}\mathbf{K}_j^{I\Gamma} \\ \mathbf{0} & \mathbf{I}_j \end{bmatrix}_{[n_j^I + n_j^{\Gamma}] \times [\tilde{m}_j + n_j^{\Gamma}]} \tag{2.7}$$

Where $\mathbf{I}_j$ is the identity matrix $(n_j^{\Gamma} \times n_j^{\Gamma})$. So we obtain the transformation matrix:

$$\begin{bmatrix} \mathbf{u}_j^{I} \\ \mathbf{u}_j^{\Gamma} \end{bmatrix} = \begin{bmatrix} \mathbf{\Phi}_j^{I} & -\mathbf{K}_j^{II}\mathbf{K}_j^{I\Gamma} \\ \mathbf{0} & \mathbf{I}_j \end{bmatrix} \begin{bmatrix} \tilde{\mathbf{q}}_j \\ \mathbf{u}_j^{\Gamma} \end{bmatrix} = \mathbf{\Psi}\mathbf{u}^* \tag{2.8}$$

Therefore substituting the Eq.2.8 in the Eq.2.2 and multiplying from the left both members for $[\Psi]^T$ we obtain the following expression:

$$\mathbf{M}_j^*\ddot{\mathbf{u}}_j^* + \mathbf{K}_j^*\mathbf{u}_j^* = 0 \tag{2.9}$$

Where $\mathbf{K}_j^*$,$\mathbf{M}_j^*$ are the reduced matrix $[(n^{\Gamma} + \tilde{m}) \times (n^{\Gamma} + \tilde{m})]$, instead the size of $\mathbf{0}$ is $[(n^{\Gamma} + \tilde{m}) \times 1]$, the reduced form are defined as follow:

$$\mathbf{M}_j^* = \mathbf{\Psi}_j^T\mathbf{M}_j\mathbf{\Psi}_j \tag{2.10a}$$

$$\mathbf{K}_j^* = \mathbf{\Psi}_j^T\mathbf{K}_j\mathbf{\Psi}_j \tag{2.10b}$$

[4] Assuming an harmonic motion $u(t) = U(\omega)\mathrm{e}^{i\omega t}$

Let $\mathbf{A}_j^*$ be the generic reduce matrix $\mathbf{M}_j^*$ or $\mathbf{K}_j^*$ of the S_j substructure, we can divide the matrix as follow:

$$\mathbf{A}_j^* = \mathbf{\Psi}_j^T \mathbf{A}_j \mathbf{\Psi}_j = \begin{bmatrix} \mathbf{A}_j^{*II} & \mathbf{A}_j^{*I\Gamma} \\ \mathbf{A}_j^{*\Gamma I} & \mathbf{A}_j^{*\Gamma\Gamma} \end{bmatrix} \tag{2.11}$$

Where the sizes are $[\mathbf{A}_j^{*II}]_{(m_j \times m_j)}$, $[\mathbf{A}_j^{*I\Gamma}]_{(m_j \times n_j^\Gamma)}$ and $[\mathbf{A}_j^{*\Gamma\Gamma}]_{(n_j^\Gamma \times n_j^\Gamma)}$. The coupling blocks for the stiffness matrix are null, this is due of the definition of the constraint modes. Hence we can finally write the equation of motion of the j-th bodies in the floating frame of reference approach , as in[1]:

$$\begin{bmatrix} \mathbf{m}_j^{RR} & \mathbf{m}_j^{R\theta} & \underline{\mathbf{m}}_j^{Rf} \\ & \mathbf{m}_j^{\theta\theta} & \underline{\mathbf{m}}_j^{\theta f} \\ Sym & & \underline{\mathbf{m}}_j^{ff} \end{bmatrix} \begin{bmatrix} \ddot{\mathbf{R}}_j \\ \ddot{\boldsymbol{\theta}}_j \\ \ddot{\underline{\mathbf{u}}}_j^f \end{bmatrix} + \begin{bmatrix} \mathbf{0} & \mathbf{0} & \mathbf{0} \\ \mathbf{0} & \mathbf{0} & \mathbf{0} \\ \mathbf{0} & \mathbf{0} & \underline{\mathbf{k}}_j^{ff} \end{bmatrix} \begin{bmatrix} \mathbf{R}_j \\ \boldsymbol{\theta}_j \\ \underline{\mathbf{u}}_j^f \end{bmatrix} + \\ + \begin{bmatrix} \mathbf{C}_{R_j}^T \\ \mathbf{C}_{\theta_j}^T \\ \underline{\mathbf{C}}_{u_j^f}^T \end{bmatrix} \boldsymbol{\lambda} = \begin{bmatrix} (\mathbf{Q}_j^e)_R \\ (\mathbf{Q}_j^e)_\theta \\ (\underline{\mathbf{Q}}_j^e)_f \end{bmatrix} + \begin{bmatrix} (\mathbf{Q}_j^v)_R \\ (\mathbf{Q}_j^v)_\theta \\ (\underline{\mathbf{Q}}_j^v)_f \end{bmatrix} \tag{2.12}$$

where :

$$\underline{\mathbf{m}}_j^{ff} = \mathbf{\Psi}_j^T \mathbf{m}_j^{ff} \mathbf{\Psi}_j \tag{2.13a}$$

$$\underline{\mathbf{k}}_j^{ff} = \mathbf{\Psi}_j^T \mathbf{k}_j^{ff} \mathbf{\Psi}_j \tag{2.13b}$$

$$\underline{\mathbf{u}}_j^f = \mathbf{\Psi}_j \mathbf{u}_j^* \tag{2.13c}$$

$$(\underline{\mathbf{Q}}_j^e)_f = \mathbf{\Psi}_j^T (\mathbf{Q}_j^e)_f \tag{2.13d}$$

$$(\underline{\mathbf{Q}}_j^v)_f = \mathbf{\Psi}_j^T (\mathbf{Q}_j^e)_f \tag{2.13e}$$

$$\underline{\mathbf{C}}_{u_j^f}^T = \mathbf{\Psi}_j^T \mathbf{C}_{u_j^f}^T \tag{2.13f}$$

$$\begin{bmatrix} \underline{\mathbf{m}}_j^{Rf} \\ \underline{\mathbf{m}}_j^{\theta f} \end{bmatrix} = \begin{bmatrix} \underline{\mathbf{m}}_j^{Rf} \\ \underline{\mathbf{m}}_j^{\theta f} \end{bmatrix} \mathbf{\Psi}_j \tag{2.13g}$$

Chapter 3

Stochastic models

The probabilistic model is built by replacing all the uncertainty parameters with random parameters, the prior probability distribution PD of the random variable are constructed by using the *Maximum Entropy Principle* (MaxEnt). For the construction of these probability density functions (PDF) we use the same approach used in [6, 7].

3.1 Maximum entropy principle

The Maximum entropy principle was introduced by Jaynes in 1957 [15] and it states that the distribution with maximal information entropy is the best choice, this is it useful to build a consistent PD, because we know that we can not choose arbitrarily the PD, for instance, see [7]. Therefore we want build the PDF $\mathbf{x} \longrightarrow p_{\mathbf{X}}(\mathbf{x}, \mathbf{s})$[1] of a $\mathbb{R}^n$-valued random variable $\mathbf{X}$, it could also be a matrix, on the probability space (Ω, Ξ, Υ) where: Ω is the sample space which is the set of all possible outcomes, Ξ is the set of events and Υ is the assignment of probabilities to the events. The MaxEnt maximize the uncertainties in the model under the constrain defined by the available information. The available information for a random variable with support in $\mathbb{R}^+$.

- Since the support of the random variable is $\mathbb{R}^+$, this implies that the support of the PDF is also $\mathbb{R}^+$.

[1] where s is a hyper-parameter that must be clearly defined.

- We can impose that the nominal model would be the model which would be used if no uncertainties were taken into account, therefore the nominal model is the mean model of the stochastic model, mathematically E{**X**}=$\underline{x}$.

- Available information directly related to the property of random solution, concerning the existence of the second order inverse moment second order moment of the norm of the inverse of the random quantities. Therefore the linearized stochastic dynamical system admits a second order solution, we will assume, as in [6], that this constraint is sufficient to guarantee the existence of a second order solution of the non-linear stochastic dynamical problem. therefore E{$\mathbf{X}^{-2}$}=C.

Where 0<C<+∞, C has no physical meaning so if the variance of the random variable is finite and it will be since we are building the PDF using the MaxEnt, we can replace C with δ that is the coefficient of variation δ_X[2] that is defined as $\delta_{M_i} = \sigma_{M_i}/\underline{m}_i$. The measure of uncertainties of a random variable **X** is defined by the Shannon entropy :

$$S(p_{\mathbf{X}}) = -\int_{\mathbb{R}} p_{\mathbf{X}}(x)\log(p_{\mathbf{X}}(x))\,d\mathbf{X} = -E\{log(p_{\mathbf{X}}(x))\} \tag{3.1}$$

Now it's an optimization problem,i.e. found the PDF contained on the set of the admissible value that maximized the entropy, this was done with the use of Lagrange multipliers, to impose the constraint provided by the available information.

Uniform distribution. We consider a real-valued random variable **X** with nothing else as a constraint than the constraint in the support. Therefore the random variable has value in [a, b]. The Shannon entropy is

$$S(p_{\mathbf{X}}) = log|b-a| \tag{3.2}$$

Therefore:

- if (b-a)=1 , $S(p_{\mathbf{X}})$=0

- if (b-a)=+ ∞ , $S(p_{\mathbf{X}})$= + ∞

[2] $0 \leq \delta \leq 1/\sqrt{2}$

- if (b-a)=0 , $S(p_{\mathbf{X}})$= - ∞

Hence, the MaxEnt is obtained when the Shannon entropy is maximum more the entropy is large more the uncertainty is high and viceversa, the case when the entropy tends to $-\infty$ correspond to the determinist case.

- The support $S_{\mathbf{X}}$=[a , b]
- the MaxEnt yields $p_x = \mathbb{1}_{[a,b]}(x)\ \frac{1}{b-a}$

Where is the indicator function with $\mathbb{1}_{[a,b]}(x)$=1 if x is within the support otherwise $\mathbb{1}_{[a,b]}(x)$=0, therefore we obtain

$$p_{\mathbf{X}}(x) = \begin{cases} \frac{1}{b-a} & \text{for } a \leq x \leq b \\ 0 & \text{for x < a or x > b} \end{cases}$$

That correspond to the uniform distribution, therefore a random value **X** with only a constraint in the support will have a PDF $p_{\mathbf{X}}(x)$ that correspond to the uniform distribution.

Gamma distribution. We now consider a positive real valued random variable **X** with values in] 0, $+\infty$ [and mean value $\underline{x}$ and it is also assumed that $E\{log(X)\} < \infty$. Therefore the constraint are :

- The support $S_{\mathbf{x}}$=]0, $+\infty$[
- E{ **X** }= $\underline{x}$
- $E\{\log(\mathbf{X})\} = C \quad , \quad |C| < \infty$

The maximum entropy principle yields :

$$p_{\mathbf{X}}(x;\delta_x) = \mathbb{1}_{]0,+\infty[}(x)\frac{1}{\underline{x}}\left(\frac{1}{\delta_{\mathbf{X}}^2}\right)^{\delta_{\mathbf{X}}^{-2}}\frac{1}{\Gamma(\delta_{\mathbf{X}}^{-2})}\left(\frac{x}{\underline{x}}\right)^{\delta_{\mathbf{X}}{}^{-2}-1} exp\left(-\frac{x}{\delta_{\mathbf{X}}^2\underline{x}}\right) \tag{3.3}$$

Where C has been replaced with $\delta_{\mathbf{X}}$ through a reparametrization, $\Gamma(\cdot)$ is the gamma function. Therefore the PDF correspond to a Gamma PDF with values in [0, ∞ [.

3.2 Construction of the Probability density functions

3.2.1 PKM Multi Body model PDF

After a preliminary analysis in the MB model seven group of parameters were selected to perform a sensitivity analysis :

1. Mass of the bodies

2. Center of mass of the bodies (COM)

3. Inertia tensor

4. Accelerometers: positions and orientation

5. Signals delay

6. Joint friction

7. Mechanical transformation

Probability density function of the random mass

Starting from physical considerations we know that the mass is a positive constant, therefore the random mass must be a positive value ($M_i > 0$), accordingly the support of the **PDF** $p_{M_i}(\mu)$ must be $\mathbb{R}^+$. The nominal model would be the model which would be used if no uncertainties were taken into account, hence the nominal model is the mean model of the stochastic model [7]. The random mass must verify the inequality $E\{M_i^{-2}\} < +\infty$[3] in order that a second-order solution exists for the stochastic multi-body dynamical system, as in [7]. Then summarizing :

$$M_i > 0 \tag{3.4a}$$

$$E\{M_i\} = \underline{m}_i \tag{3.4b}$$

$$E\{\log(M_i)\} = C_{M_i} \quad , \quad |C_M| < \infty \tag{3.4c}$$

[3]can be proven that this inequality can be replaced with $|\, E\{\log(M_i)\}| < +\infty$

Where $\underline{m}_i$ is the nominal mass. The probability distribution function is written as follow:

$$p_{M_i}(\mu;\delta_{M_i}) = \mathbb{1}_{]0,+\infty[}(\mu)\frac{1}{\underline{m}_i}\left(\frac{1}{\delta^2_{M_i}}\right)^{\delta^{-2}_{M_i}}\frac{1}{\Gamma(\delta^{-2}_{M_i})}\left(\frac{\mu}{\underline{m}_i}\right)^{\delta^{-2}_{M_i}-1} exp\left(-\frac{\mu}{\delta^2_{M_i}\underline{m}_i}\right) \quad (3.5)$$

Where $\Gamma\left(\delta^{-2}_{M_i}\right)$ is the *gamma function* and $\mathbb{1}_{]0,+\infty[}(\mu)$ is the *indicator function* .

Probability density function of the random Signal delay

These parameters simulate propagation delay, that is the amount of time it takes for the head of the signal to travel from the sender to the receiver. For the random signal time delay we apply the same consideration of the random mass, time is also a positive constant such as the mass so the random signal time delay $T_i > 0$, summarizing all the constraints:

$$T_i > 0 \quad (3.6a)$$

$$E\{T_i\} = \underline{t}_i \quad (3.6b)$$

$$E\{\log(T_i)\} = C_{T_i} \quad , \quad |C_T| < \infty \quad (3.6c)$$

As before we combine the *Shannon entropy* definition with the constraints (equation 3.6) to build the PDF $\tau \longrightarrow p_{T_i}(\tau)$, therefore we obtain the following expression of the PDF:

$$p_{T_i}(\tau;\delta_{T_i}) = \mathbb{1}_{]0,+\infty[}(\tau)\frac{1}{\underline{t}_i}\left(\frac{1}{\delta^2_{T_i}}\right)^{\delta^{-2}_{T_i}}\frac{1}{\Gamma(\delta^{-2}_{T_i})}\left(\frac{\tau}{\underline{t}_i}\right)^{\delta^{-2}_{T_i}-1} exp\left(-\frac{\tau}{\delta^2_{T_i}\underline{t}_i}\right) \quad (3.7)$$

Probability density function of the random joint friction parameter

The aim of these parameters is to simulate the friction in the joints, the exact same considerations are applied to these parameters as well as time delay and mass. Hence the random friction is a positive constant with expected value setted to be equal to the corresponding value of the nominal model with finite fluctuations. Summarizing all the constraints:

$$D_i > 0 \quad (3.8a)$$

$$E\{D_i\} = \underline{d}_i \quad (3.8b)$$

$$E\{\log(D_i)\} = C_{D_i} \quad , \quad |C_D| < \infty \quad (3.8c)$$

Using again the *maximum entropy principle* we obtain the PDF $\kappa \longrightarrow p_{D_i}(\kappa)$ we obtain the expression of the PDF:

$$p_{D_i}(\kappa;\delta_{D_i}) = \mathbb{1}_{]0,+\infty[}(\kappa)\frac{1}{\underline{d}_i}\left(\frac{1}{\delta^2_{D_i}}\right)^{\delta^{-2}_{D_i}}\frac{1}{\Gamma(\delta^{-2}_{D_i})}\left(\frac{\kappa}{\underline{d}_i}\right)^{\delta^{-2}_{D_i}-1} exp\left(-\frac{\kappa}{\delta^2_{D_i}\underline{d}_i}\right) \tag{3.9}$$

Probability density function of the random mechanical transformation

The purpose of these parameters is to simulate the mechanical transformation between torque input to ideal motor, and torque applied to modelled joint. The considerations are the same as in the previous cases:

$$F_i > 0 \tag{3.10a}$$

$$E\{F_i\} = \underline{f}_i \tag{3.10b}$$

$$E\{\log(F_i)\} = C_{F_i} \quad , \quad |C_F| < \infty \tag{3.10c}$$

Using again the *maximum principle entropy* we obtain the PDF $\eta \longrightarrow p_{F_i}(\eta)$ we obtain the expression of the PDF:

$$p_{F_i}(\eta;\delta_{F_i}) = \mathbb{1}_{]0,+\infty[}(\eta)\frac{1}{\underline{f}_i}\left(\frac{1}{\delta^2_{F_i}}\right)^{\delta^{-2}_{F_i}}\frac{1}{\Gamma(\delta^{-2}_{F_i})}\left(\frac{\eta}{\underline{f}_i}\right)^{\delta^{-2}_{F_i}-1} exp\left(-\frac{\eta}{\delta^2_{F_i}\underline{f}_i}\right) \tag{3.11}$$

Probability density function of the random centers of mass

These parameters represents the position of the center of mass of the rigid bodies. A continuous uniform distribution was adopted for these parameters, this is due to a constrain imposed in the distribution's support, in this way all the value of the support are equally probable. The support is defined by two parameters **a** and **b** which are the minimum and maximum value that that parameter can take. The PDF is expressed as follow:

$$p_{com}(\nu) = \begin{cases} \frac{1}{b-a} & \text{for } a \le \nu \le b \\ 0 & \text{for } \nu < \text{a or } \nu > \text{b} \end{cases}$$

This distribution is the maximum entropy probability distribution for a random variable with under no constraint other than being contained in the distribution's support.

Probability density function of the random sensors position and orientation

These parameters represent the position and orientation in space of the sensor used in the acquisition of the experimental data. For both cases they have been provided confidence intervals, therefore a maximum and a minimum value that the parameters can assume. This constraint lead us to choose a continuous uniform distribution, the PDF is expressed as follow in both case:

$$p(\theta_j)^4 = \begin{cases} \frac{1}{b_j - a_j} & \text{for } a_j \leq \theta_j \leq b_j \\ 0 & \text{for } \theta_j < a_j \text{ or } \theta_j > b_j \end{cases}$$

Probability density function of the random inertia tensor

For the development of the PDF of the inertia tensor we will refer to [6]. Since the mass distribution around the random center of mass is uncertain, as a consequence, the inertia tensor is also uncertain. The inertia matrix $\mathbf{J}_i$ depends on the mass through the density $\rho(\mathbf{x})$, therefore the random variable M_i and $\mathbf{J}_i$ are not independent. Accordingly we introduce $\mathbf{I}_i = \mathbf{J}_i / m_i$ so that $\mathbf{J}_i$ depends on the normalized distribution of mass $\rho(\mathbf{x})/m_i$ and so $\mathbf{I}_i$ is independent of the total mass and we can construct the probability model of $\tilde{\mathbf{I}}_i$ with respect to $\mathbf{I}_i$. We can now introduce the positive definite matrix $\mathbf{Z}_i$ defined as follow:

$$\mathbf{Z}_i = \frac{1}{m_i} \left\{ \frac{tr\,(\mathbf{J}_i)}{2} [\,I\,] - \mathbf{J}_i \right\} \tag{3.12}$$

where with $[\,I\,]$ we indicate the identity matrix, rewriting the equation 3.12 we obtain:

$$\mathbf{J}_i = \frac{tr\,(\mathbf{J}_i)}{2} [\,I\,] - m_i \mathbf{Z}_i \tag{3.13}$$

Taking the trace of 3.13 and substituting into the equation 3.12 we obtain an explicit form of $\mathbf{J}_i$

$$J_i = m_i \left\{ tr\,(Z_i)\,[\,I\,] - \mathbf{Z}_i \right\} \tag{3.14}$$

We now introduce the random matrix $\tilde{\mathbf{Z}}_i$ and using the equation 3.14 we obtain the following expressions

$$\tilde{\mathbf{Z}}_i = \frac{1}{M_i} \left\{ \frac{tr\,(\tilde{\mathbf{J}}_i)}{2} [\,I\,] - \tilde{\mathbf{J}} \right\} \tag{3.15}$$

[4] the j index indicate the two different PDF

$$\tilde{\mathbf{J}} = M_i \left\{ tr\left(\tilde{\mathbf{Z}}_i\right) [\, I\,] - \tilde{\mathbf{Z}}_i \right\} \tag{3.16}$$

In order to use the *maximum entropy principle* we must collect all the available information about $\tilde{\mathbf{Z}}_i$. Since the matrix $\mathbf{Z}_i$ is positive defined, consequently its stochastic model $\tilde{\mathbf{Z}}_i$ must be a random matrix with values in $\mathbb{M}_3^+(\mathbb{R})$[5]. Indicating with $\underline{\mathbf{Z}}_i$ the nominal value of the deterministic matrix $\mathbf{Z}_i$ such that:

$$\underline{\mathbf{Z}}_i = \frac{1}{m_i} \left\{ \frac{tr(\underline{\mathbf{J}}_i)}{2} [\, I\,] - \underline{\mathbf{J}}_i \right\} \tag{3.17}$$

Due to the construction the mean value of the random matrix $\tilde{\mathbf{Z}}_i$ is equal to $\underline{\mathbf{Z}}_i$. In order to obtain a second-order stochastic solution of the dynamical system we introduce the last constraint that is $|\,\mathrm{E}\{\log(\tilde{\mathbf{Z}}_i)\}| < +\infty$. Summarizing all the constraints:

$$\tilde{\mathbf{Z}} \in \mathbb{M}_3^+(\mathbb{R}) \tag{3.18a}$$

$$E\{\tilde{\mathbf{Z}}_i\} = \underline{\mathbf{Z}}_i \tag{3.18b}$$

$$E\{\log\left(det|\tilde{\mathbf{Z}}_i|\right)\} = C_i^l \quad , \quad |C_i^l| < +\infty \tag{3.18c}$$

We can rewrite $\underline{\mathbf{Z}}_i$ with his Cholesky decomposition

$$\underline{\mathbf{Z}}_i = \underline{\mathbf{L}}_{\mathbf{Z}_i}^T \underline{\mathbf{L}}_{\mathbf{Z}_i} \tag{3.19}$$

Where $\underline{\mathbf{L}}_{\mathbf{Z}_i}$ is a upper triangular matrix, Therefore the random matrix can be rewritten as

$$\tilde{\mathbf{Z}}_i = \underline{L}_{Z_i}^T \tilde{\mathbf{G}}_i \underline{L}_{Z_i} \tag{3.20}$$

the matrix $\tilde{\mathbf{G}}_i$ is the random matrix with the following constraints:

$$\tilde{\mathbf{G}}_i \in \mathbb{M}_3^+(\mathbb{R}) \tag{3.21a}$$

$$E\{\tilde{\mathbf{G}}_i\} = [\, I\,] \tag{3.21b}$$

$$E\{\log\left(det|\tilde{\mathbf{G}}_i|\right)\} = C_i^{l'} \quad , \quad |C_i^{l'}| < +\infty \tag{3.21c}$$

where $C^{l'} = C_i^l - \log\left(det\,[\,\underline{Z}_i\,]\right)$. Hence the *maximum entropy principle* is applied to $\tilde{\mathbf{G}}_i$, hence $\tilde{\mathbf{Z}}_i$ is build from the equation 3.20. Using the constrains in the equation

[5] $\mathbb{M}_3^+(\mathbb{R})$ is the set of all (3 x 3) real symmetric positive-definite matrices

3.21 the PDF $p_{\mathbf{G}_i}(\mathbf{G}_i)$ of the random matrix $\tilde{\mathbf{G}}_i$ with respect to the volume element $\tilde{d}G = 2^{\frac{2}{3}} \prod_{1<j<k<3} dG_{jk}$ is written as

$$p_{\tilde{\mathbf{G}}_i} = \mathbb{1}_{\mathbb{M}_3^+(\mathbb{R})}(G) \times C_{G_i} \times (det|G|)^{-\lambda} \times \mathrm{e}^{-tr[\mu][G]} \tag{3.22}$$

in which the positive valued parameter C_{G_i} is a normalization constant, the real parameter $\lambda < 1$ is a Lagrange multiplier relative to the constraint defined by the equation 3.21c and the positive definite matrix $[\mu]$ is a Lagrange multiplier relative to the constraint 3.21b. The statistical fluctuations of $\tilde{\mathbf{G}}_i$ is controlled by the dispersion parameter δ_{G_i} which must be chosen such that $0 < \delta_{G_i} < \sqrt{1/2}$. This probability density function is a particular case the Kummer-Beta matrix variate distribution, for more detail see [6]. The available information defined in the equation 3.18 and the equation 3.16 allow us to deduce the following properties for the random matrix $[\mathbf{J}_i]$. [6]

$$\frac{1}{2}tr(\tilde{\mathbf{J}}_i)\,[\,I\,] - \tilde{\mathbf{J}}_i \in \mathbb{M}_3^+(\mathbb{R}) \tag{3.23a}$$

$$E\{\tilde{\mathbf{J}}_i\} = \underline{\mathbf{J}}_i \tag{3.23b}$$

$$\lambda < -2 \Rightarrow E\{\|\,[\mathbf{J}_i]^{-1}\,\|^2\} \tag{3.23c}$$

The equation 3.23a implies that the random matrix $\tilde{\mathbf{J}}_i$ is positive definite. The equation 3.23c is necessary for guaranty the existence of a second-order solution of the non-linear stochastic dynamical system.

3.2.2 PKM Flexible Multi Body model

The non-parametric probabilistic model is constructed by replacing the uncertain parameters with random parameters, the prior probability distribution of the random variable are constructed by using the Maximum Entropy Principle, that maximize the uncertainties in the model under the constrain defined by the available information, for a detailed description of the construction of the PDF fo to see [17, 7, 16]. Therefore we replace the deterministic reduced-order of the stiffness $\mathbf{K}_j^*$ matrices with random matrices $\tilde{\mathbf{K}}_j^*$,for the moment we only take into account symmetric positive-defined matrices[7]. The generic random matrix $\tilde{\mathbf{A}}_j^*$

[6] more detail about it in [6]

[7] hence no rigid body modes are considered

can be written as follow:

$$\tilde{\mathbf{A}}_j^* = \mathbf{L}_j \mathbf{G}_j \mathbf{L}_j^T \tag{3.24}$$

Where $\mathbf{L}_j$ is the lower triangular matrix obtained with the Cholesky factorization of the matrix $\mathbf{A}_j^*$ while $\mathbf{G}_j$ is a normalized random matrix where a generator of independent realizations is shown in [6], in which the level of the statistical fluctuations depends on the dispersion parameter δ_A.

$$\delta_A = \left(\frac{E\{\|\mathbf{G}_j - \mathbf{I}\|_F^2\}}{\|\mathbf{I}\|^2} \right)^{\frac{1}{2}} \tag{3.25}$$

Where $E\{\cdot\}$ is the mathematical expectation and $\|\cdot\|_F$ is the Frobenius norm[8]. Therefore we obtain the following expression of the equation of motion of the j-th substructure.

$$\mathbf{M}_j^* \ddot{\mathbf{u}}_j^* + \tilde{\mathbf{D}}_j^* \dot{\mathbf{u}}_j^* + \tilde{\mathbf{K}}_j^* \mathbf{u}_j^* = \mathbf{F}_j^* \tag{3.26}$$

In presence of substructure that have the possibility of rigid body motion therefore not attached to a fixed frame, the stiffness matrix is positive semidefinite therefore the Cholesky factorization can not longer be used, instead we will use the eigen-decomposition. Therefore the generic matrix $\mathbf{A}_j^*$ will can be written as

$$\mathbf{A}_j^* = \mathbf{V}_j \mathbf{\Lambda}_j \mathbf{V}_j^{-1} \tag{3.27}$$

where $\mathbf{V}_j$ is the square (n×n) matrix whose i-th column is the eigenvector $\boldsymbol{v}_i$ of $\mathbf{A}_j^*$ and $\mathbf{\Lambda}_j$ is the diagonal matrix whose diagonal elements are the corresponding eigenvalues. For every real symmetric matrix, the eigenvalues are real and the eigenvectors can be chosen such that they are orthogonal to each other. Thus a real symmetric matrix $\mathbf{A}_j^*$ can be decomposed as

$$\mathbf{A}_j^* = \mathbf{V}_j \mathbf{\Lambda}_j \mathbf{V}_j^T \tag{3.28}$$

Since there are rigid modes, the corresponding eigenvalues will be null, hence we ca write the eigenvalue square matrix as

$$\mathbf{\Lambda}_j = \begin{bmatrix} \mathbf{0} & \mathbf{0} \\ \mathbf{0} & \mathbf{H}_j \end{bmatrix} \tag{3.29}$$

[8] $\|[B]\|_F = \sqrt{tr([B] * [B]^T)}$

$\mathbf{H}_j$ is a diagonal square matrix that contains all the non null eigenvalues, hence we can then decompose it as

$$\mathbf{H}_j = \mathbf{L}_j^T \mathbf{L}_j \tag{3.30}$$

so that we can write the random matrix $\mathbf{H}_j$

$$\tilde{\mathbf{H}}_j = \mathbf{L}_j^T \mathbf{G}_j \mathbf{L}_j \tag{3.31}$$

replacing the deterministic matrix $\mathbf{H}_j$ with the random matrix $\tilde{\mathbf{H}}_j$ we obtain the probabilistic model of the random reduced-order matrix.

$$\tilde{\mathbf{A}}_j^* = \mathbf{V_j} \tilde{\mathbf{\Lambda}}_\mathbf{j} \mathbf{V_j^T} \tag{3.32}$$

Therefore we can finally obtain the same stochastic model as in the Eq.3.26, by replacing the random matrices in the equation of motion of the system[9].

[9] even if $\mathbf{D}_j$ is a positive defined matrix, when we construct the probabilistic model of a flexible body with rigid body modes, we must use the eigen-decomposition approach to remain congruent with what is done with the stiffness matrix

Chapter 4

Sensitivity analysis

Satelli, in [18], define the sensitivity analysis as

> "The study of how uncertainty in the output of a model (numerical or otherwise) can be apportioned to different sources of uncertainty in the model input."

The global sensitivity analysis it is used to identify the group of parameters which once fixed led to the smallest variance of the output, it is usually performed before the model calibrations. The sensitivity analysis is a useful tool because allow us to understand how the uncertainty in the output of a mathematical model can be apportioned to the various source of uncertainty. This process is functional for a various range of purpose, in this case, it was used to increase the understanding of the relationship between input and output, also to found with a Sampling based methods the most sensitive parameters of the model then, only for the MB model, apply a Variance-based sensitivity analysis on the group of parameters previously found in order to quantify the influence on the system output. The sensitivity analysis was performed through the Monte Carlo method which consists to randomly sampling the PDF (see figure 4.1 and figure 4.2) of the parameters of interest to get a series of uncorrelated numbers used as a inputs of the mathematical model of interest, see table below. Therefore, all the system outputs are collected and mean value and relative standard deviation are evaluated, this will help us to qualitative understand which parameters influence the most the output of the system. The Relative standard deviation (**RSD**) is defined as the ratio of the standard deviation and the mean value.

$$RSD_i = \frac{\sigma_i}{|\mu_i|} * 100 \tag{4.1}$$

It shows the extent of variability in relation to the mean, The **RSD** tells you whether the regular standard deviation is small or large when compared to the mean for the data set. For an appropriate execution of the Monte Carlo method,

Algorithm 1 Monte Carlo method

initialization	▷ loading the data
$\mathbf{X}_i = 1, \ldots\ldots, n_p;$	▷ Generate all n_p random variable n_t times
parfor $j = 1, \ldots\ldots, n_t$	▷ where n_t is the number of realization
run the mathematical model;	▷ using as input the j-th random sampling
end	

the mean value of the realization must converge to the true value, this usually requires lots of realization it follows a not negligible computational cost. The computational cost is not only due to the number of realization but it depends also to the complexity of the mathematical model, in fact, the FMB model requires much more time for single realization than the MB model. Another aspect that contributes to increasing the computational cost is a large number of parameter that in a MB model can be considered uncertain not only due to the multiple individual structures but also due to the fact that the MBS is often multidisciplinary, so different dynamics are combined. Not counting the mechanical part of rigid and flexible bodies, there are also actuators and controllers or other mathematical law may be present in the model. There are some procedure to try to reduce the computational cost such as more efficient way of sampling techniques or reducing the number of uncertain parameters that of course cannot be known *a priori* because as already mentioned the equation of motion is non linear, so with a change of configuration of the system or with the simple evolving of the system in time the influence of the parameters can variate over time. A time savings approach is to parallelize the realizations this is the approach that we used to perform the sensitivity analysis in both models.

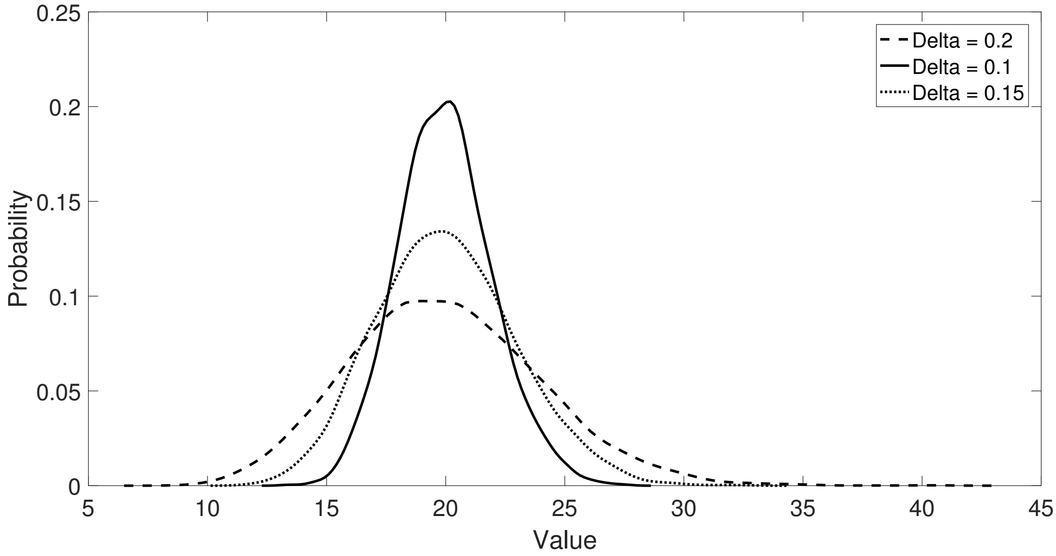

Figure 4.1: Gamma probability density function

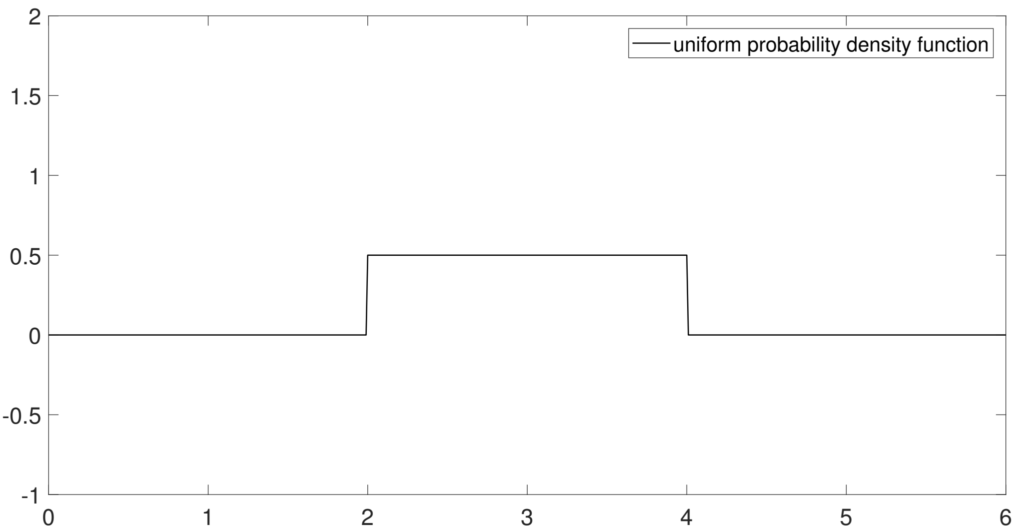

Figure 4.2: uniform probability density function

4.1 PKM MTC model

The first MB model of the Exechon PKM provided by the MTC has shown that the frequency response of the MB model was not in agreement with the experimental data, as shown in the figure 4.3 and figure 4.4.

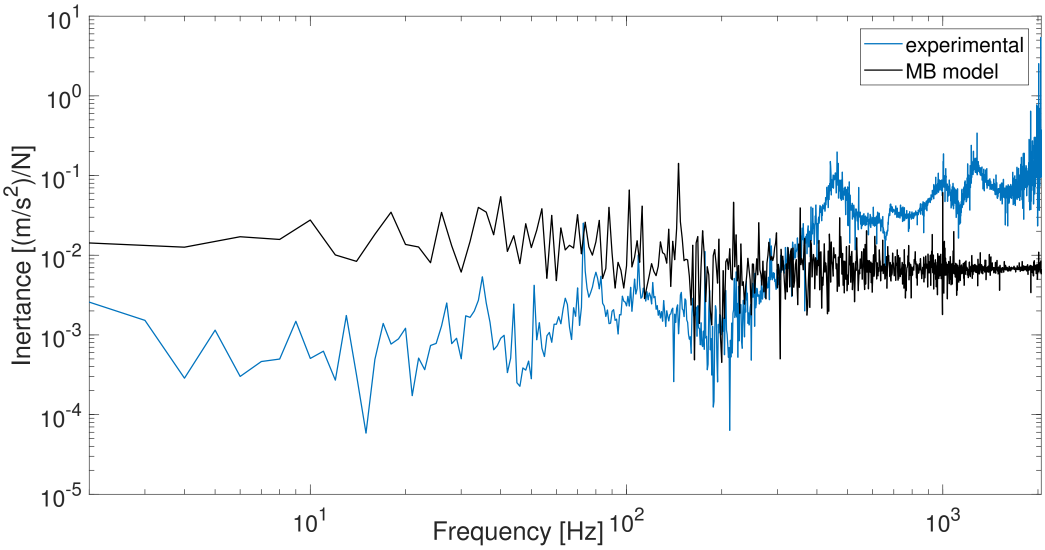

Figure 4.3: frequency response of the first MB model **sensor 1**

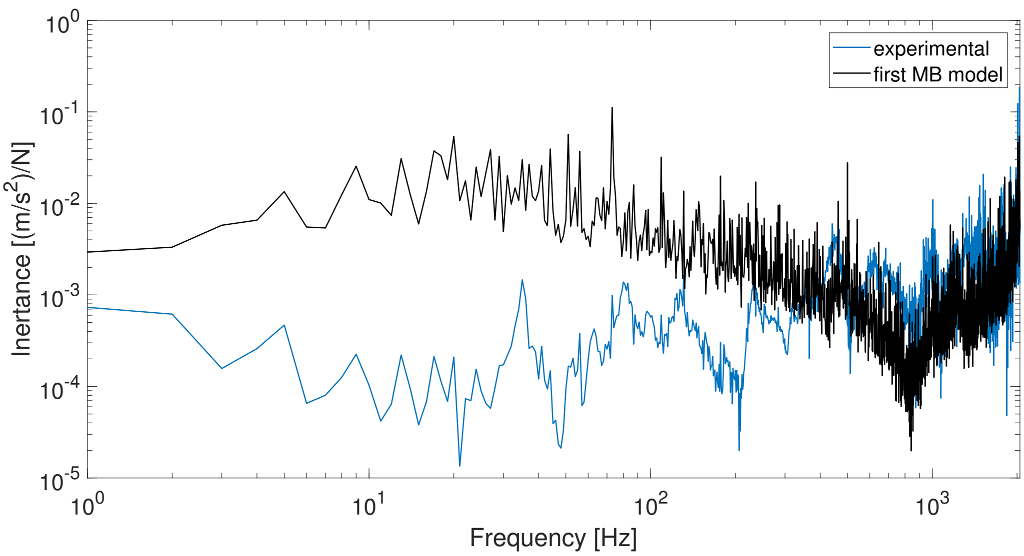

Figure 4.4: frequency response of the first MB model **sensor 3**

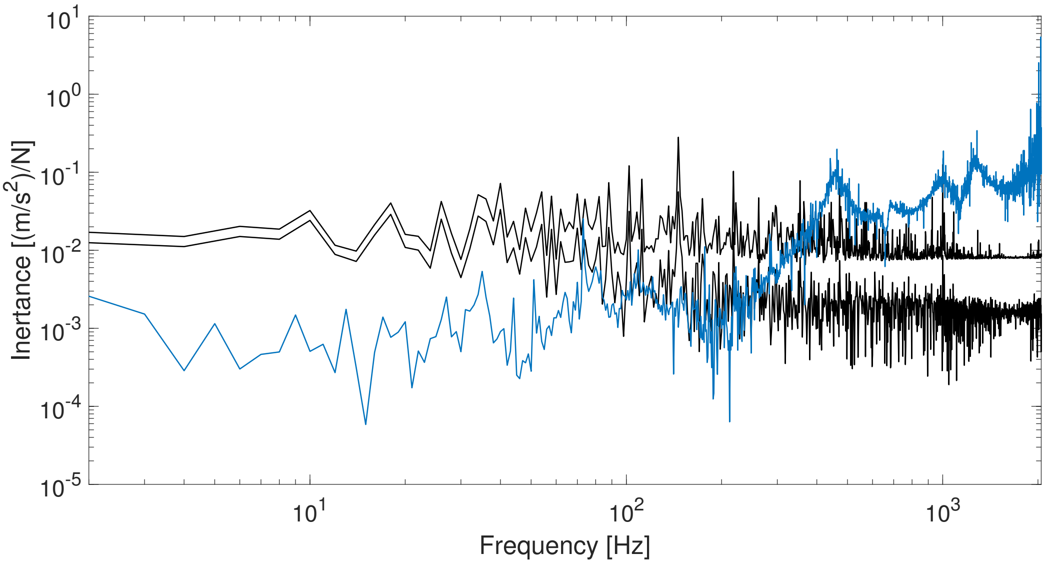

Figure 4.5: -**Black lines** - confidence region of the MBS -**blue line**- Experimental response **sensor 1**

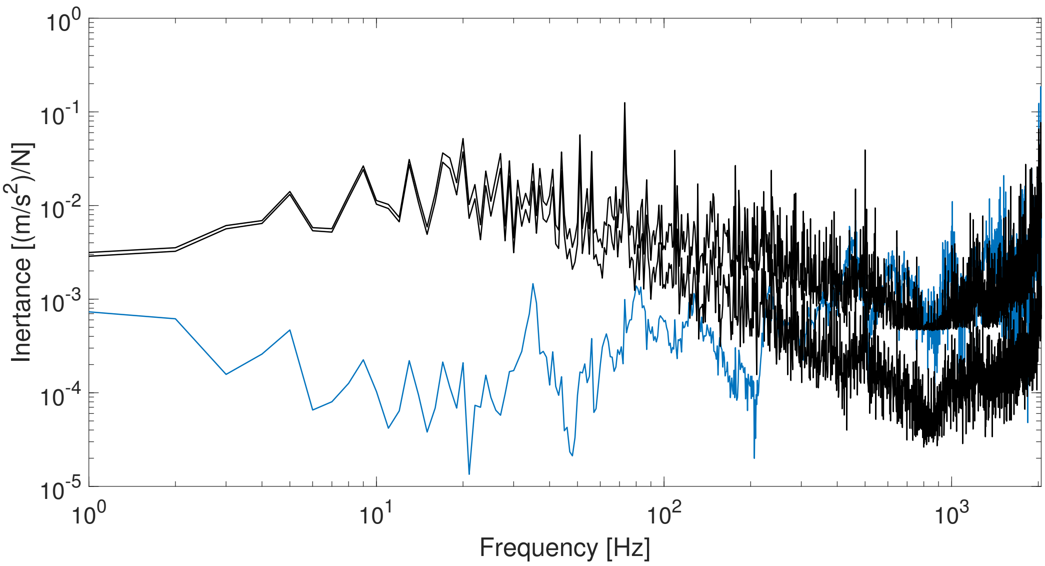

Figure 4.6: -**Black lines** - confidence region of the MBS -**blue line**- Experimental response **sensor 3**

After the first sensitivity analysis which produced poorly result, as we can see in figure 4.5 and figure 4.6. In front of these results updates have been made to the MB model, in particular they were focused on the control system architecture and on the joint stiffness. The previous control architecture was based on referential information about the actual control system, which includes two PI feedback loops, one for position and other for speed , figure 4.7. The parameters

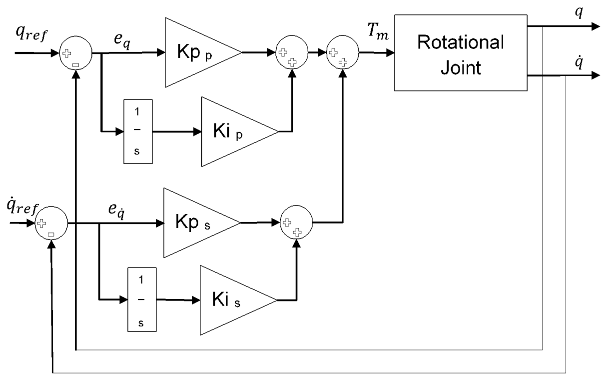

Figure 4.7: Previous control architecture

of these controllers were estimated from the time domain experiment, therefore if the configuration of the machine changed, the parameters of the controllers has to be reevaluated. This representation also neglect the effect of the filters from the true control architecture as well as considering the motor dynamic ideal, it is clear why these representation of the controller architecture was inadequate. The new architecture was obtained from the machine control system provider this architecture was implemented into the PKM dynamics model, with some simplifications. The other change to the model was to remove the joint compliance that was implemented in the previous model that is not appropriate to define the physical phenomena around the joint, instead the Joint damping model is still being considered as a representation of the joints friction, i.e. resisting relative motion of solid surfaces. It is proportional to the relative speed between the bodies the joint relates. These changes lead to a new FRF of the MB model shown in figure 4.9 and figure 4.10. It is clear, however, that even with this update the MB model is not yet in completely agreement with the experimental data, all the images of the first sensitivity analysis can be found in the appendix A.

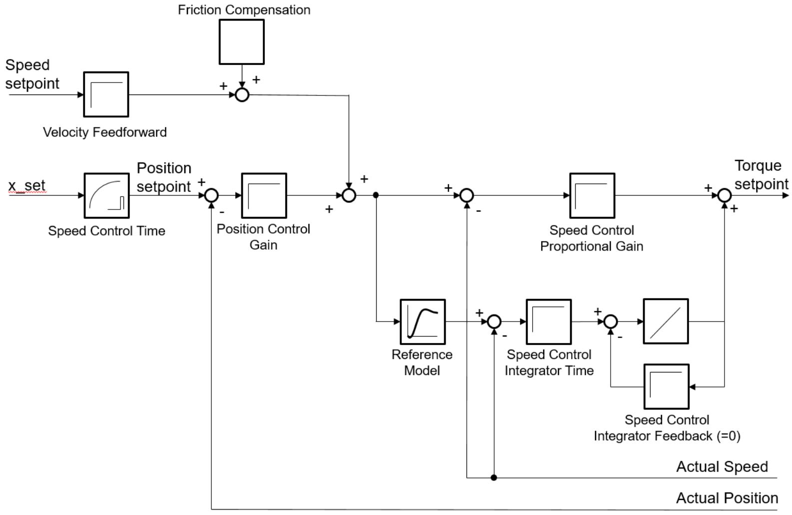

Figure 4.8: New control architecture

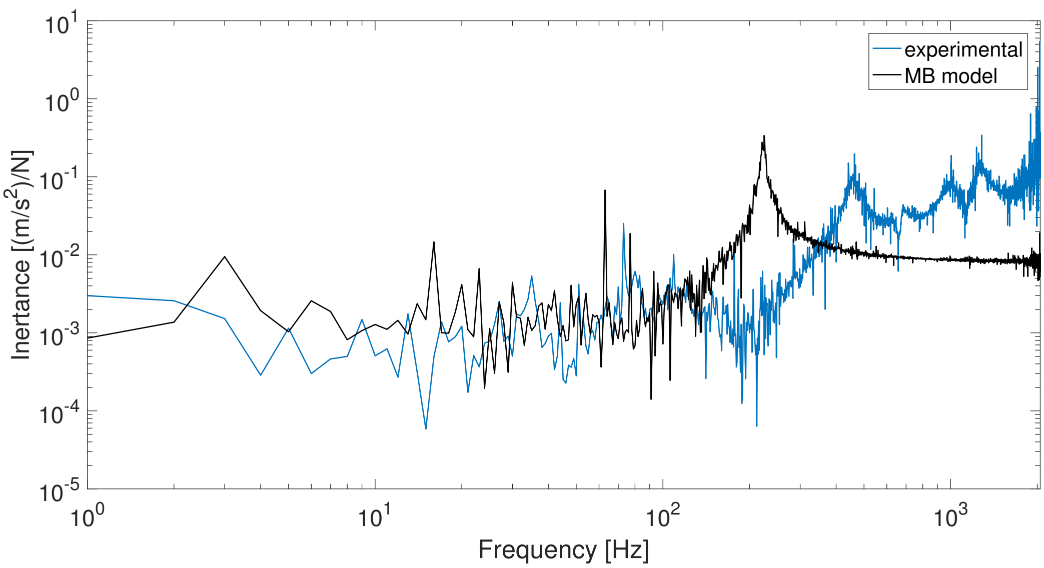

Figure 4.9: New model Frequency response **sensor 1**

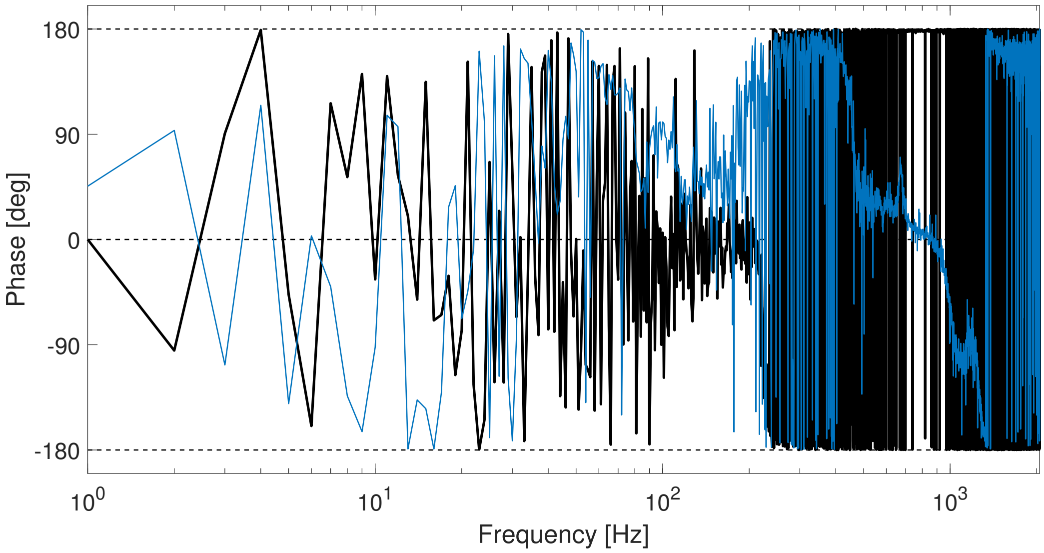

Figure 4.10: New model phase diagram **sensor 1**

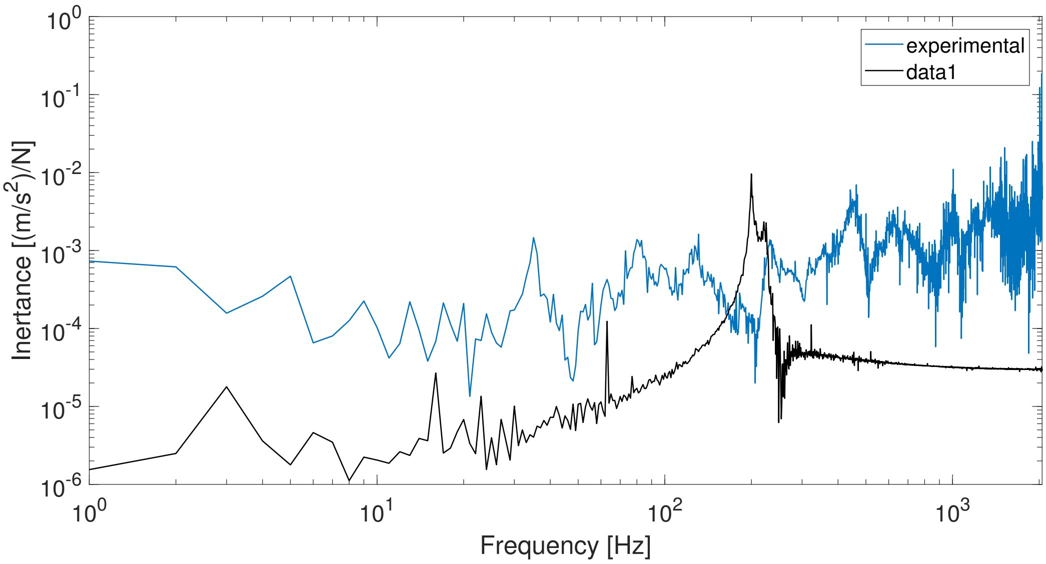

Figure 4.11: New model Frequency response **sensor 3**

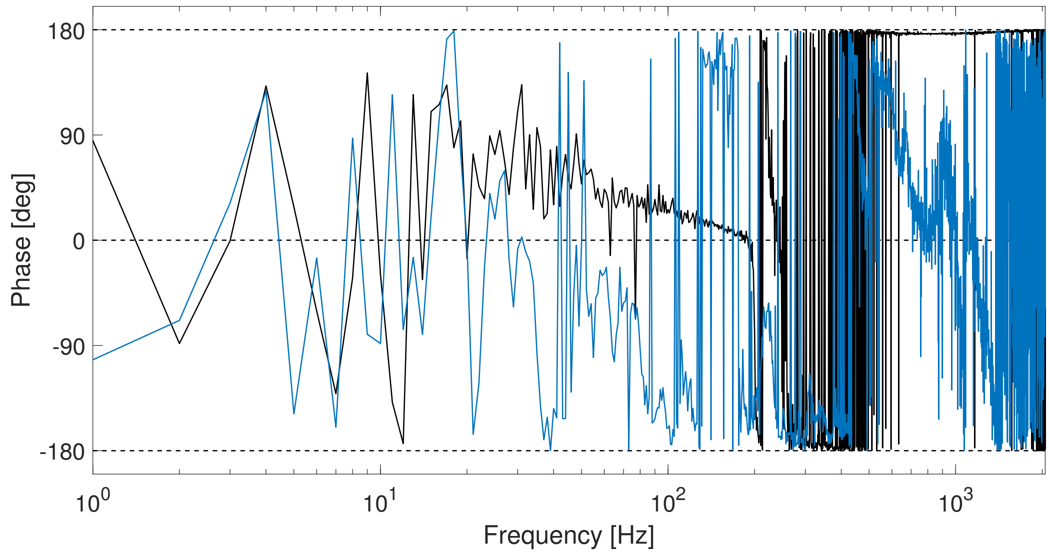

Figure 4.12: New model phase diagram **sensor 3**

4.1.1 sensitivity analysis results

The sensitivity analysis has been organized with seven different Monte Carlo Simulation, one for each group of parameters. This choice to treat group of parameters instead the single parameters is due to the high number of parameters to analyze, table 4.1. The statistics for the response of the system have been es-

Group of parameters	**number of parameters for group**
Mechanical transformation (from CtrlParams)	5
Signal time delay	5
Inertial data (mass , center of mass, inertia tensor)	39
Joint friction parameters	14
Sensor positions and orientation	2
TOTAL	65

Table 4.1: Group of parameters under study

timated using the Monte Carlo simulation method with 200 independent realizations for each different case. Once all the responses of the system has been computed, the output data were ordered with respect to the amplitude at each time step, then starting from the mean of the sorted[1] data we selected the confident region with a probability P_c[2], meanwhile the RSD figure can be found in the appendix C.

Case 1 In this case all the 13 centers of mass (COM) are random instead the other group of parameters are deterministic. With reference to what has been said in the sub-section 3.2.1,

$$\begin{cases} a_i = \underline{COM}_i - 10 \\ b_i = \underline{COM}_i + 10 \end{cases}$$

Where $\underline{COM}_i$ it is the mean value of the COM position of the i-th body, the value of $\pm$ 10 expressed in [mm] is provided by the MTC. We can see in the Figure 4.13 how these parameters affects widely the response of the system, but these parameters do not explain the difference on the resonance peak.

Case 2 In this case the 13 tensor of inertia are the random instead the other parameter are all deterministic. We have chosen a preliminary value for the dispersion parameter $\delta_J = 0.2$. We can see in the Figure 4.14 how these parameters affects the response of the system.

Case 3 In this case the masses of the rigid bodies are the random parameters and the other are all deterministic. For these parameters we have chosen a value for the dispersion parameter $\delta_M = 0.2$. We can see in the Figure 4.15 how these parameters affects the response of the system.

[1]this is usually different from the response of the nominal model

[2]for all cases it was used $P_c = 80\%$

Case 4 In this case the sensors position and orientation are random the other parameters are deterministic, as done previously we define the

$$\begin{cases} a_j^{pos} = \underline{S_{pos}}_j - 10 \\ b_j^{pos} = \underline{S_{pos}}_j + 10 \\ a_j^{or} = \underline{S_{or}}_j - 10^\circ \\ b_j^{or} = \underline{S_{or}}_j + 10^\circ \end{cases}$$

Where $\underline{S_{pos}}_j$ it is the mean value of the j-th sensor position and $\underline{S_{or}}_j$ is the mean value of the j-th sensor orientation, the value $\pm$ 10 is expressed in [mm] instead the valeu $\pm 10^\circ$ is expressed in [Deg] . We can see in the Figure 4.16 how these parameters affects the response of the system.

Case 5 In this case the mechanical transformation parameters are setted to be random and the other are all deterministic. For these parameters we have chosen a value for the dispersion parameter $\delta_F = 0.2$. We can see in the Figure 4.17 how these parameters affects the response of the system, It can be seen that the fluctuations of the response decrease with frequency since the spatial wave lengths decrease with frequency.

Case 6 In this case the time delay signal parameters are setted to be random and the other are all deterministic. For these parameters we have chosen a value for the dispersion parameter $\delta_T = 0.2$. We can see in the Figure 4.18 how these parameters affects the response of the system.

Case 7 In this case the joint friction parameters are setted to be random and the other are all deterministic. For these parameters we have chosen a value for the dispersion parameter $\delta_D = 0.2$. We can see in the Figure 4.19 how these parameters affects the response of the system.

Case 8 In this last case all the parameters are setted to be random, with the same values used for the individual cases. We can see in the Figure 4.20 all these parameters affects the response of the system.

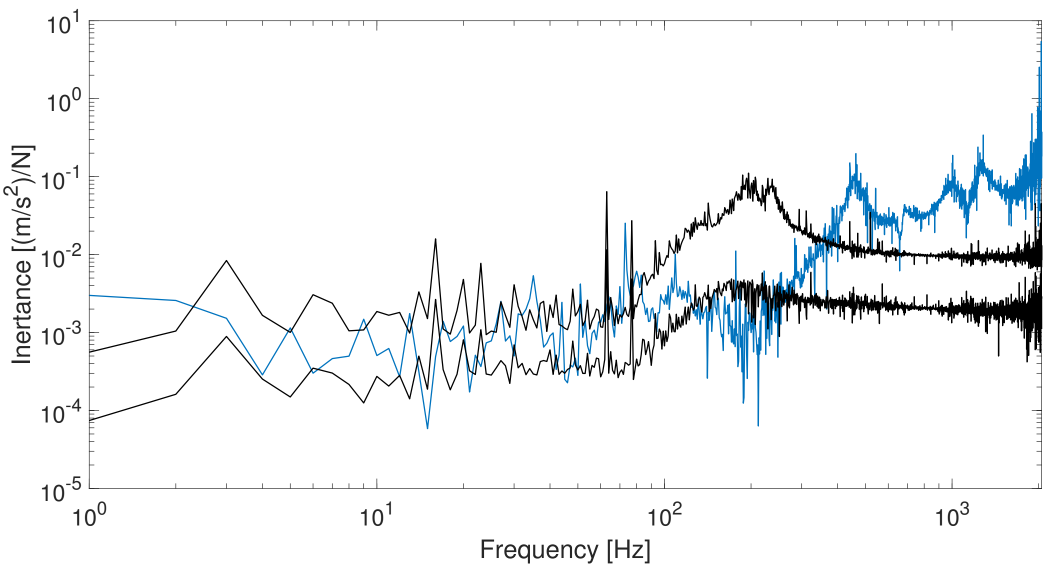

Figure 4.13: **CASE 1** - the **black** lines indicate the confidence region of the MB model- the **blue** indicate the experimental response **sesor 1**

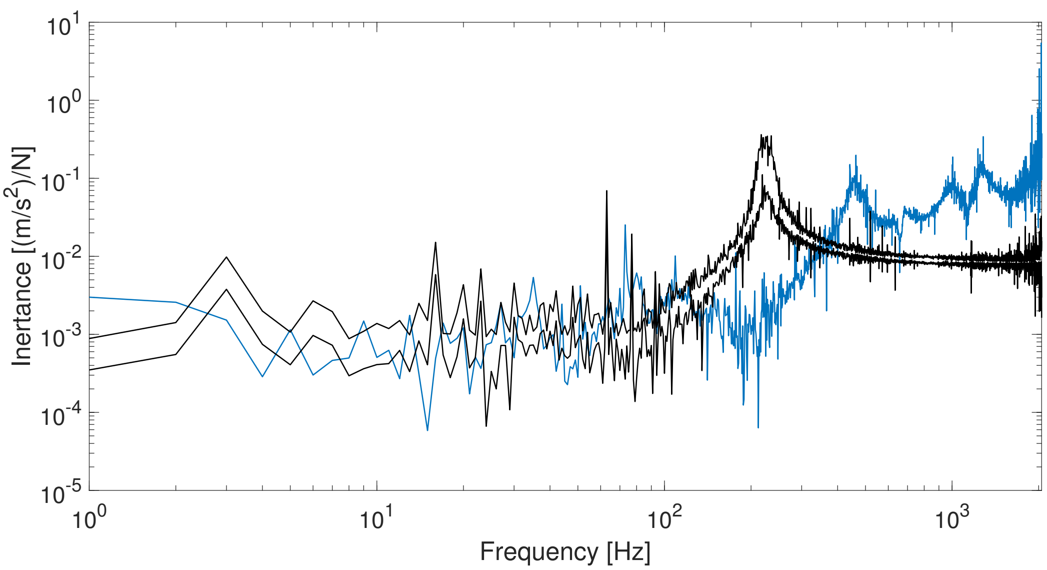

Figure 4.14: **CASE 2** - the **black** lines indicate the confidence region of the MB model- the **blue** indicate the experimental response **sesor 1**

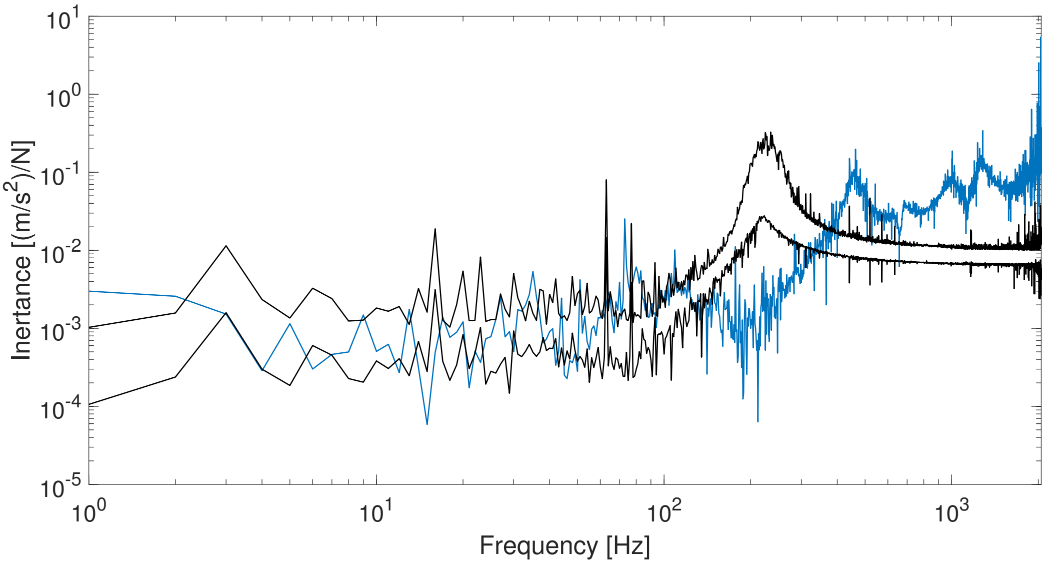

Figure 4.15: **CASE 3** - the **black** lines indicate the confidence region of the MB model- the **blue** indicate the experimental response **sesor 1**

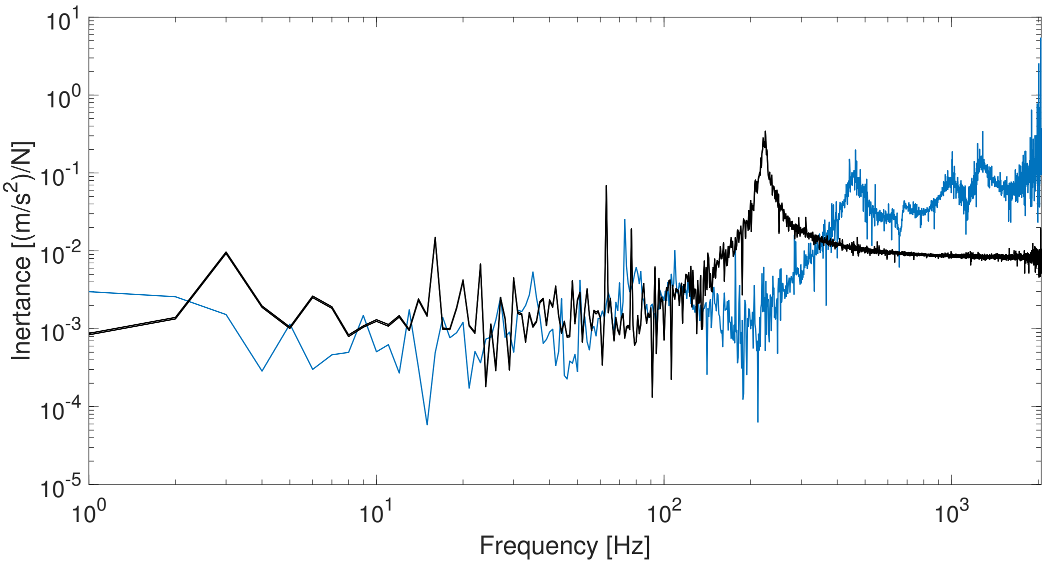

Figure 4.16: **CASE 4** - the **black** lines indicate the confidence region of the MB model- the **blue** indicate the experimental response **sesor 1**

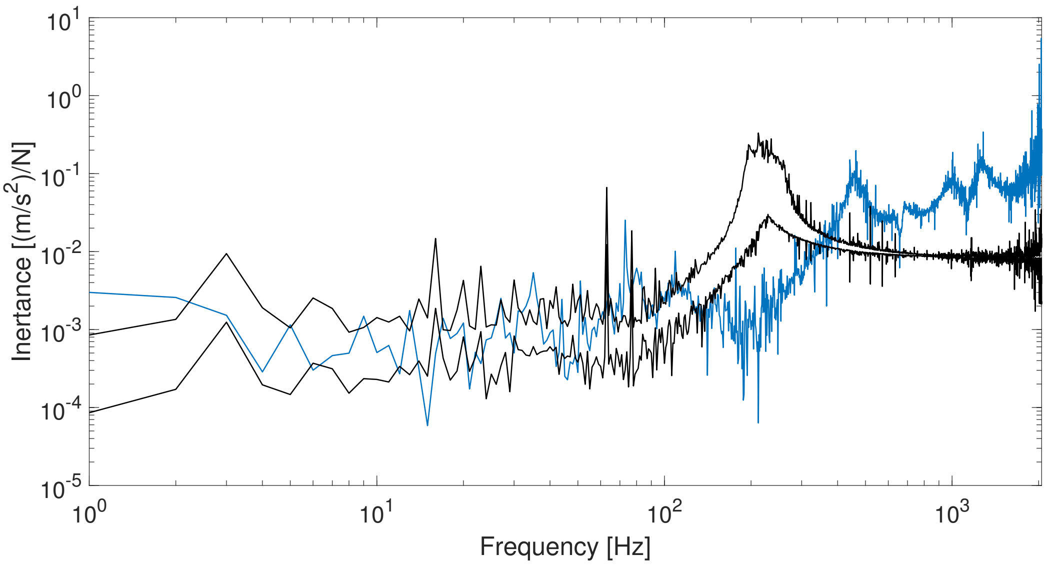

Figure 4.17: **CASE 5** - the **black** lines indicate the confidence region of the MB model- the **blue** indicate the experimental response **sesor 1**

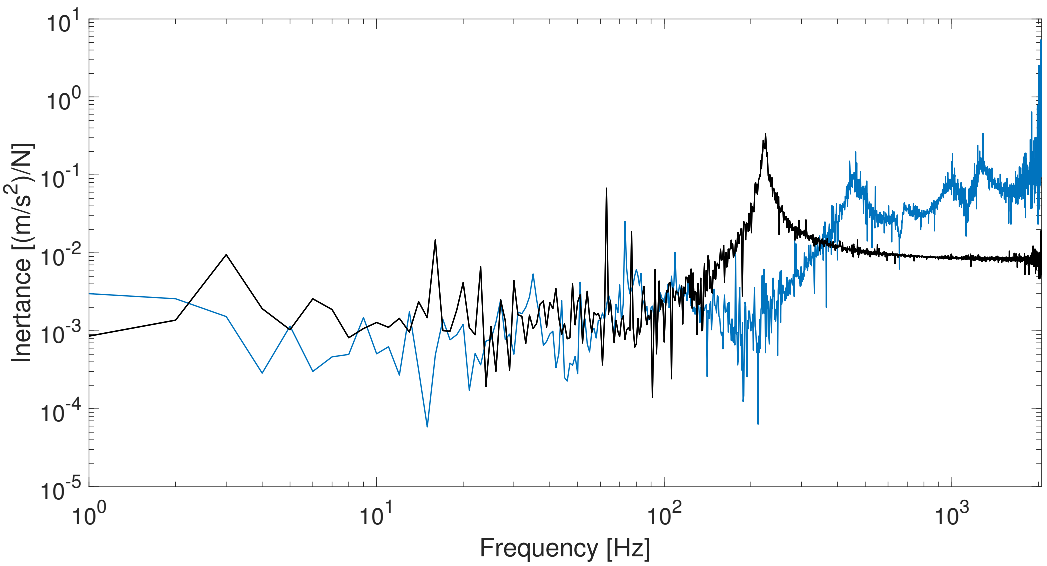

Figure 4.18: **CASE 6** - the **black** lines indicate the confidence region of the MB model- the **blue** indicate the experimental response **sesor 1**

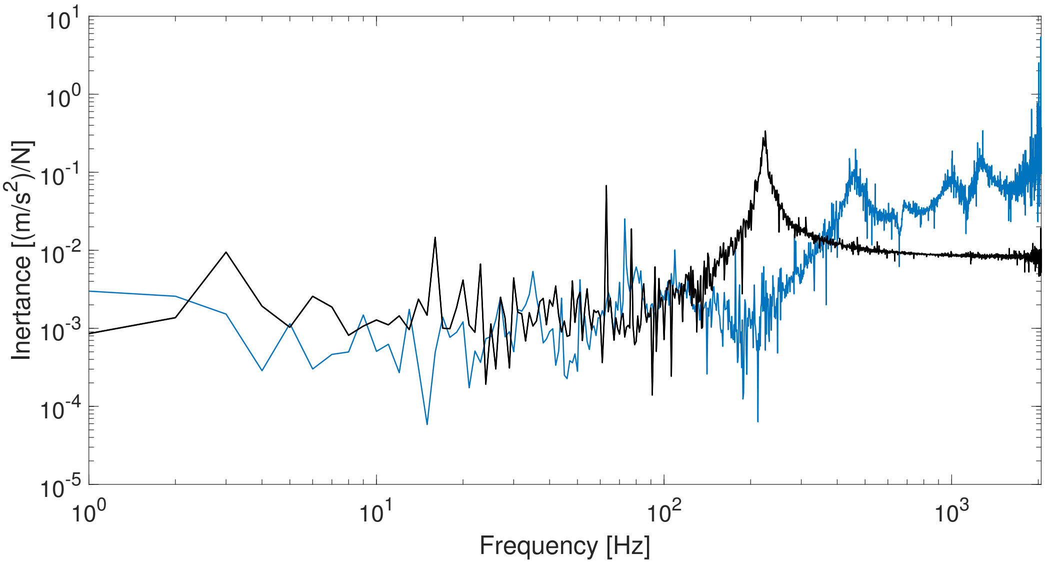

Figure 4.19: **CASE 7** - the **black** lines indicate the confidence region of the MB model- the **blue** indicate the experimental response **sesor 1**

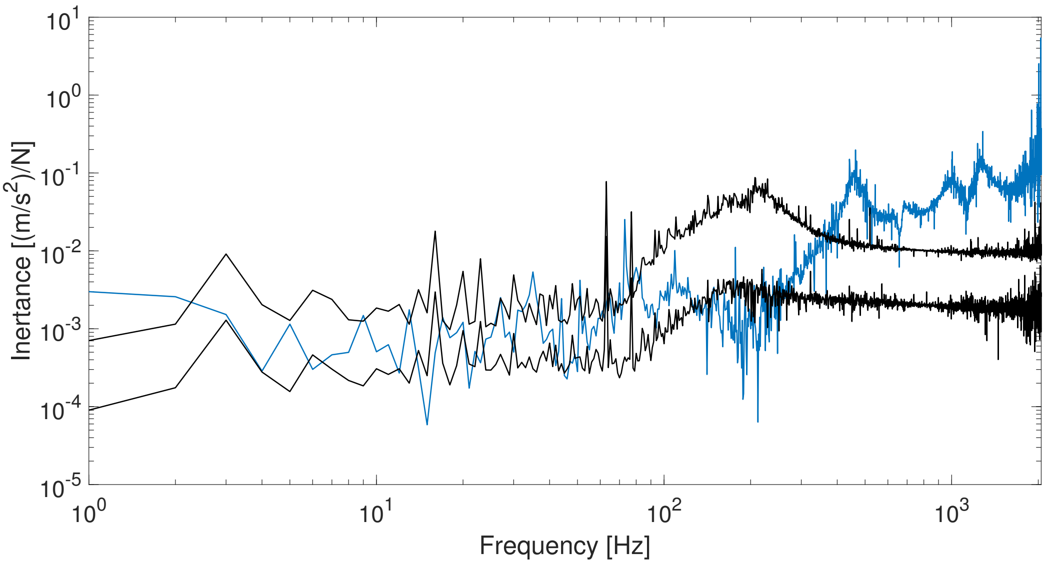

Figure 4.20: **CASE 8** - the **black** lines indicate the confidence region of the MB model- the **blue** indicate the experimental response **sesor 1**

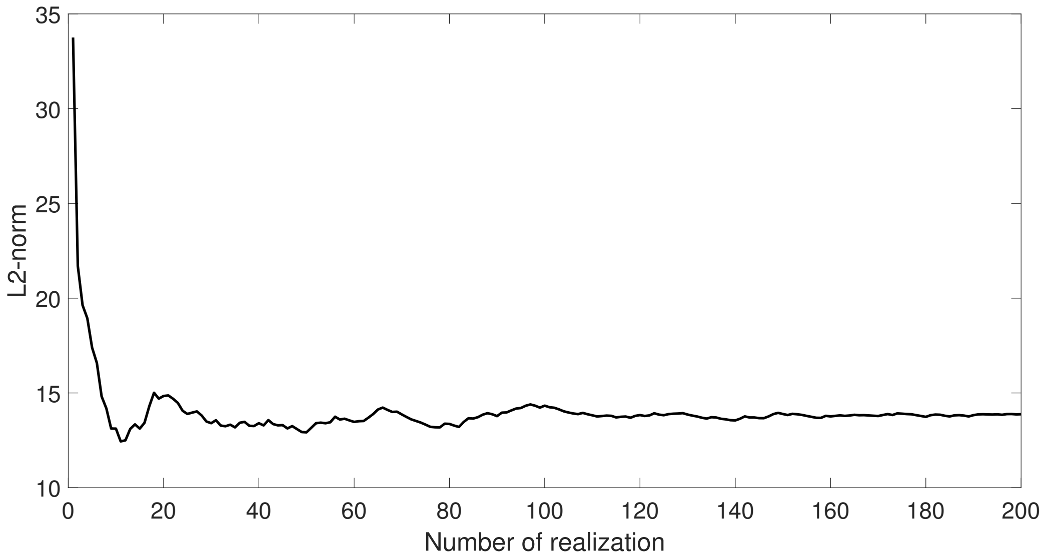

Figure 4.21: convergence of the mean value with respect to the number of Monte Carlo simulations

4.1.2 Summary of the preliminary sensitivity analysis

As shown in the figures in the previous section the most sensitive parameters are:

1. center of mass position
2. Tensor of inertia
3. Mass of the bodies
4. mechanical transformation parameters

The remaining parameters can be neglected in this configuration of the machine. In the figure 4.21 we can see the convergence of the mean value with respect to the number of Monte Carlo simulations, for sick of simplicity we only put here the sensitivity analysis of the **sensor 1** the result of the **sensor 3** can be found in Appendix B. Each simulation lasted roughly 1 minutes so the but even with such a low simulation time, the times to carry out a sensitivity analysis with only one core are relatively high, in fact since there was 200 realization for 8 different cases the computational cost with only one core was about 26.5 hours the process was parallelized with 32 cores and lasted only one hour, a summary of the simulation times can be seen in the table 4.2.

number of simulations	Time (1 core)	Time (32 core)
1	1 min	1 min
200	200 min	7 min
1600	1600 min	50 min

Table 4.2: Computational cost comparison MB model

Usually, after a preliminary analysis that helps us to identify the most sensitive parameters, we should perform a calibration of the probability distribution parameters, such as the δ dispersion parameter, using the experimental data through an inverse problem, or construct a predictive probabilistic model and analysis of the variability of its outputs but until the MB model is not enough in agreement with the dynamic behavior of the machine, this procedure can not be performed.

4.1.3 Variance based sensitivity analysis

Once the most influential parameters have been identified through a qualitative sensitivity analysis we can now quantify the influence of these four parameters as the frequency changes. It was used a variance-based sensitivity analysis [19], often referred as Sobol method or Sobol indices, that is a form of a global sensitivity analysis. This method basically decompose the variance of the output of the model in fraction that can be attributed to the groups of parameters, hence the sensitivity of the output to an input variable is evaluated by the variance in the output caused by that input. This method it is useful because it can dealt with non linearity. We can evaluate the total effect index through the following formula, [19].

$$S_{Tik} = \frac{E_{\mathbf{X}_{\sim i}}\left(\mathrm{Var}_{X_i}(Y \mid \mathbf{X}_{\sim i})\right)}{\mathrm{Var}(Y)} \tag{4.2}$$

where Y is the output, **X** is the vector of the uncertain parameters, k indicate the frequency to which the index is referred and i the group of parameters. In this case since we are measuring the output variance considering also the variance caused by the interaction with the other parameters

$$\sum_{i=1}^{d} S_{Tik} \geq 1 \tag{4.3}$$

The indices can be evaluated analytically, most of the time as in this case, they are estimated with the Monte Carlo method through the following formula:

$$E_{\mathbf{X}_{\sim i}}\left(\mathrm{Var}_{X_i}\left(Y \mid \mathbf{X}_{\sim i}\right)\right) \approx \frac{1}{2N}\sum_{j=1}^{N}\left(f\left(\mathbf{A}\right)_j - f\left(\mathbf{A}_B^i\right)_j\right)^2 \tag{4.4}$$

The procedure is articulate as follow:

1. We generate two (A and B) independent set of random parameters sampled with the PDF that we built with the maximum entropy principle

2. with the first group A of parameters we generate the first N simulations

3. then we will switch a group of B of random parameters into A and we will generate other N simulation, and we will repeat this procedure to change a group of parameters at a time until they have all been changed.

4. then using the formula 4.4 in the formula 4.2 we are able to evaluate for each group of parameters at each frequency the Sobol indices.

This sensitivity analysis requires lots of simulation in order to have an appropriate convergence, therefore the preliminary sensitivity analysis result were used to understand on which parameters we had to focus, in order to avoid long simulation on useless parameters. We found that the most influential parameters are:

- Mass
- Control parameter
- Center of mass
- Tensor of inertia

In this case for each group we lunched one-thousand of simulation, therefore since the group are four we had to lunch five-thousand of simulation. We used the same dispersion parameters of the previous analysis. Summarized in the table 4.3 we can see the number of simulations and the computational time necessary to evaluate the indices.

number of simulations	Time (1 core)	Time (72 core)
1	1 min	1 min
1000	1000 min	14 min
5000	5000 min	70 min

Table 4.3: Computational cost to evaluate the Sobol indices

The results of this analysis are shown in the figure 4.22 and figure 4.23, the graphs show the trend of the index referred to the frequency. The influence of the groups of parameters for both sensor is similar, as we can see the most important group of parameters are the position of the center of mass of the bodies. The very similar trend of all the index may be due to the fact that we are measuring the contribution to the output variance including all the variance caused by the interaction between the other parameters. In figure 4.24 we can see a convergence of one of the index.

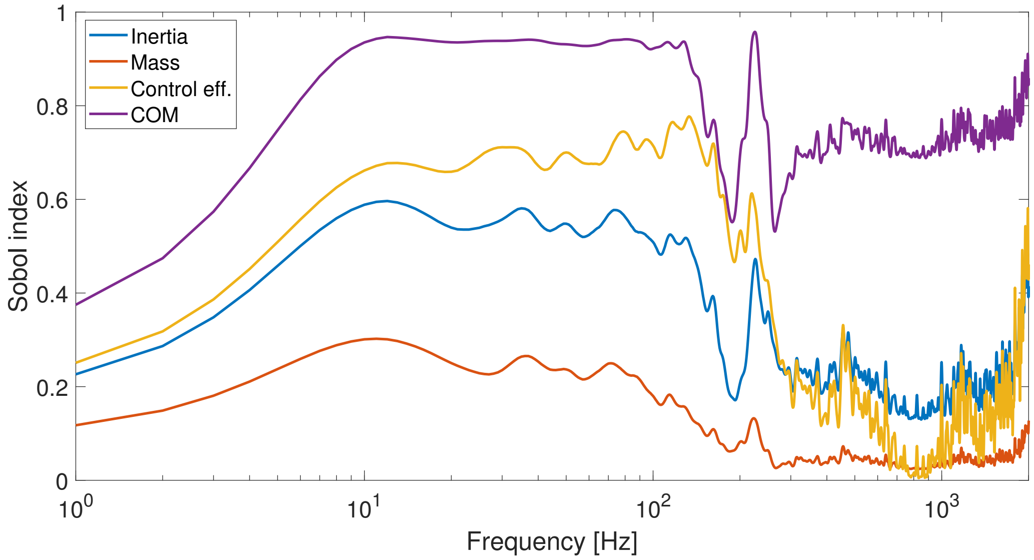

Figure 4.22: Sobol index for the sensor 1

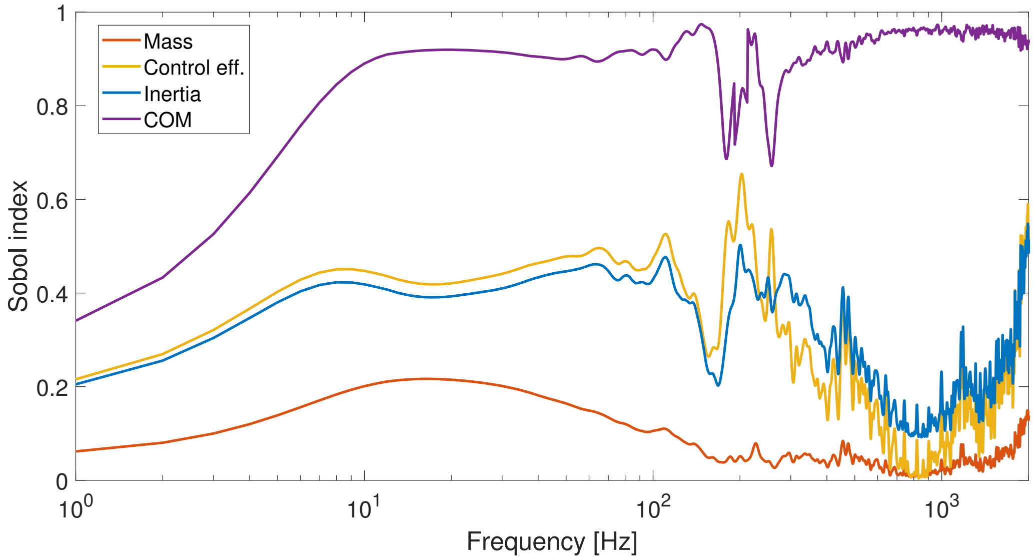

Figure 4.23: Sobol index for the sensor 3

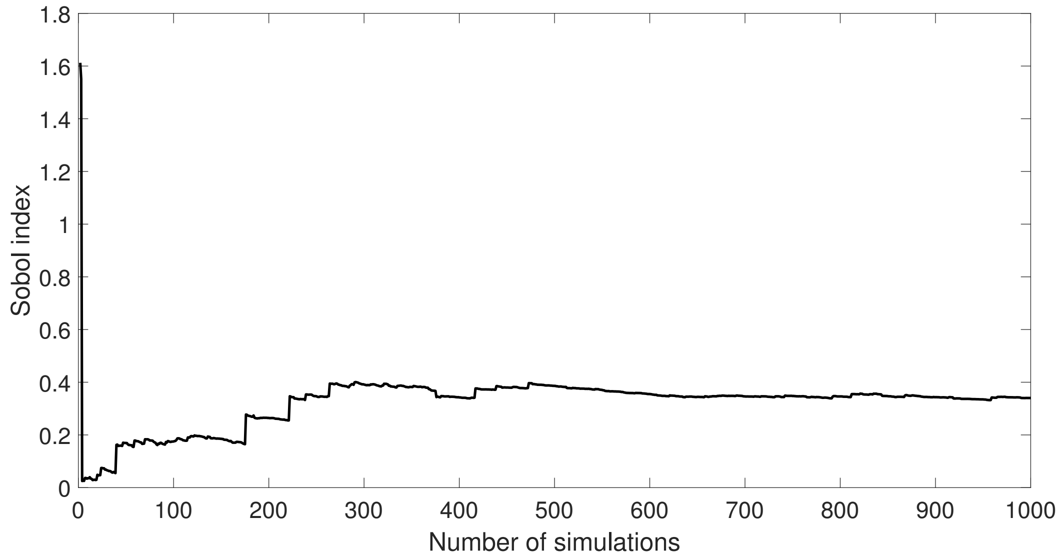

Figure 4.24: Convergence Sobol index, sensor 1 2000 Hz Mass

4.1.4 MB model comment

As we can see from the frequency response of the new model figure 4.9 and figure 4.11, the update model is not still in complete agreement with experimental results and we have done some investigation about it. Looking at the frequency response, figure 4.25, of the MB model we can see a peak of the MB model at 225 Hz show the same slope as the first peak of experimental data at 463.1 Hz. Instead of a random excitation to better understand which components is due this peak, we excited the system with an harmonic excitation with frequency ω=225 Hz. Visually and also through the use of sensors in SimMechanics, we have noticed that the base tool, figure 4.26 started oscillating along his revolution axis. As already mentioned the PKM has 5 active controllers, in our sensibility analysis we didn't take into account all the machine parameters such as the proportional, derivative and integrative gain of the controllers. From the theory we know that the active controllers influence the dynamic response of a system, ans also affect the free behaviour as well as the forced behaviour [14]. Since the system has no stiffness in the joint all the stiffness is provided by the controllers. In the MB scheme of the PKM the sensor and actuator are co-located, from the theory we know that for these simplified controllers:

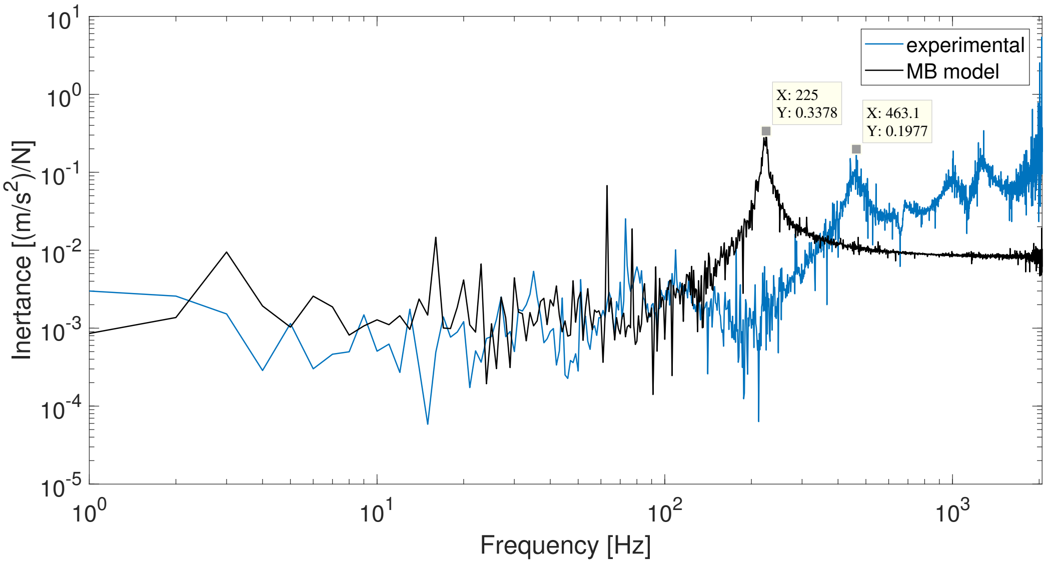

Figure 4.25: comparison of resonance peaks

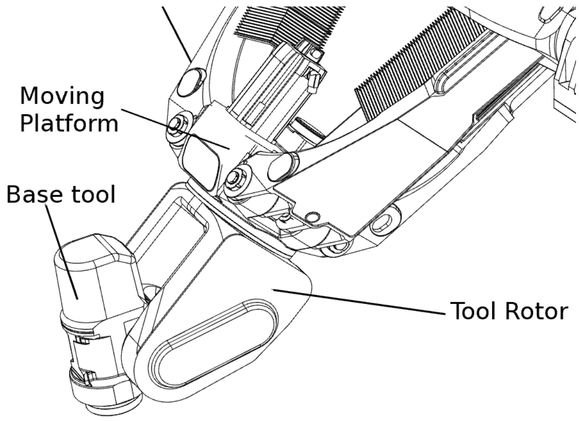

Figure 4.26: Base tool

- the proportional part of the controllers act like a restoring force similar to a stiffness.
- the derivative part is similar of the action of damping
- the integrative part introduce a behaviour different from that obtainable for non controlled system.

we have at least two ways to tune the peak of the MB model in the experimental response that is or increase the proportional gain of the machine or decrease the mass. As we can see from the figure 4.27 - 4.30 both solutions seem to

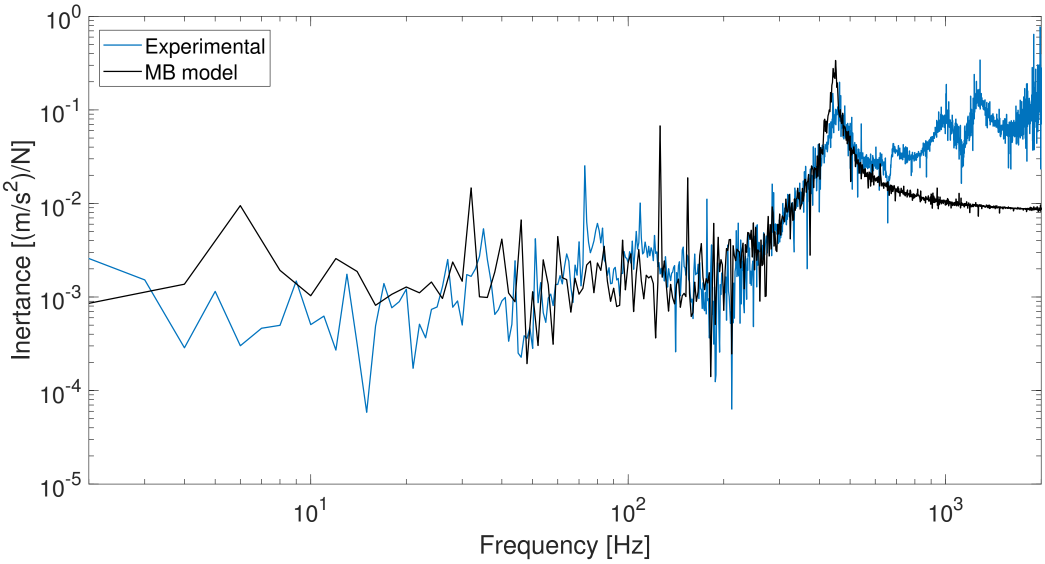

Figure 4.27: New frequency response by changing the proportional gain **sensor 1**

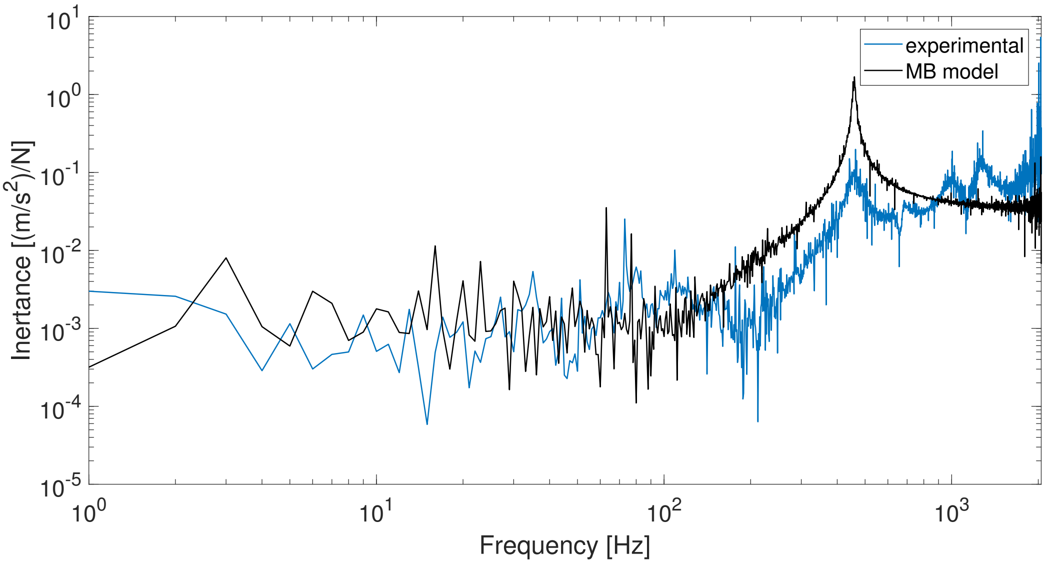

Figure 4.28: New frequency response by changing the inertial property **sensor 1**

represent the peak in the frequency response obtained with the acceleration data from the sensor 1, the solution obtained increasing the proportional gain seem to follow better the trend of the experimental frequency response because it covers the curve also following the same slope. In the frequency response of the system, obtained from the acceleration data from the sensor 3, we see that with respect to the first frequency response the appearance of another peak that roughly together

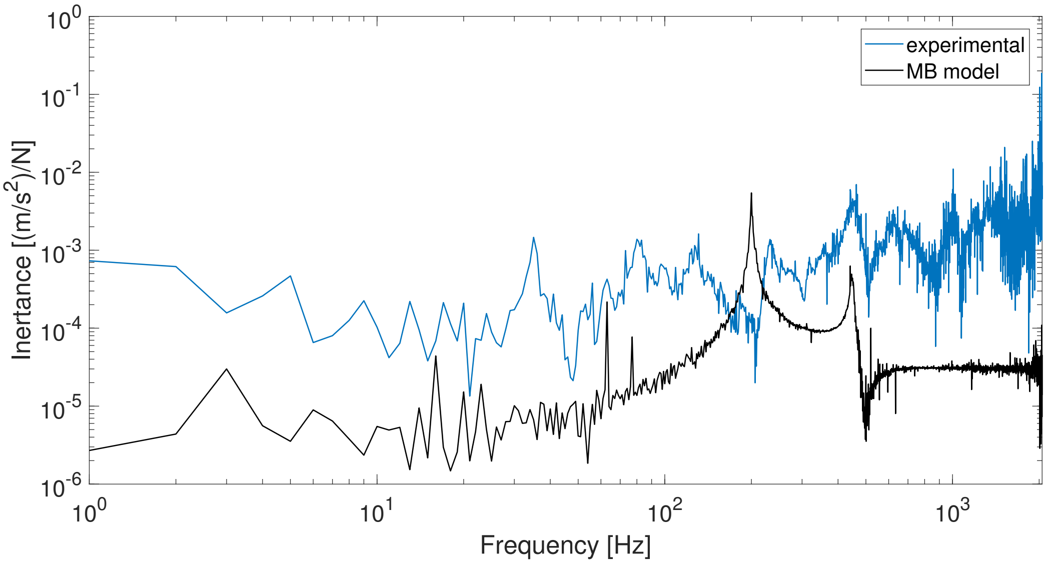

Figure 4.29: New frequency response by changing the proportional gain **sensor 3**

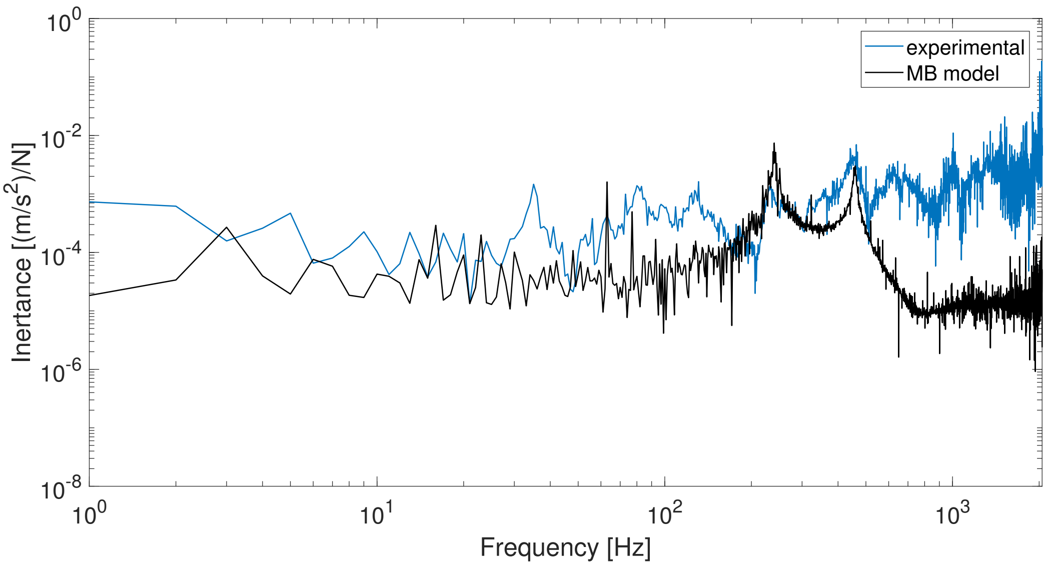

Figure 4.30: New frequency response by changing the inertial property **sensor 3**

with the already present peak follow the trend of the experimental frequency response the test performed to obtain the frequency response of the figure 4.28 was obtained decreasing the mass (thus also changing inertia) of the base tool. However, it must be kept in mind that without an experimental confirmation of these parameters we can not know if this representation is physically possible or is correct, in fact this difference in the peaks could also be due to a combination of the two effects or some stiffness that was not considered when the MB model was built or it could also easily be a purely accidental phenomenon, hence the peak represents a phenomenon present only in the MB model and therefore not present in the real machine.

4.2 PKM FMB model

Before start to apply this new strategy of model uncertainty on a complex system such as the Exechon PKM, it was necessary to apply this method to a simpler system, such as a crank slider system, in this way is easier understand the results and also understand if this approach leads to meaningful results, in appendix D can be found this example briefly reported. Since the system is made up of several bodies and joints for sick of simplicity and also to avoid long computational times, only five bodies were considered flexible which are the three arms and the two support beams figure 4.31. To avoid an excessive computational cost some geometry simplifications were made avoiding to model the details of the structure, but focusing on the dimensional and kinematic aspect of the structure. These simplifications led to a considerable reduction of the degrees of freedom of the flexible bodies and therefore in the dimensions of the stiffness matrices which was further reduced thanks to the Craig Bampton substructuring method.
The discretization of the bodies was performed with **SALOME**, that is an open source software, then the meshed bodies were saved in a **UNV** format that convert the mesh in node, element and group. The latest property of this format has been exploited selecting group of the boundary element i.e. the element in contact with other body that are used as master node in the Craig Bampton method. Then the mesh was imported in Matlab and through the shape function of the 4 node element (tetrahedrons) the stiffness matrix was created. In order to kinematically simulate the system it was imposed an harmonic motion of the prismatic joints, thus obtaining an almost harmonic motion along the Z-axis, figure 4.32. Six different cases were generated since we considered five flexible bodies, in five of those cases the uncertainty was imposed on one body at a time and in one case the uncertainty was imposed in all the body, this is necessary to understand

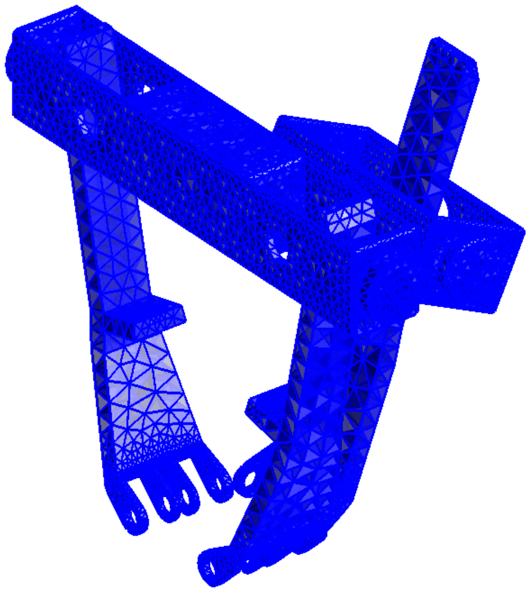

Figure 4.31: Flexible part representation

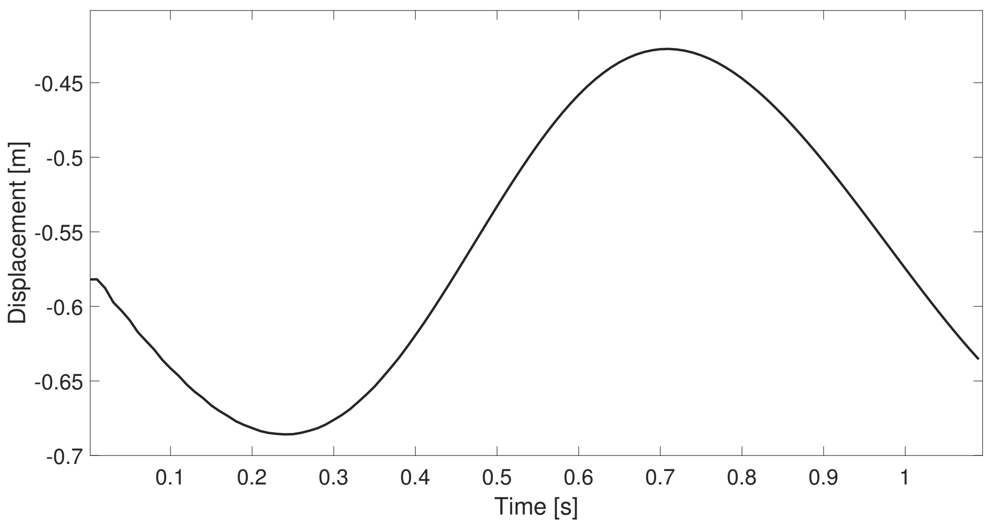

Figure 4.32: Displacement along z-axis of the COM against time of the nominal model

which body give us the greatest dispersion respect to the nominal trajectory.
The statistics for the system response were estimated using the Monte Carlo simulation method with n_s=150 independent realizations, the confidence region were built removing the nominal response in all realization and then data were ordered

with respect to the amplitude of the displacement at each time step of all the realization. In this case the probability that the data of the system's response are inside the confidence region is of the $P_c = 90\%$ with the dispersion parameter $\delta = 0.2$ that control the dispersion of the random stiffness matrices for each different case alternately.

4.2.1 Summary of the results FMBS

A problem not to be underestimated in the FMB models is the computational cost in this case each simulation lasted around the 40 minutes, so since we used 150 independent realization for 6 different case the analysis should have lasted roughly 600 hours, fortunately the process was parallelized with 72 cores and the analysis lasted about 8.5 hours, a summary of the simulation times can be seen in the table 4.4. In the figure 4.35 we can see the convergence of the mean value with respect to the number of Monte Carlo simulation. As we can see from the Fig.4.33 and Fig.4.34 the body that most influence the system's response is the upper support beam, because it has the biggest confidence region, instead the other bodies introduce almost the same level of fluctuation in the system's response, therefore in order to reduce the level of uncertainty in the motion of the machine we must act on the upper support beam and also on the lower support beam. These results give us an idea of how the stiffness of some bodies affects the trajectory of the system, but to have a true estimate of the size of the deviation from the imposed trajectory we should have a control system architecture closer to the real one and also recreate a more detailed geometry, in this example the aim was to demonstrate how to take into account the global uncertainties of the stiffness matrix and to find the body that introduced the greatest one. Respect to the previous sensitivity analysis this one is really intrusive respect to the commercial code because he needs to have access to the stiffness and damping[3] matrices of the bodies.

[3]if the damping is of the Rayleigh type $\mathbf{D}=\alpha\ \mathbf{M}+\ \beta\ \mathbf{K}$

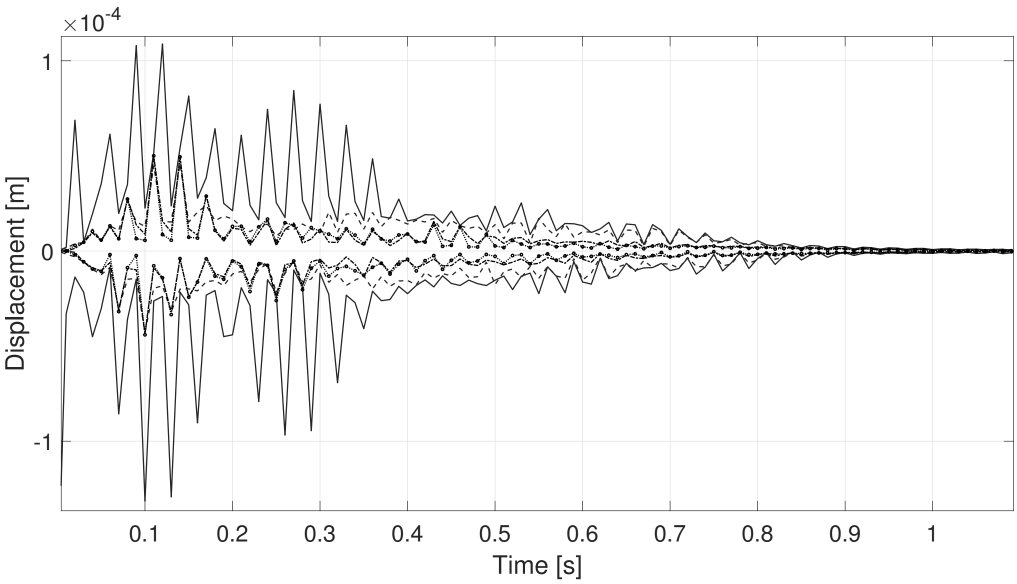

Figure 4.33: Confidence Region - **Case 1**thin solid lines $\delta = 0.2$ for all bodies - **Case 2** dashed line dispersion only in the left arm - **Case 3** dotted line dispersion only in the right arm - **Case 4** dashed-dotted marked line dispersion only in the middle arm

number of simulations	Time (1 core)	Time (72 core)
1	40 min	40 min
150	6000 min	120 min
900	36000 min	520 min

Table 4.4: Computational cost comparison FMB model

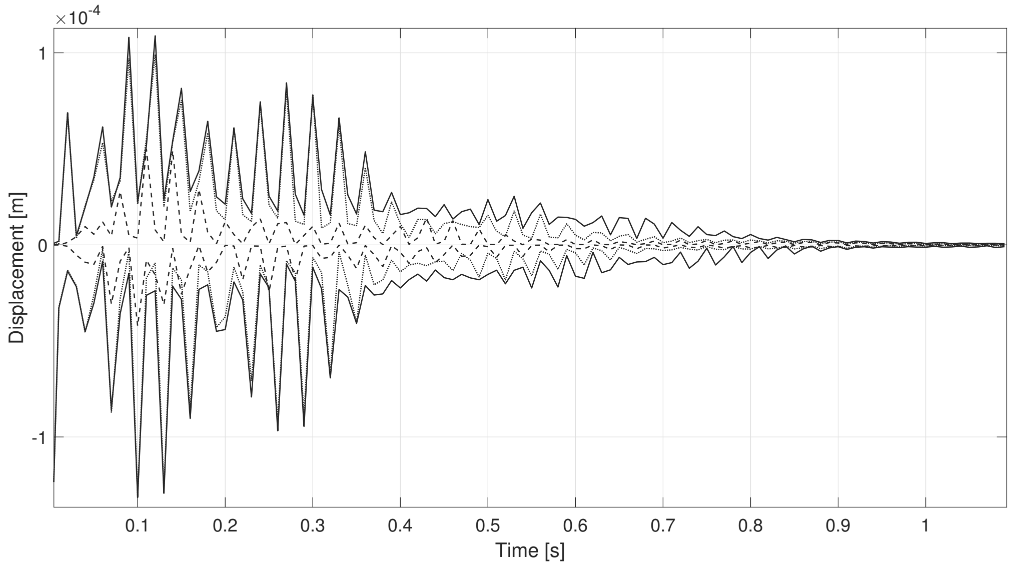

Figure 4.34: Confidence Region - **Case 1**thin solid lines $\delta = 0.2$ for all bodies - **Case 5** dashed line random stiffness only in the lower support beam - **Case 6** dotted line random stiffness only in upper support beam

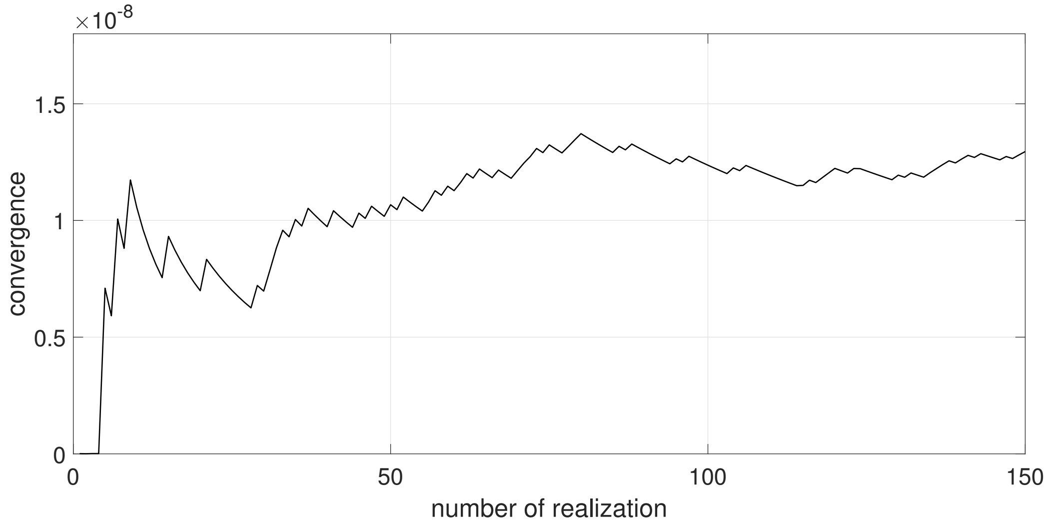

Figure 4.35: convergence of the mean value with respect to the number of Monte Carlo simulations

Chapter 5

Conclusion

Over the years the study of complex system with MB or FMB system has gained interest thanks to the possibility to solve interdisciplinary problems. However, the parameters may be really uncertain therefore to improve the predictability of the model uncertainties must be take into account. In this report through a sensitivity analysis we were able to:

- propose a new strategy based on a non parametric probabilistic approach to model the uncertainties in the stiffness matrices of a FMB system based on the floating frame of reference approach.
- identify the parameters that most influence the dynamic and kinematic response of the machine in a given configuration
- understand how these uncertainties affect the system response

It must be noticed that these results can change by changing the configuration of the system. There are few drawback in the use of this approach such as:

- the **computational cost**, especially in the FMB models that usually require much more time than the MB models to perform a simulation. Of course, as already mentioned, since these method lends itself very well to parallel computing, the computational time can be drastically reduced.
- the **invasiveness** of the new approach for the FMB system respect to the commercial code, because to implement it we need to have access to the stiffness matrices of the flexible bodies, which are usually not available.

5.1 Further development

5.1.1 PKM MB model

Once a more representative MB model is developed, the next step is to perform a calibration of the probability distribution parameters solving an inverse stochastic problem through experimental data, with the final goal to validate also the dynamic models for its posterior use in related dynamic predictions and for control purposes.

5.1.2 PKM FMB model

Some interesting future developments of this approach could regard:

- perform a sensitivity analysis of the frequency response of the system and comparing it with the experimental data, to see how flexible component affect the frequency response of the system.
- extend this new approach, which now includes only the uncertainty due to the stiffness matrices, also the uncertainty due to the mass matrix.

Appendix A

First MB model sensitivity analysis results

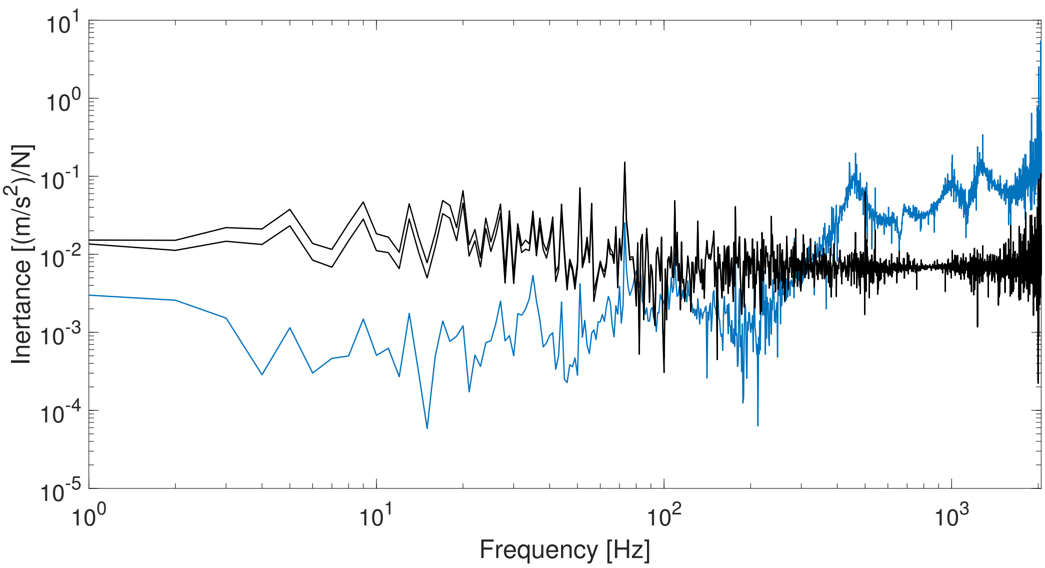

Figure A.1: **Case 1**: Random joint mechanical properties, δ=0.4 coefficient of variation with a 80% confidence region (black) and experiments (blue))

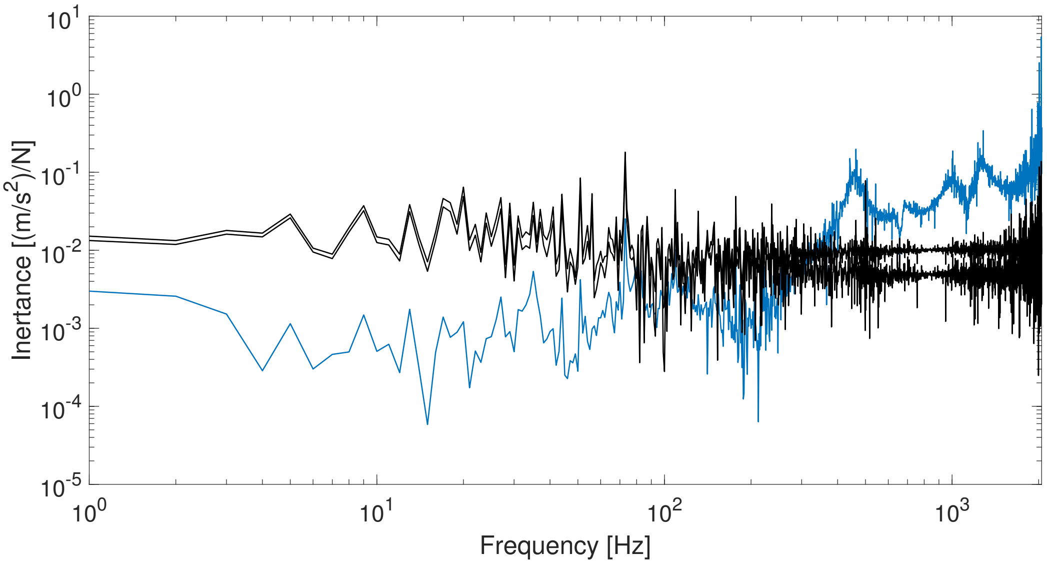

Figure A.2: **Case 2**: Random masses, δ=0.4 coefficient of variation with a 80% confidence region (black) and experiments (blue))

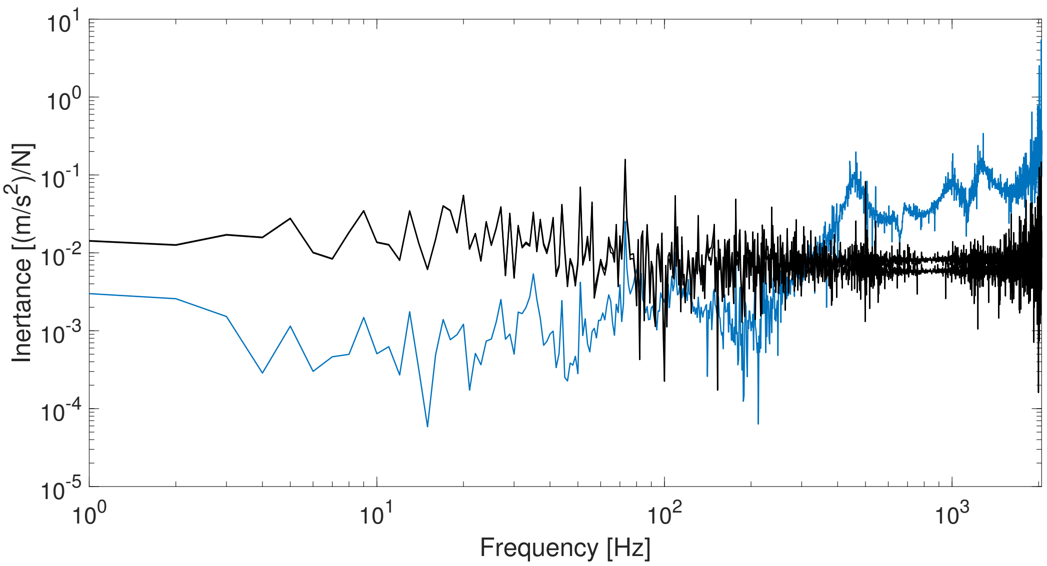

Figure A.3: **Case 3**: Random inertia matrices, δ=0.4 coefficient of variation with a 80% confidence region (black) and experiments (blue))

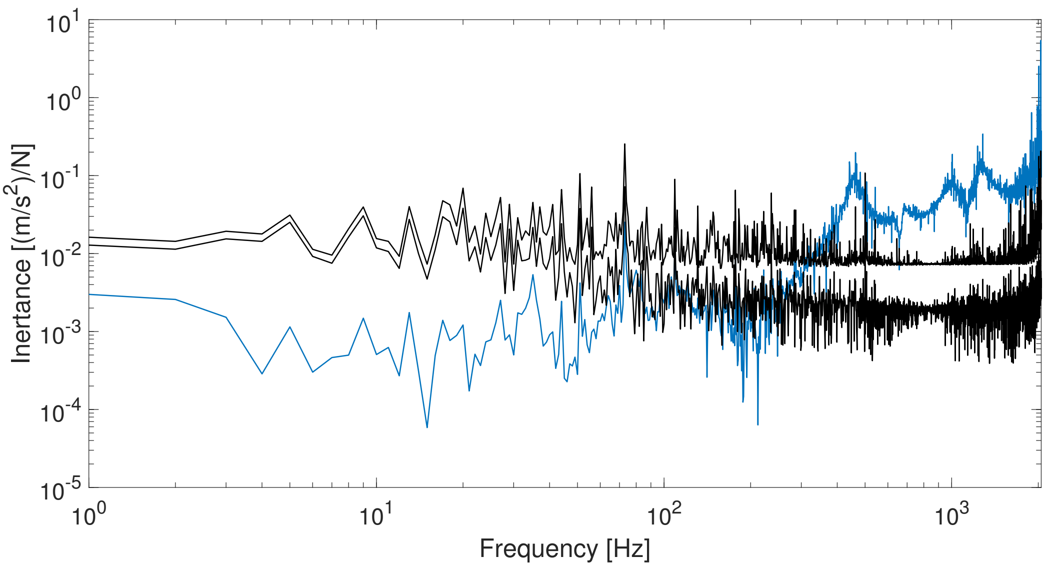

Figure A.4: **Case 4**: Random inertia matrices, δ=0.4 coefficient of variation with a 80% confidence region (black) and experiments (blue))

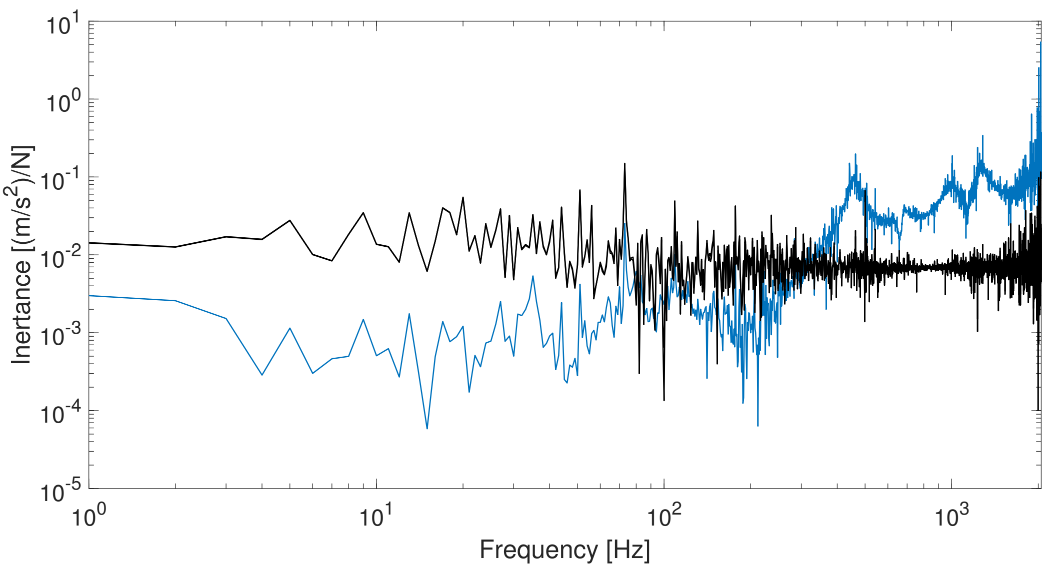

Figure A.5: **Case 5**:Random sensors positions, uniform random variables $\pm$ 20 mm and $\pm$ 20 deg with a 80% confidence region (black) and experiments (blue))

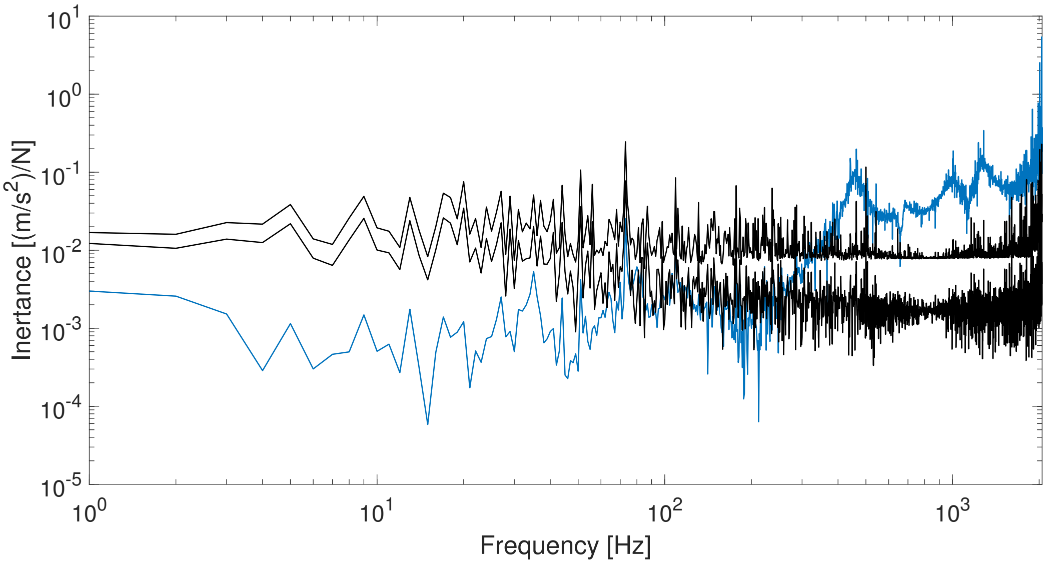

Figure A.6: **Case 6**:All random , 80% confidence region (black) and experiments (blue))

Appendix B

Second model Sensitivity analysis figures

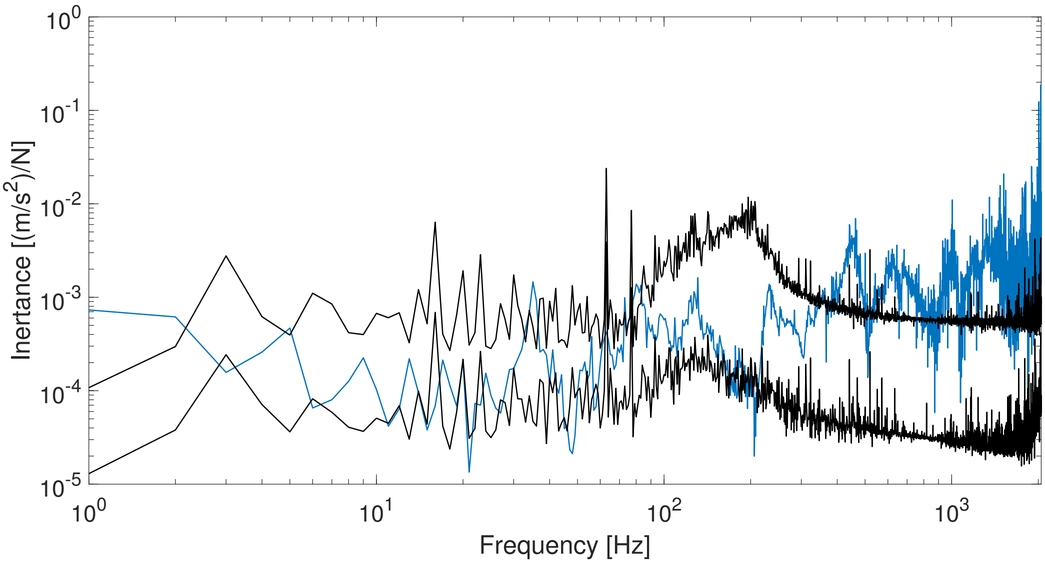

Figure B.1: **CASE 1** - the **black** lines indicate the confidence region of the MB model- the **blue** indicate the experimental response **sensor 3**

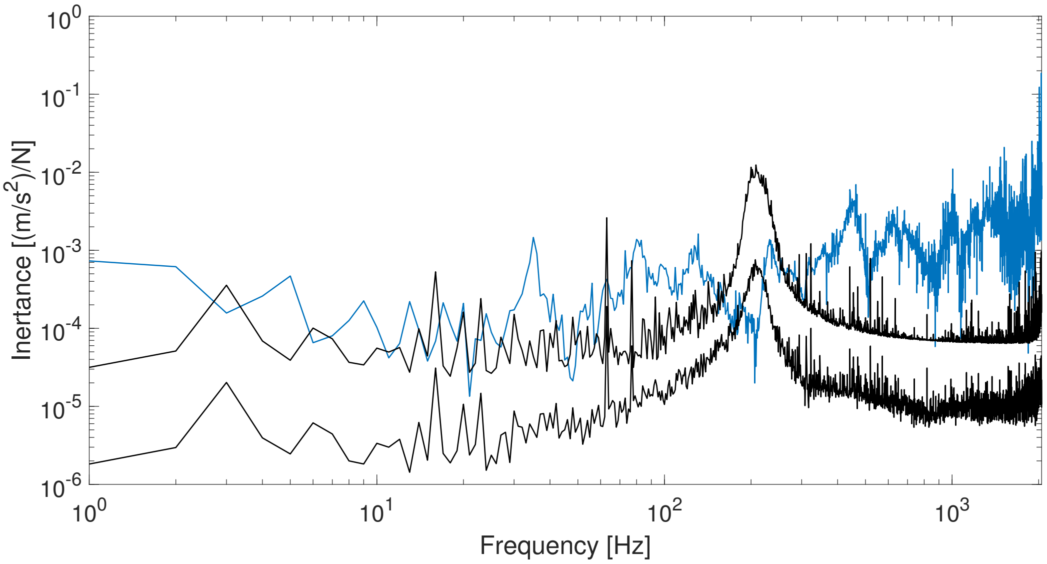

Figure B.2: **CASE 2** - the **black** lines indicate the confidence region of the MB model- the **blue** indicate the experimental response **sensor 3**

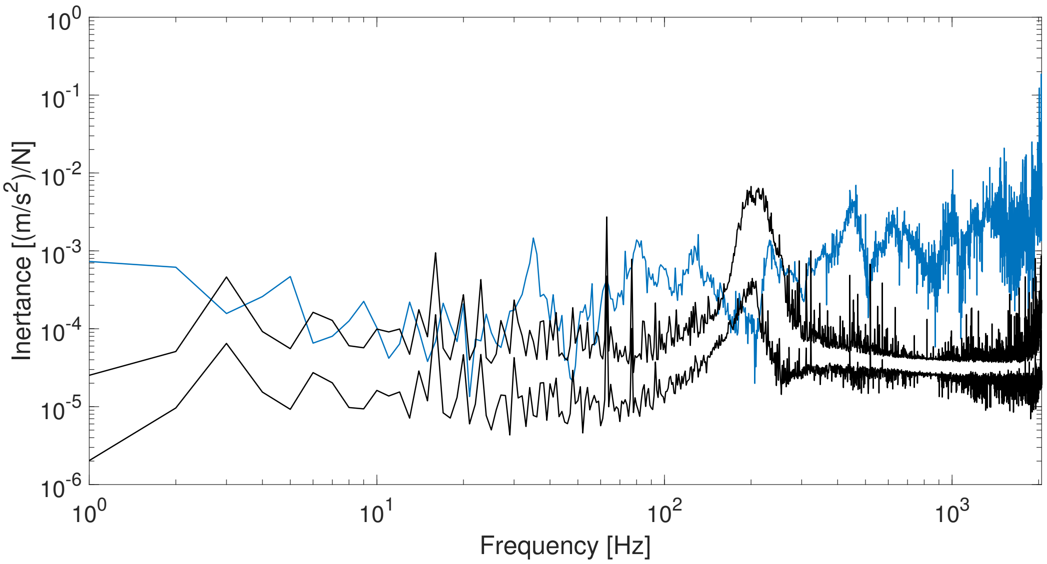

Figure B.3: **CASE 3** - the **black** lines indicate the confidence region of the MB model- the **blue** indicate the experimental response **sensor 3**

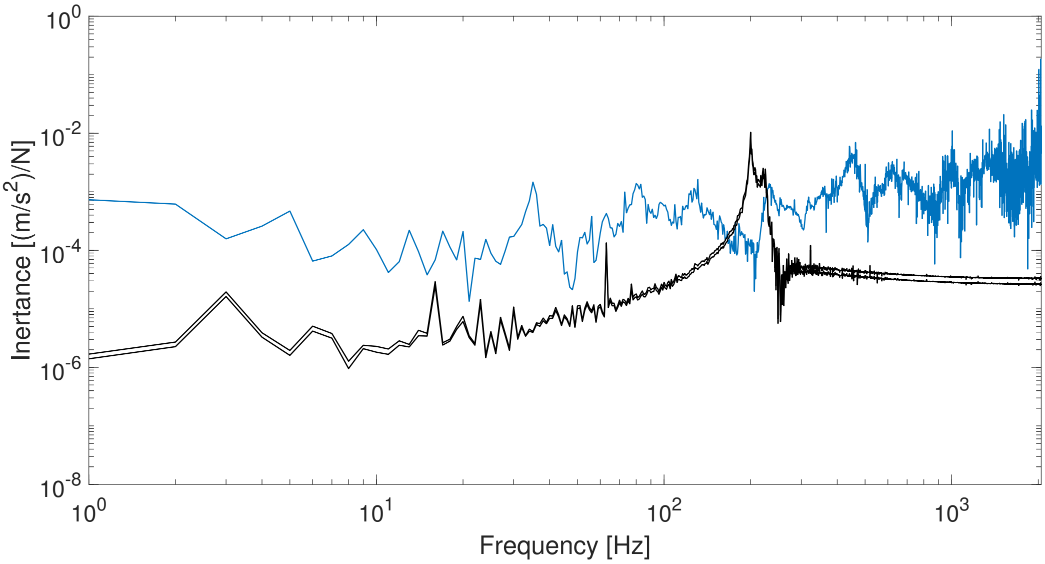

Figure B.4: **CASE 4** - the **black** lines indicate the confidence region of the MB model- the **blue** indicate the experimental response **sensor 3**

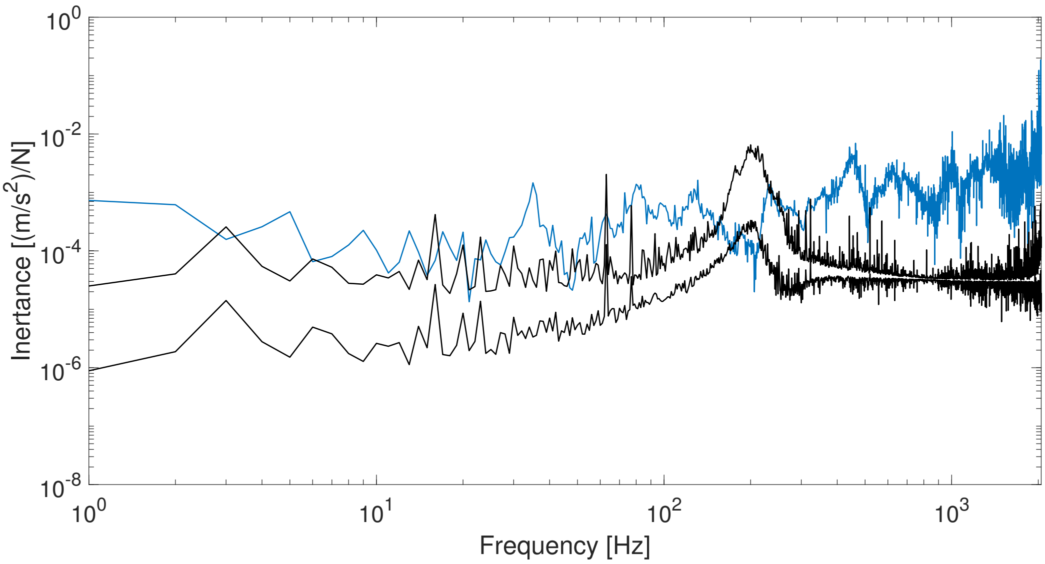

Figure B.5: **CASE 5** - the **black** lines indicate the confidence region of the MB model- the **blue** indicate the experimental response **sensor 3**

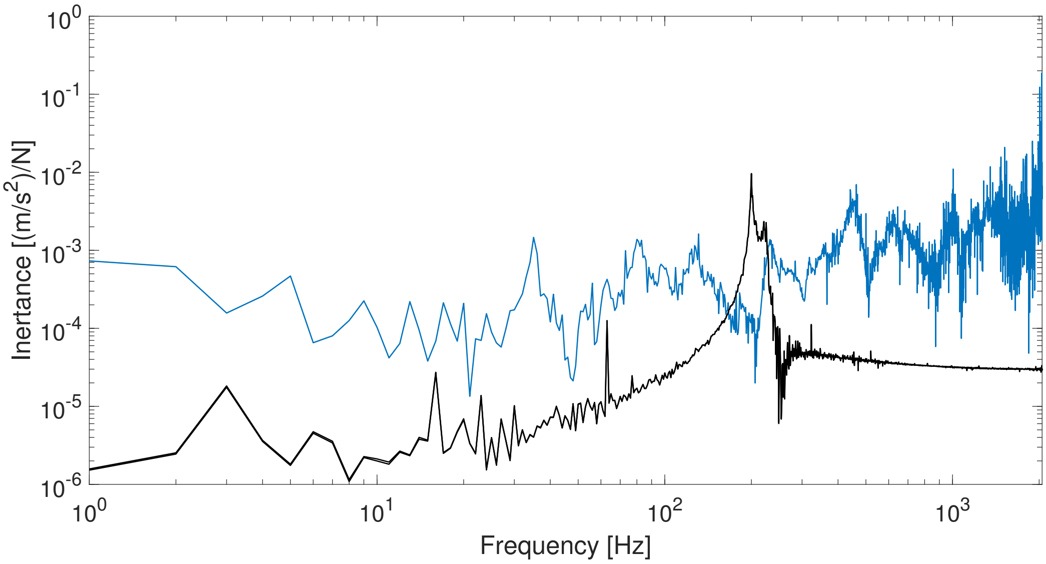

Figure B.6: **CASE 6** - the **black** lines indicate the confidence region of the MB model- the **blue** indicate the experimental response **sensor 3**

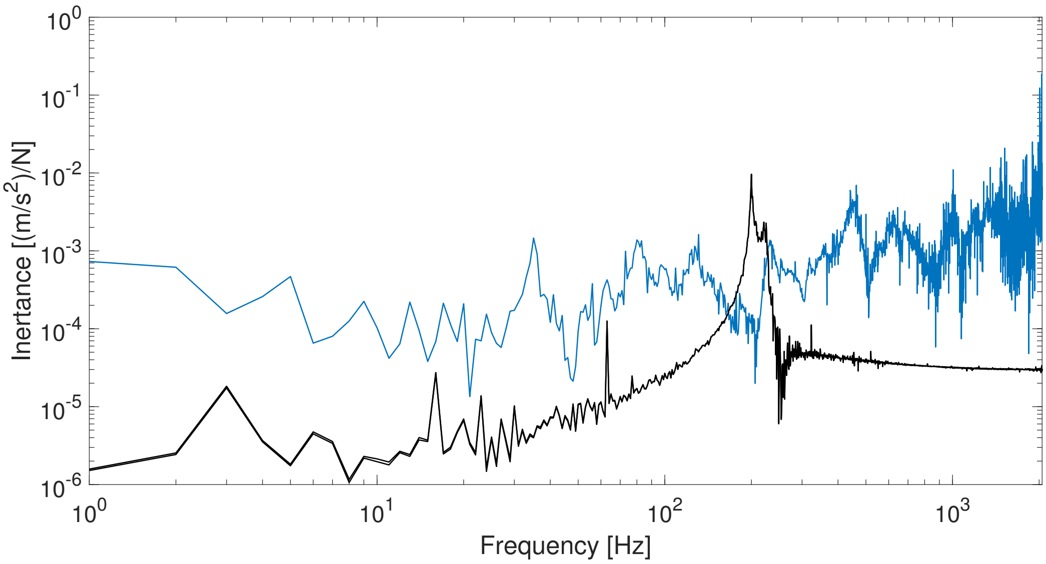

Figure B.7: **CASE 7** - the **black** lines indicate the confidence region of the MB model- the **blue** indicate the experimental response **sensor 3**

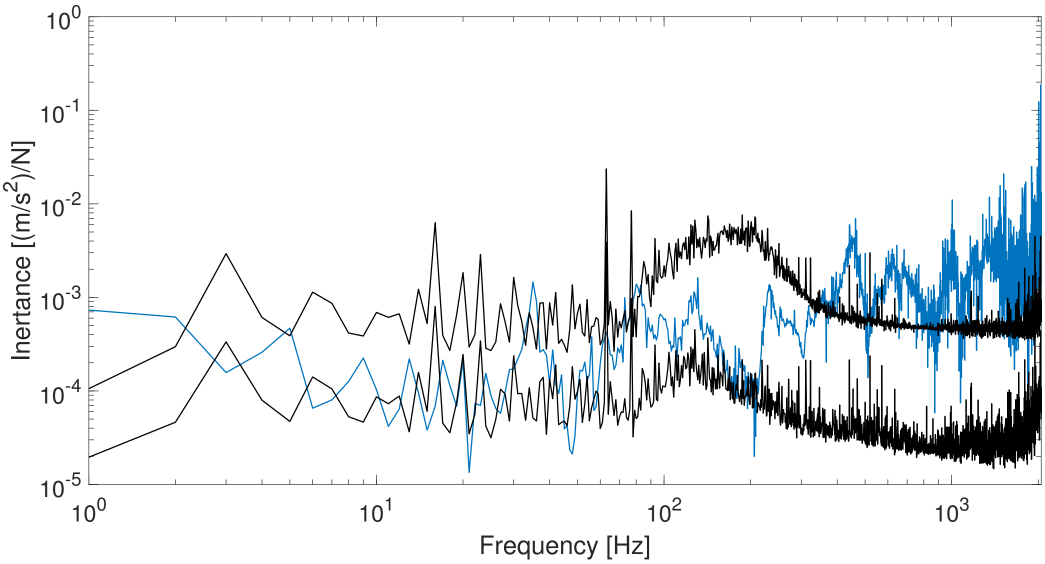

Figure B.8: **CASE 8** - the **black** lines indicate the confidence region of the MB model- the **blue** indicate the experimental response **sensor 3**

Appendix C

Relative standard deviation

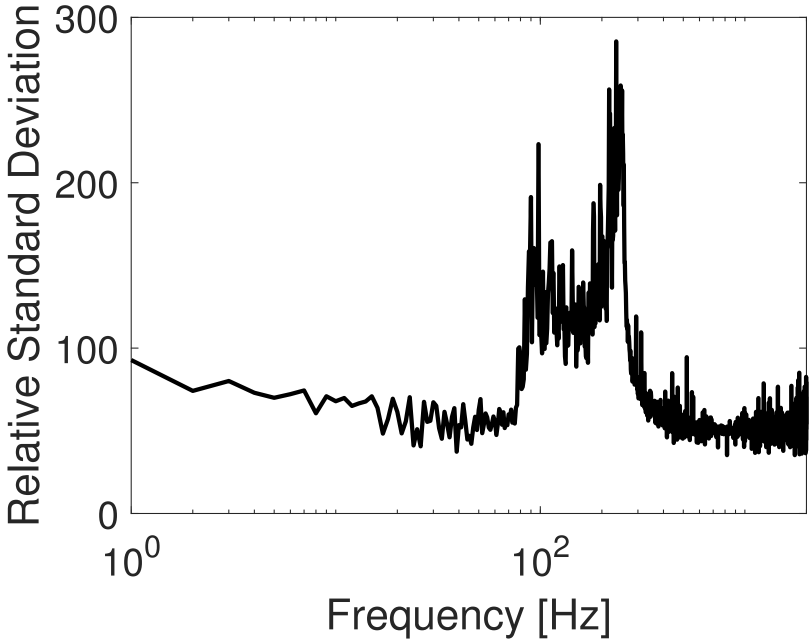

Figure C.1: **CASE 1** Relative standard deviation **sensor 1**

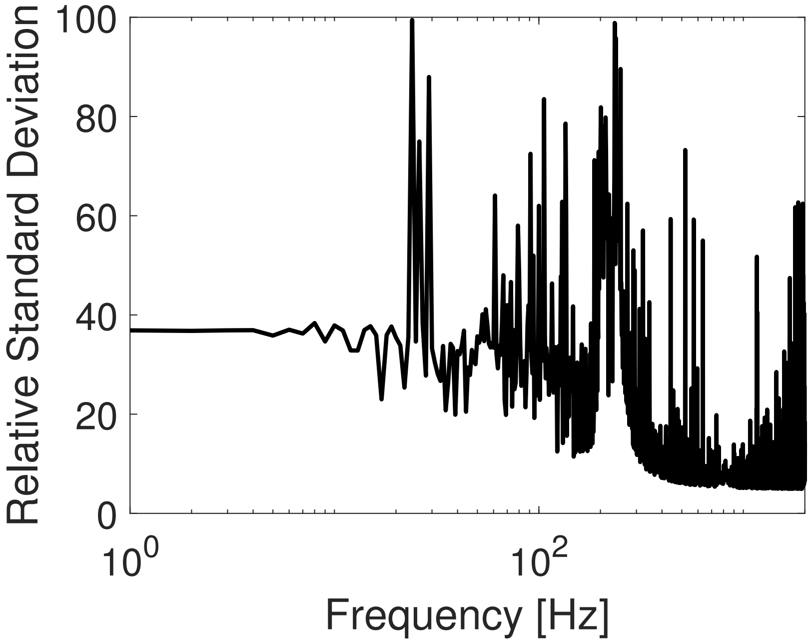

Figure C.2: **CASE 2** Relative standard deviation **sensor 1**

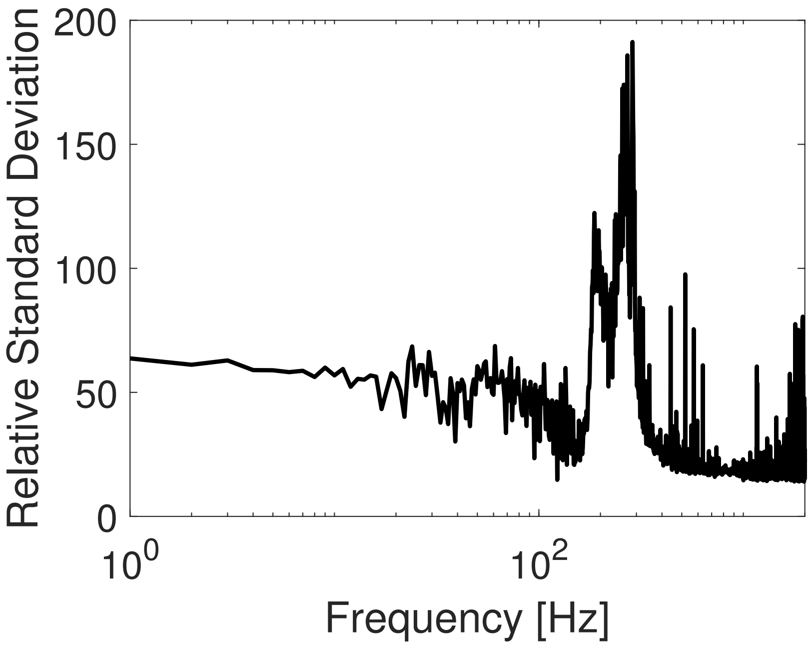

Figure C.3: **CASE 3** Relative standard deviation **sensor 1**

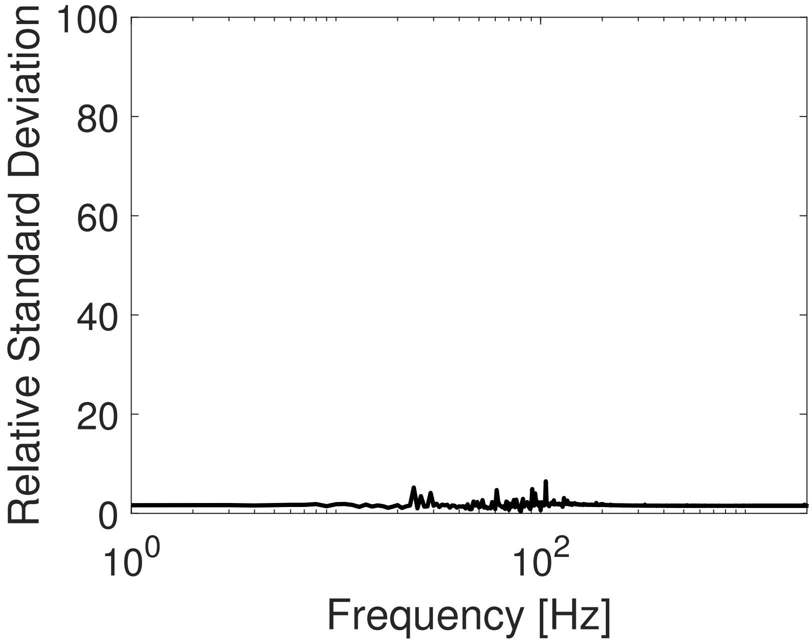

Figure C.4: **CASE 4** Relative standard deviation **sensor 1**

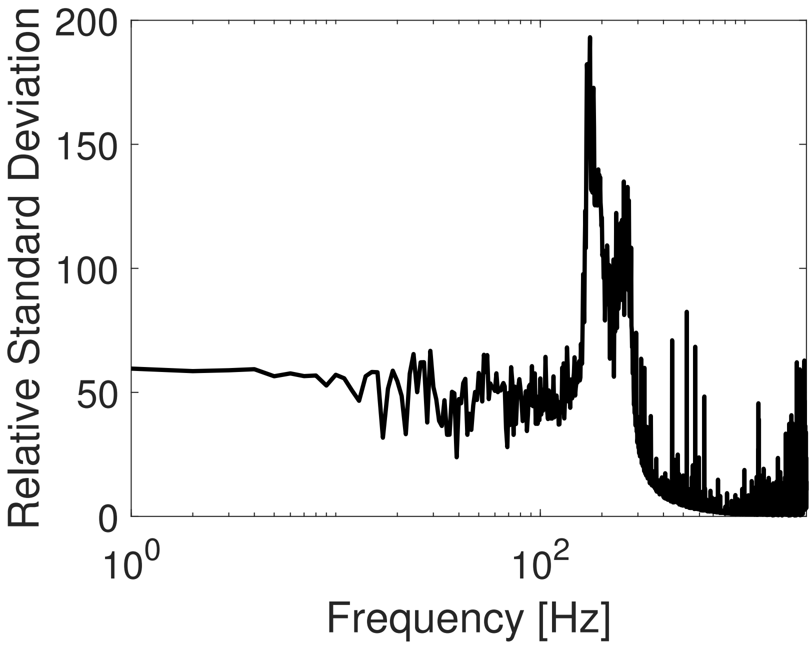

Figure C.5: **CASE 5** Relative standard deviation **sensor 1**

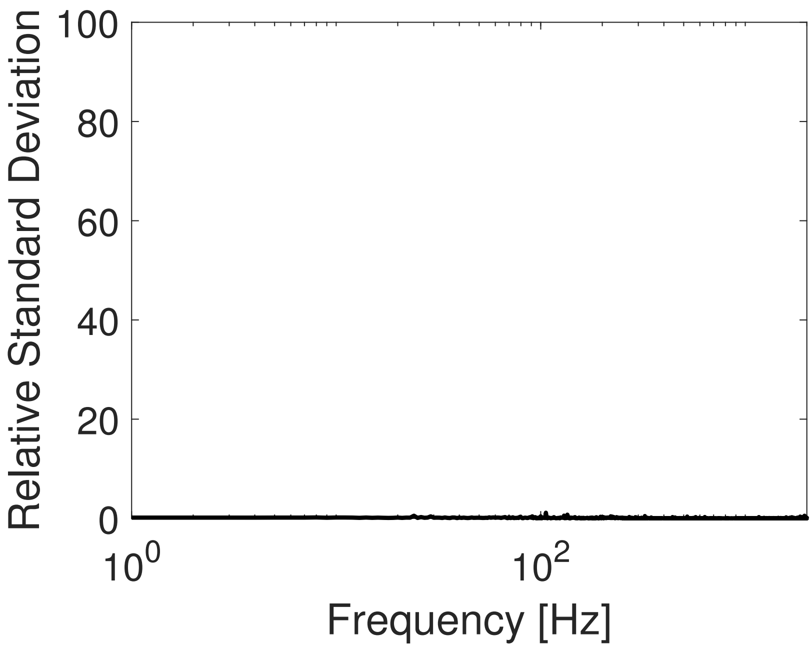

Figure C.6: **CASE 6** Relative standard deviation **sensor 1**

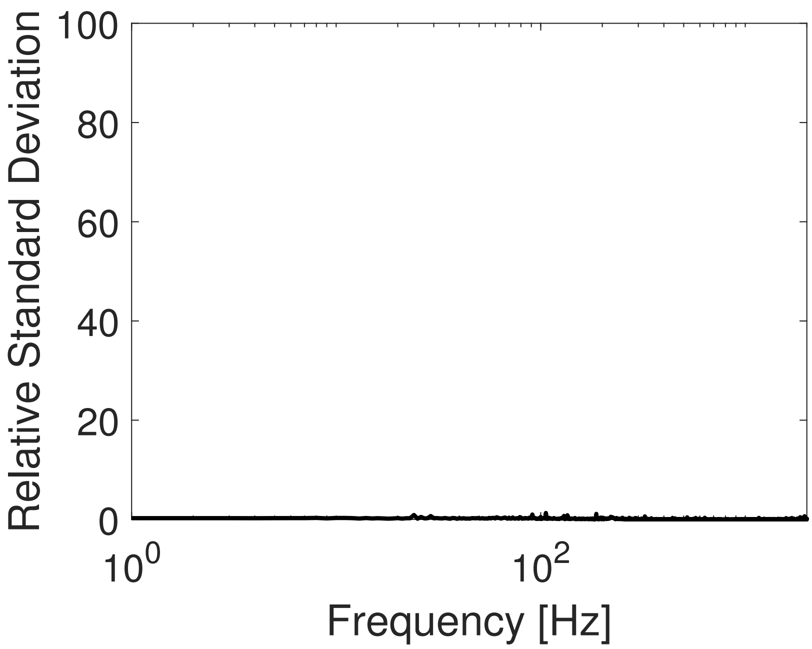

Figure C.7: **CASE 7** Relative standard deviation **sensor 1**

Appendix D

Crank-Slider

We will perform two different numerical simulations of the crank slider mechanism, for the first application we will confront the results obtained from the MB and FMB model of the system, on the second application we will perform a sensitivity analysis on the stiffness matrices of the flexible part to show which one of the bodies is the most sensible at the uncertainty.

First application

In this first application we trace the trajectory of two significant points, this points are shown in the Fig.D.1.1. To simulate the system a rotation is imposed respect to

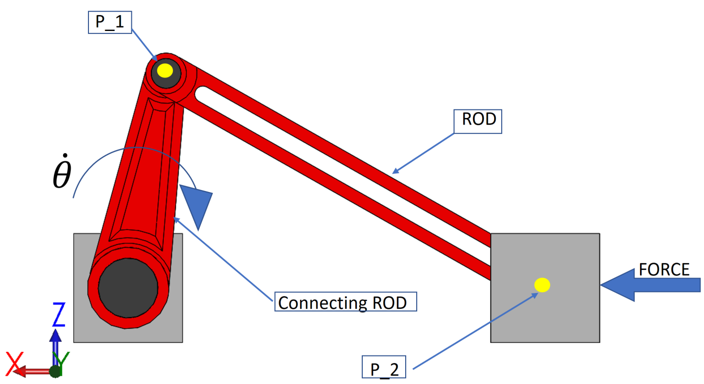

Figure D.1: representation of the system

the revolution joint of the connecting rod, and also a force that always is against the motion of the prismatic joint, to do that a PD controller was built. When we consider all the bodies rigid what we aspect to see is that the point P_1 that is the point of the connecting rod describe in the three dimension a circular trajectory, but what we see is that the point is not exactly describing a circular trajectory Fig.D.2.2. What we aspect from a rigid body solution, according to the reference

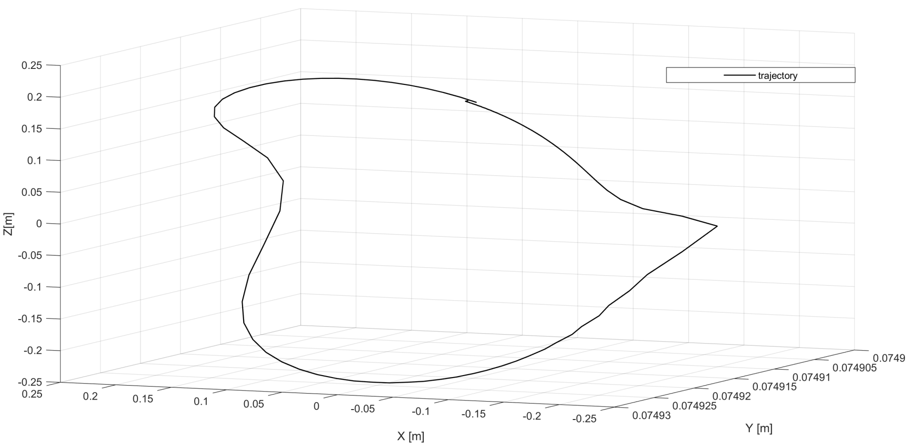

Figure D.2: trajectory P_1 in a flexible Multi-body system

frame shown in figure D.1, is that the trajectory is a should be a circle in fact if we look the trajectory in figure D.3 that is the trajectory of the MB system. This

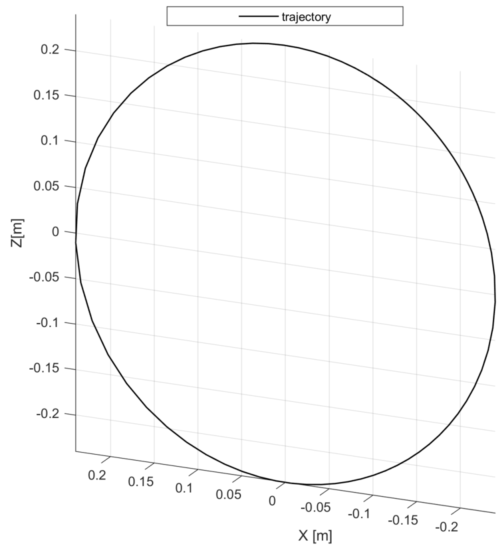

Figure D.3: trajectory P_1 in a Multi-body system

difference is due to the stiffness of the connecting rod and rod, in fact what we can notice is that if we increase the Young Modulus of the two flexible part is that the trajectory when $E \longrightarrow \infty$ the trajectory of the flexible system tends to a circle, as in figure D.4.

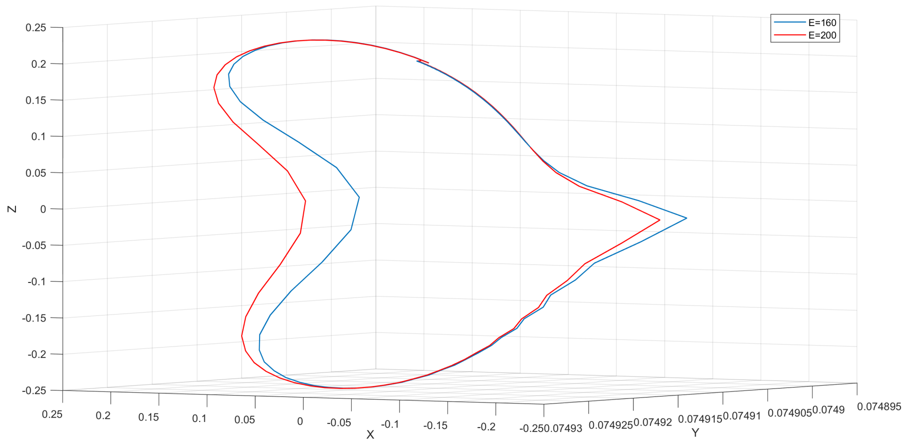

Figure D.4: trajectory P_1 increasing the Young Modulus

We also want to control the effect of flexibility on the stroke of the Crank-slider. The trajectory no matter we are considering the body rigid of flexible is a straight line. What we aspect that change is the length of this line, so we want now understand how the stroke is affected by the flexibility of the bodies to do that we trace the point P_2 that correspond to the center of mass of the brick body attached at the end of the rod. As we can see in figure D.5. The trend of P_2 respect to time is almost harmonic to understand which body is the most important to the length of the stroke we will change the Young modulus making three cases:

- "Nominal" E_{rod}=40 GPa, $E_{condord}$=40 GPa
- "case 1" E_{rod}=35 GPa, $E_{condord}$=40 GPa
- "case 2" E_{rod}=40 GPa, $E_{condord}$=35 GPa

We chose a lower value of Young Modulus only to highlight the influence of flexible bodies in the stroke. In the following application we will see that the bodies that most influence the length of the stroke is the rod.

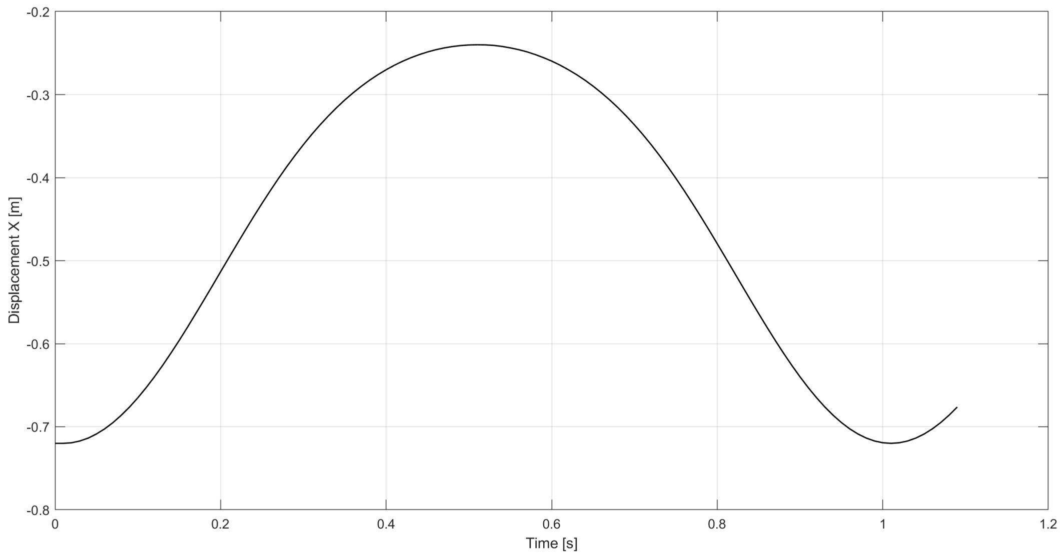

Figure D.5: trajectory P_2 E=40 GPa

second application

For the second application we will use a Crank-Slider mechanism, shown in Fig.D.6. The Flexible Multi-Body system is made up of five bodies of which only two are assumed to be flexible, the flexible body are denominated as **Fb** in the figure. The inertial frame of reference is it fixed to the center of mass of the rigid body (**Rb**) called world. In this system are used one prismatic joint along x-axis, and three revolution joints along y-axis where the revolution joint 1 (Rj1) pass to the center of mass (COM) of the world, Rj2 pass to the COM of the Rb2 and the Rj3 pass to the COM of the Rb1. A rotation is imposed in the Rj1 and it is also applied a force $F_x = 3,3kN$ which is always opposite to the motion of the Rb1, and it is applied to the COM of the latter. The material characteristic of the flexible bodies are Young Modulus E= 40 GPa, density ρ = 1700 kg/m^3 and Poisson's ratio $\nu = 0.29$. In the initial configuration the positions of center of mass expressed in [mm], are World= [0 0 0], Rb2 = [-240 94.5 0], Rb1= [-720 114 0], Fb1= [-93.868 79.5 0], Fb2=[-480 114 0]; The respective weight of the rigid bodies Rb1= 12.6 kg and Rb2= 0.42 kg. The respective moments of inertia of the two rigid bodies taken at the center of mass are J_{Rb1} =[23898712.61 0 0 ; 0 43876679.43 0 ;0 0 43876679.43] [g mm^2], J_{Rb2} =[197504.57 0 0; 0 57841.19 0 ;0 0 197504.57] [g mm^2]. The system is

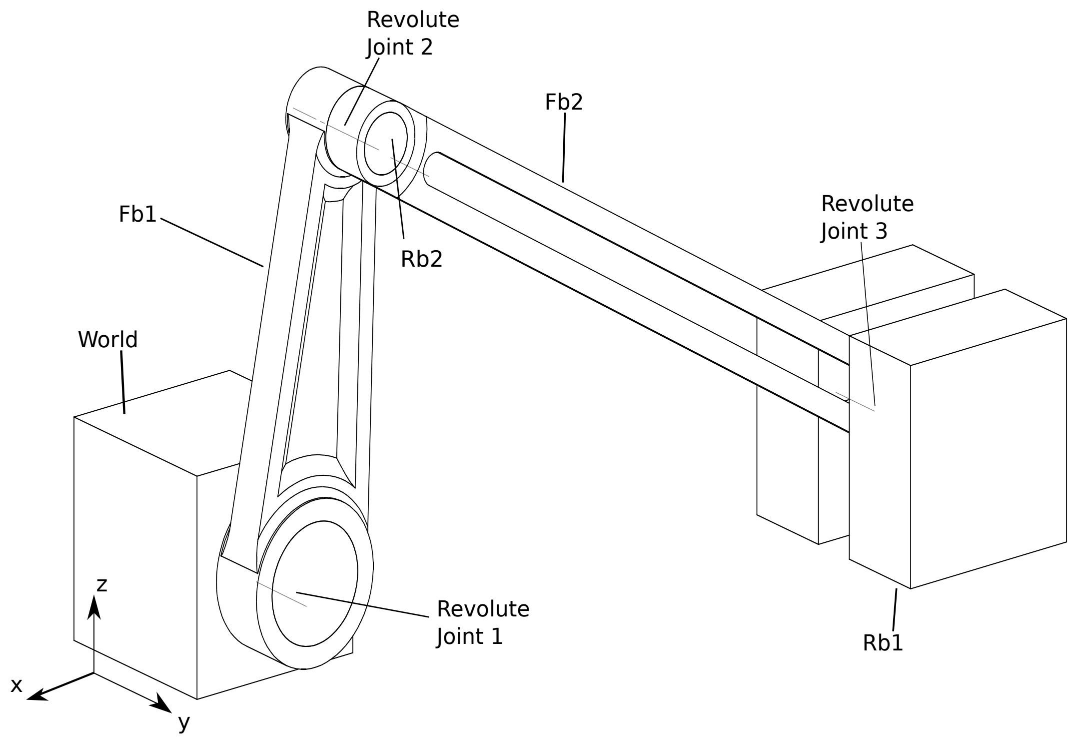

Figure D.6: Crank-Slider mechanism

	δ_{Fb1}	δ_{Fb2}
Case 1	0.2	0.2
Case 2	0.001	0.2
Case 3	0.2	0.001

Table D.1: dispersion parameters in the different cases

simulated for a time of t=1.1s with a circular frequency f= 1 Hz. In order to individuate the flexible body that most influence the system behavior were developed three cases, summarized in the table D.1, the dispersion parameter is it referred to the Damping matrix and also to the Stiffness matrix. The statistics for the system response were estimated using the Monte Carlo simulation method with 300 independent realizations. Once all the responses of the system has been computed, from each realization was removed the nominal response Fig.D.7 and then the output data were ordered with respect to the amplitude at each time step, then starting from the mean of the sorted data we selected the confident region with a probability $P_c = 90\%,$ As we can see from the Fig.D.8 the largest confident region

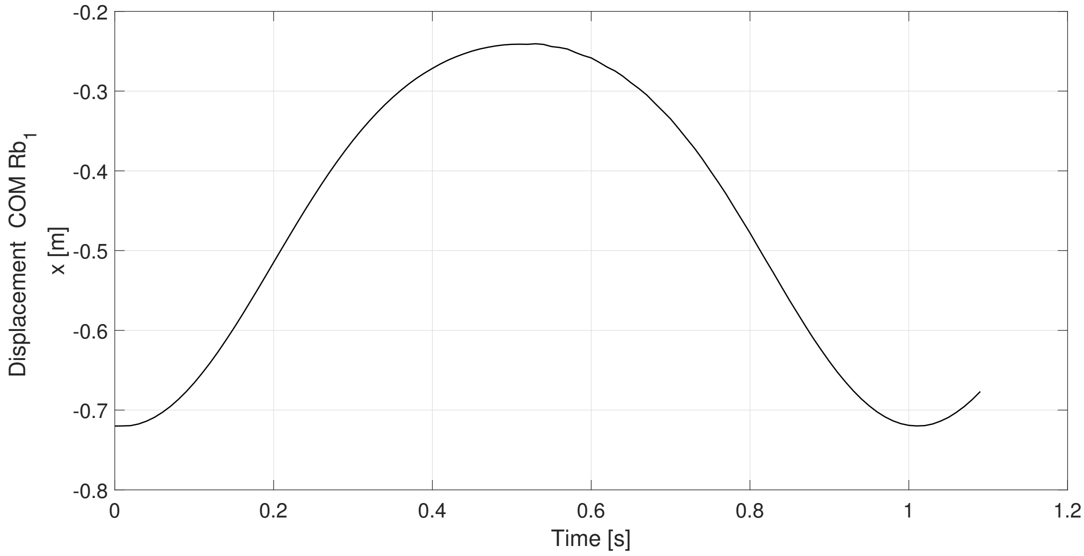

Figure D.7: Displacement along x-axis of the COM Rb_1 against time of the nominal model

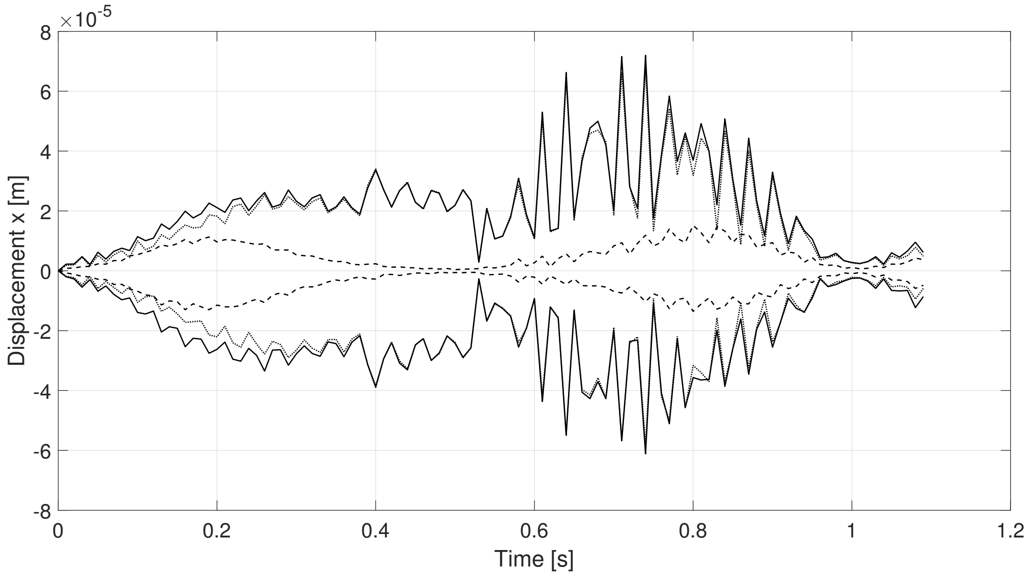

Figure D.8: Difference between the nominal displacement and the displacement of the n realization -**confidence regions** - **Case 1** upper and lower thin solid lines - **Case 2** upper and lower thin dotted lines -**Case 3** upper and lower thin dashed lines

is the one of the case 1 as expected, the smallest confidence region is the one in which the stiffness and damping matrix of the Fb1 are considered as uncertain.

From this results is it obvious that the Fb2 is the one where the uncertainty most influence the response of the system since at equal conditions has a confidence region bigger then the one of the Fb1. So in order to reduce drastically the uncertainty on the stroke of the system we must reduce the uncertainty related to the Fb2. In the Fig.D.9 , we show the convergence of the L2 norm, of displacement of the COM of the Rb1 respect of the number of Monte Carlo simulations.

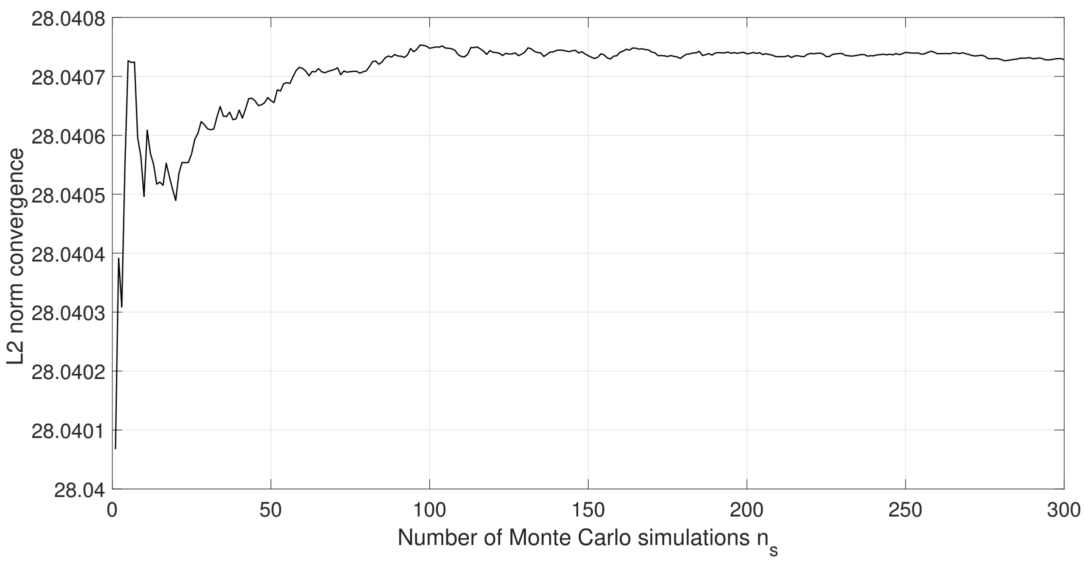

Figure D.9: Convergence of the mean value respect to the number of Monte Carlo simulations **Case 1**

List of Symbols

E	Young modulus
ρ	density
$\mathbf{R}$	Reference coordinate for the location of the body
$\boldsymbol{\theta}$	Reference coordinate for the orientation of the body
$\mathbf{u}^f$	Elastic coordinate
$\mathbf{Q}^v$	Quadratic velocity vector
$\mathbf{Q}^e$	Generalized forces
$\mathbf{C}$	Constraint Jacobian matrix
$\boldsymbol{\lambda}$	Lagrange multipliers vector
$\mathbf{m}$	Mass matrix
$\mathbf{k}$	Stiffness matrix
$\square^I$	Inner DOF
$\square^\Gamma$	Interface DOF
$\tilde{q}$	Generalize coordinate to normal modes
$\square^{ff}$	matrix associated with elastic coordinate
$\square^{\mathbf{R}f}$	coupling between elastic and location coordinate
$\square^{\boldsymbol{\theta}f}$	coupling between elastic and orientation coordinate
$\boldsymbol{\Phi}$	Modal matrix
$\boldsymbol{\Psi}$	Craig Bampton transfer matrix
$\mathbf{M}^*$	Reduced mass matrix
$\mathbf{K}^*$	Reduced stiffness matrix
Ω	Sample space
Ξ	Set of events
Υ	Probability of the events
δ	Dispersion parameter
σ	variance
$\mathbf{J}$	Inertia matrix
$\mathbf{I}$	Normalized inertia matrix
$\mathbf{L}$	Cholesky decomposition matrix
$\mathbf{G}$	Random matrix
$\mathbf{V}$	Eigen-decomposition matrix
$\boldsymbol{\Lambda}$	Eigen-decomposition diagonal matrix
$E\{\cdot\}$	Expected value
$E\{\square^{-2}\}$	Second order inverse moment
$\Gamma\{\cdot\}$	Gamma function
$p_{\mathbf{x}}$	Probability density function

List of Figures

List of Tables

Bibliography

[1] Shabana, A. (2005). Dynamics of Multibody Systems. 3rd ed. Cambridge: Cambridge University Press.

[2] GeÌĄradin, M. and Cardona, A. (2001). Flexible multibody dynamics. Chichester: John Wiley.

[3] Walz N, Hanss M. (2013). Fuzzy Arithmetical Analysis of Multibody Systems with Uncertainties. Archive of Mechanical Engineering, 60(1), 109-125. `https://doi.org/10.2478/meceng-2013-0007`

[4] Sandu A, Sandu C, Ahmadian M. (2006). Modeling Multibody Systems with Uncertainties. Part I: Theoretical and Computational Aspects. Multibody System Dynamics, 15(4), 369-391. `https://doi.org/10.1007/s11044-006-9007-5`

[5] Sandu C, Sandu A, Ahmadian M. (2006). Modeling multibody systems with uncertainties. Part II: Numerical applications. Multibody System Dynamics, 15(3), 241-262. `https://doi.org/10.1007/s11044-006-9008-4`

[6] Batou A, Soize C. Rigid multibody system dynamics with uncertain hrigid bodies, Multibody System Dynamics, 27(3), 285-319 (2012) `https://doi.org/10.1007/s11044-011-9279-2`.

[7] Soize, C. (2017). Uncertainty quantification - an accelerated course with advanced applications. 1st ed. New York: Springer.

[8] Robert, C. and Casella, G. (2010). Monte Carlo statistical methods. New York: Springer.

[9] Sobol', I. (2001). Global sensitivity indices for nonlinear mathematical models and their Monte Carlo estimates. Mathematics and Computers in Simulation, 55(1-3), pp.271-280. https://doi.org/10.1016/S0378-4754(00)00270-6

[10] Trinh, C., Zlatanov, D., Zoppi, M. (2016). Direct Kinematics of the Exechon Tripod. Volume 5B: 40th Mechanisms and Robotics Conference. http://dx.doi.org/10.1115/detc2016-60038

[11] Bampton MCC and Craig RR Jr. Coupling of substructures for dynamic analyses. AIAA Journal, Vol. 6, No. 7 (1968), pp. 1313-1319. https://doi.org/10.2514/3.4741

[12] Oshea, J. J., Jayakumar, P., Mechergui, D., Shabana, A. A., Wang, L. (2018). Reference Conditions and Substructuring Techniques in Flexible Multibody System Dynamics. Journal of Computational and Nonlinear Dynamics, 13(4), 041007. http://dx.doi.org/10.1115/1.4039059

[13] The equations of Lagrange for a continuous deformable body with rigid body degrees of freedom, written in a momentum based formulation - Scientific Figure on ResearchGate. Available from: https://www.researchgate.net/Floating-frame-of-reference-formulation_fig1_267339371 [accessed 4 Oct, 2018]

[14] Genta G, editor. Vibration Dynamics and Control. Mechanical Engineering Series [Internet]. Springer US; 2009; Available from: http://dx.doi.org/10.1007/978-0-387-79580-5

[15] Jaynes, E. (1957). Information Theory and Statistical Mechanics. Physical Review, 106(4), pp.620-630.

[16] Real, F., Fontanela, F., Ritto, T., Batou, A. and Desceliers, C. (2017). A probabilistic model of uncertainties in the substructures and interfaces of a dynamical system: application to the torsional vibration of a drill-string. Archive of Applied Mechanics, 87(4), pp.685-698.

[17] Soize, C.: A nonparametric model of random uncertainties on reduced matrix model in structural dynamics. Probabilistic Engineering Mechan-

ics. 15(3), 277âĂŞ294 (2000). https://hal-upec-upem.archives-ouvertes.fr/hal-00686293

[18] Saltelli, A., Chan, K. and Scott, E. (2000). Mathematical and statistical methods for sensitivity analysis. Chichester: Wiley.

[19] Variance-based sensitivity analysis. In Wikipedia. Retrived October 08, 2018, from https://en.wikipedia.org/wiki/Variance-based_sensitivity_analysis

[20] Soize C. (2005). Random matrix theory for modeling uncertainties in computational mechanics. Computer Methods in Applied Mechanics and Engineering, 194(12-16), 1333-1366. http://dx.doi.org/10.1016/j.cma.2004.06.038